Anna Á. Rauscher

INTERNAL FRICTION IN ENZYME REACTIONS

PhD Thesis

Supervisor: András Málnási-Csizmadia DSc.

Structural Biochemistry Doctoral Program

Doctoral School in Biology

Program leaders: Prof. László Nyitray DSc. , Prof. László Gráf DSc.

Head of the School: Prof. Anna Erdei DSc.

Department of Biochemistry, Eötvös Loránd University, Budapest, Hungary

2013

Table of contents

List of figures and tables

List of abbreviations

HuTry4	human trypsin 4
193A, 193G	Ala/Gly residue at position 193
NATA	N-Acetyl-L-tryptophanamide
ATP-N	gamma-amido-adenosine triphosphate
k_B	Boltzmann constant, $1.3806488 \times 10^{-23}$ m^2 kg s^{-2} K^{-1}

T	absolute temperature in Kelvin (K)
ΔE_a ΔE_A ΔE_σ ΔH ΔG	activation energy in J/mol
η	viscosity of the solvent in cP
σ	internal viscosity in cP
σ_0	internal viscosity at T=0 K
σ_{300}	internal viscosity at T=300 K
σ_M	internal viscosity in the mechanistic model in cP
τ	relaxation time , $1/k$ in s
k	rate constant, $1/\tau$ in s^{-1}
A	temperature and viscosity independent preexponential constant
p	exponent of viscosity, $0<p<1$
I	ionic strength

1. Introduction

1.1. Introduction to the energy landscape

Even though the Greeks did not study protein dynamics, the famous quote from Heraclitus that "*You cannot step twice into the same stream"* illustrates well how we see proteins today. When we consider the conformational diversity of proteins, we may come to a similar conclusion as "it is unlikely (…) that a protein returns twice to the same [conformational] substate" (cited from (3)). The theoretical energy landscape (BOX 1) characterizes this enormous conformational space of a protein by assigning an energy/probability to each conformational state. The conformational transitions, enzyme reactions, folding-unfolding processes, etc., could be precisely predicted if we knew the complete energy landscape. However, the detailed energy landscape cannot be

BOX 1 Timescales in protein dynamics

The different types of movements occur on different time- and spatial scales (1). The folding funnel is often used for illustrating the potential surface of the slow (minutes-hours) folding reactions, which involve large conformational changes. The bottom of this funnel contains the enzyme reaction space, i.e. all native enzyme conformations that transform into each other on the millisecond-second timescale. This might be the most frequently used scale in enzyme kinetics, as Arrhenius plots often reflect to this model: two enzymatic states and a simple energy barrier, a transitional state, in between. This energy barrier, however can be further structured, which has been referred to as 'roughness' of the energy landscape (2).

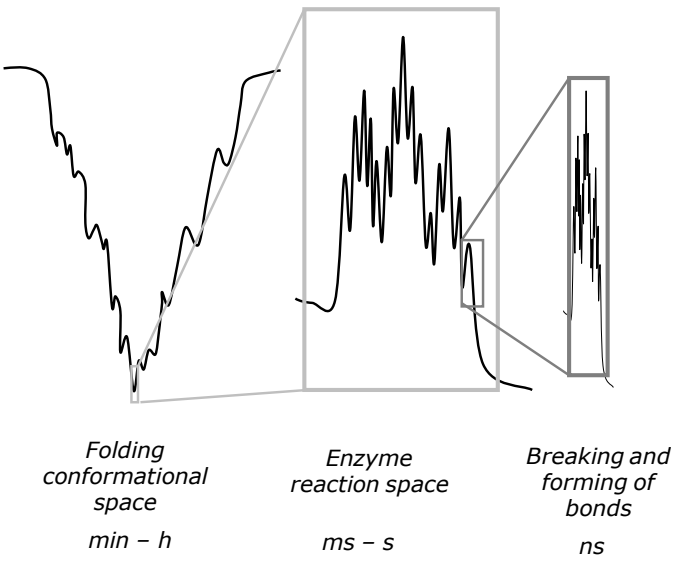

Figure 1 Hierarchical structure of the energy landscape

determined experimentally because of its vast complexity. Therefore, in order to characterize the general features of enzyme reactions, empirical parameters are usually introduced. The long-known parameters as activation energy, preexponential factor, activation entropy describe the observed temperature dependence of enzyme reactions. Internal viscosity is a more recently introduced parameter, which characterizes the

viscosity dependence of reactions. Ideally, the empirically introduced parameters should become physically meaningful and reflect important characteristics of the energy landscape. This way the infinitely complex energy landscape can be simplified.

1.2. Short history of enzyme dynamics

The first experimental approach towards obtaining a simple energy landscape, an energy barrier for chemical reactions was the Arrhenius plot, i.e. the determination of the temperature dependence of the rate constant (4). The transition state theory (TST) provided theoretical background for the Arrhenius equation at the molecular level. TST is a good approximation for gas phase reactions of small molecules. For reactions in condensed phase, the theory was extended by Kramers (see BOX 2), who introduced parameters that describe the effects of the constant energy exchange between the reactants and their surroundings (5, 6). Since enzyme reactions are accomplished in condensed phase, the approximation of the energy landscape by Kramers theory came into the focus of interest. Assuming that enzyme reactions are highly damped by friction, the Kramers formula predicts that the rate constant (k) is inversely proportional to the friction coeffiecent, γ (see BOX 2). Based on the Stokes law this friction coefficient is proportional to the viscosity of the solvent (η), which results in:

$$k(T,\eta) = \frac{A}{\eta}\exp\left(\frac{-\Delta E_a}{k_B T}\right) \qquad \text{Eq 1}$$

where k_B is the Boltzmann constant, T is the absolute temperature, ΔE_a is the activation free energy, and A is a temperature and viscosity independent constant. Nevertheless, several early experiments indicated that Kramers theory was not sufficient to describe the viscosity dependence of certain enzyme reactions. In these cases the relaxation time of the reaction (the reciprocal for the rate constant) was found not to be linearly proportional to viscosity; instead, weaker viscosity dependences were observed (7, 8).

BOX 2 Basics of Kramers theory

Kramers theory is excellently summarized, explained and put into context in the review of Peter Hänggi et al entitled 'Fifty years after Kramers'. A figure and a relevant part of this review is copied below:

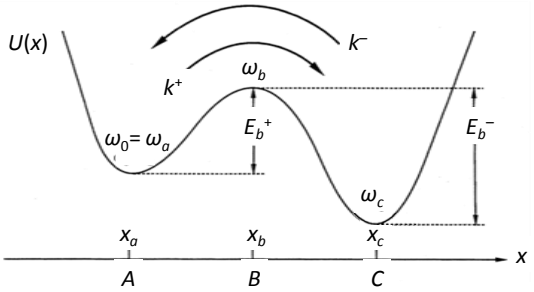

Figure 2 Energy landscape in Kramer's model

Potential U(x) with two metastable states A and C. Escape occurs via the forward rate k^+ and the backward rate k^-, respectively, and $E_b^{\pm}$ are the corresponding activation energies. When calculating the rates $E_b^{\pm} \equiv E_b >> k_BT$ is always assumed (Fig. 3 of (6), modified).
For strong friction the rate in the overdamped regime, i.e., for $\gamma >> \omega_0$ is given by

$$k_{A\to C}^{\text{overdamped}} = \frac{\omega_0 \omega_b}{2\pi\gamma} \exp\left(-\beta E_b\right)$$

which approaches zero as $\gamma \to \infty$. E_b is the activation energy ($E_b^{\pm} \equiv E_b >> k_BT$), β is inversion temperature $(k_BT)^{-1}$, ω_0 is the angular frequency of the metastable state, ω_b is the positive-valued angular frequency of the unstable state at the barrier, γ is the damping relaxation rate.

1.3. The concept of internal friction

In order to explain the observed deviation from Kramers theory the concept of internal friction was introduced. Friction characterizes the energy and momentum exchange caused by the movement and collision of all atoms involved in the reaction during a conformational change (9). Therefore, the friction encountered by the protein during an enzyme reaction comes from two sources: friction due to the movement of solvent molecules (external friction) and friction due to the reorganization of the protein interior (internal friction) (8). The sum of these two types of friction was inserted into the Kramers relationship:

$$k(T,\eta) = \frac{A}{\sigma + \eta} \exp\left(\frac{-\Delta E_a}{k_B T}\right) \qquad \text{Eq 2}$$

As friction originating from the solvent is directly proportional to its viscosity (η), in the equation, the friction inside the protein is also characterized by a parameter (σ) with units of viscosity to match dimensions. This newly introduced σ parameter is later referred to as internal viscosity.

1.4. Alternative models for the viscosity dependence of enzyme reactions

The earliest observations of the viscosity dependence of the relaxation time that showed deviation from proportionality were fitted by a power function (7)

$$k(T,\eta)=\frac{A}{\eta^{p}}\exp\left(\frac{-\Delta E_{a}}{k_{B}T}\right) \qquad \text{Eq 3}$$

,where p is the exponent of the power function ($0<p<1$).

Without much justification another, admittedly empirical mathematical formulation of internal viscosity appeared in the literature: the $1/(\sigma+\eta)$ term of Eq 2 was changed to $(\eta_0+\sigma)/(\eta+\sigma)$, where η_0=1 cP (10). This modification predicts a rather unlikely behavior, rendering this formula less appealing: supposing that $\eta>\eta_0$, the rate constant increases with increasing internal viscosity.

The viscosity dependence of the rate constant of an enzymatic reaction has been phenomenologically described by two groups of models which are not mathematically equivalent: the first group assumes a linear relationship between the solvent viscosity and the reciprocal of the rate constant (by introducing internal viscosity as in Eq 2), whereas the other group hypothesizes a power law dependence of the rate constant on the viscosity (Eq 3). There is no agreement in the scientific community as to which relationship (i.e., Eq 2 or Eq 3) is valid, or a single relationship should hold for every reaction at all. It is very challenging to distinguish the two formulae (i.e., Eq 2 or Eq 3) in viscosity-dependence experiments, as in narrow viscosity range they fit the data equally well. Although several studies using wide ranges of viscosities have indicated that the reciprocal of the rate constant has a sub-linear dependence on the viscosity (such as in Eq 3), it is questionable whether this behavior is directly related to the viscosity or it originates from some other effects of the high concentration of the viscogenic material (and low concentration of water, which, e.g., decreases the permittivity of the buffer). Even though Eq 2 seems to fail when fitted to wide viscosity ranges, an appealing feature of Eq 2 is that the reaction cannot be infinitely fast at zero viscosity (i.e. it has a non-zero limit to the reaction time, Figure 3). Moreover, there are more and more ideas that link the empirically introduced internal friction to the energy landscape and explore its physical background (11-14).

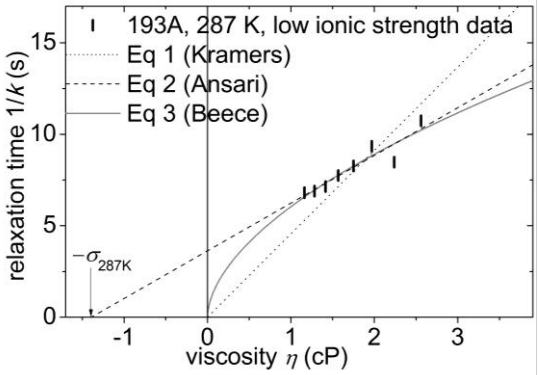

Figure 3 Viscosity dependence of the relaxation time

The viscosity dependence of trypsin activation at 287 K for the 193A HuTry4 in solutions containing 0-0.8 M maltose. Three different models are fitted to the data: i) the Kramers formula for overdamped reactions (6) (Eq 1, dotted line going through the origin); ii) the internal viscosity model introduced by Ansari (8) (Eq 2, dashed line), internal viscosity is derived from the intercept with the viscosity-axis; iii) the power-law dependence suggested by Beece (7) (Eq 3, solid line)

1.5. Viscosity dependence of enzyme reactions in the literature

Several types of enzymes have been investigated concerning internal viscosity. Besides the experiments directly aimed at determining internal viscosity of enzyme reactions, viscosity dependence measurements are often a tool for determining whether a reaction is diffusion-limited or whether a reaction is accompanied by a conformational change, so valuable viscosity-dependence data are available also from measurements that do not directly aim to investigate internal viscosity.

A significant amount of data has been gathered about ligand binding to heme proteins. Besides their historical importance (deviation from Kramers behavior was first observed in myoglobin (7), and the "classical concept" of internal friction was first introduced also in the analysis of myoglobin (8)) the heme proteins provide an excellent experimental system: flash-photolysis breaks the ligand-protein bond and the rebinding can be comfortably followed by spectrophotometric methods (7, 8, 15-26). Other techniques in the investigation of the internal viscosity of heme proteins include the spin labeling of residues (27), transient hole burning spectroscopy (28) and vibrational echo spectroscopy (29).

The viscosity-dependence of electron transfer (ET) reactions between two proteins in a complex has been extensively studied by the Kostic group; in order to see whether the ET is coupled to a conformational change, they quickly discovered the deviation from Kramers behavior (30), later they found that internal viscosity is temperature-dependent (10) and its value can change due to a dynamical phase transition at certain temperature (31). Various ET reactions have been studied by other groups as well: ET between a peptide and cyt c (32), within a hemoglobin tetramer (33), between the two

subunits of Mo-dependent nitrogenase (34), internal ET in cytochrome P450 reductase (35, 36), although (34) and (36) only analyze the effects of cosolvent concentration and not viscosity. Besides interprotein ET experiments, the viscosity dependence of intraprotein ET was studied in nitric oxide synthase (37), and in sulphite oxidase (38).

The internal friction in H-tunneling reactions has also become an area of interest recently: hydride tunneling in morphinone reductase (39), proton and hydride tunneling in protochlorophyllide oxidoreductase (40) were investigated and studies on dihydrofolate reductase (41-43) and the proton transfer in EGFP (44) were published in the past few years.

Other types of enzyme reactions investigated include photoswitching kinetics of Dronpa (45) and the radical pair reaction of coenzyme B12-dependent ethanolamine ammonia lyase (46). There is also an interesting, very extensive early study of the viscosity dependence of a voltage gated Na+ channel (47) with several cosolvents (ethylene glycol, erythritol, sorbitol and PEG 600). Very few data are published on motor enzymes: Chase et al investigated the viscosity dependence of single, skinned fiber mechanics (48) and the viscosity dependence of myosin heads in motility and ATPase assays (49). There are several other enzyme reactions where only steady-state kinetic parameters are available (50-60).

Often the quenching of intrinsic fluorescence is used as a reporter on the internal dynamics of proteins. Viscosity dependence of quenching of Trp fluorescence by acrylamide (61, 62) or the quenching of porphyrin fluorescence in horseradish peroxidase by the benzhydroxamic acid ligand (63), the lifetime of GFP fluorescence (64) or Trp phosphorescence (65) were studied. Other means to characterize the viscosity dependence of enzyme dynamics include ultrasonic absorption of BSA (66) or measuring the rate of isotope exchange (67). Interestingly, a Hungarian scientist is the first author of this latter paper from 1988 that demonstrates “the validity of Kramers model for […] a reaction that takes place in a highly viscous protein matrix” and mentions the concept of internal friction as “friction effects in reaction space”. According to the authors, Somogyi et al, the novelty of their paper is that they characterize the dynamics of lysosime more directly, compared to the previous works in the field where ligand binding reactions with low activation barriers were investigated.

Folding in general is considered to be a multi-step, more complex conformational change than what happens in enzyme reactions, but the results of folding experiments can still be valuable and theoretical considerations may be applicable to enzyme reactions, especially when folding from a compact state is investigated (68). Hagen reviewed solvent viscosity and friction in protein folding dynamics recently (69), presenting the results of Protein L (70), CspB (71), cyt c (68), TripCage (72), gly-ser repeat peptide (73), alpha-helical peptide (74) folding data. He also mentions villin subdomain (75) and Trp zipper (76) folding as recent examples of multi-step folding where viscosity affects the individual steps to a varying extent. Since the publication of this informative review the viscosity dependence of the folding of the Pit1 homeodomain (77) and the small binding domain BBL (78) were also investigated and the folding of spectrin domains have been studied extensively (11-13). Interestingly, through the viscosity dependence the internal friction of the unfolded state itself was also characterized for a series of proteins (14).

From the above listed published viscosity dependence data internal viscosity values were derived, which are summarized in Table 1.

internal viscosity values published	
internal viscosity (cP)	**type of reaction**
4.1	Myoglobin CO photolysis, CO rebinding (8)
7.46	equilibrium conformational fluctuation of Zn-myoglobin (28)
2.2	Myoglobin CO photolysis, protein conformational averaging (24)
2.0	Myoglobin CO photolysis, relaxation (19)
1.5-5	horseradish peroxidase, phosphorescence quenching within the protein (63)
0.27, 0.81, 0.67	trypsinogen activation, Gly, Ala, Arg mutants, respectively (79)
3, 15	electron transfer electrostatic and covalent complex, respectively (80)
0.14,3.8, 5.6	folding of spectrin domains R15, R16 and R17, respectively (13), similar data in (11, 12, 81, 82)
internal viscosity values calculated by us based on published viscosity-dependence data	
internal viscosity (cP)	**type of reaction**
0.18	proton tunneling in light-activated protochlorophyllide oxidoreductase (40)
3 – 30 *	electron transfer between Zn cytochrome c and Cu plastocyanin at different temperatures (10)
0.8 – 3.5 *	electron transfer between Zn cytochrome c_6 and cytochrome f (31)
1 and 1.5	electron transfer between cytochrome c and two negatively charged metallopeptides (32)
0.78	intramolecular electron transfer in sulphite oxidase (38)
-0.5	nitric oxide synthase intraprotein electron transfer (37)
-0.2 – -0.6	H^+ tunneling in light-activated protochlorophyllide oxidoreductase (40) (imprecise viscosity data)
2 – 5	electron transfer between Zn cytochrome c and plastocyanin at different temperatures (83)
3.8, 2.6	electron transfer between plastocyanin and Zn or Sn cytochrome c, respectively (30)

3.7	electron transfer between ZnCyt C and plastocyanin (84)
1, 3 *	electron transfer between cyt P450 reductase and (NADPH)-linked diflavin oxidoreductase (35)
0.14	H^+ transfer in EGFP (44)
1.5, ~3 – 4	ethanolamine ammonia lyase (46), depending on the cofactor
580 – 4300	NO spin label bound to hemoglobin at different temperatures (27)
2 – 3.2	isotope exchange in lysosime at different temperatures (67)
50, 3.3	acrylamide quenching of Trp fluorescence of parvalbumin and RNAse T1, respectively (61)
~30 *	protoheme CO release rate at 257 K (7)
8 *	O_2 escape from hemerythrin (16)
0.8-1.9	cyt c folding 290-303K (68)
2.04-0.12	small cold shock protein, depending on denaturant concentration (14)
0.77, 0.17	prothymosin α depending on ionic strength (14)
reactions where no viscosity dependence was observed	
	GFP fluorescence decay (64)
	H-tunneling in dihydrofolate reductase (41, 42)
	catalysis by dihydrofolate reductase (43)
	H-tunneling, morphinone reductase (39)
	hydride tunneling in light-activated protochlorophyllide oxidoreductase (40)
~350	O_2 internal recombination in hemerythrin (16)

* outstanding datapoints were excluded from our calculation, e.g. where the cosolvent concentration was very high or data were not readable.

Table 1 Internal viscosity values from published viscosity dependence data (Table S1 from (85), extended)

1.6. Structural background of the viscosity dependence of reactions

Understanding the structural background of the viscosity dependence of reactions is an important step in understanding the structural background of internal friction. In the literature there is agreement that the viscosity dependent reactions must be coupled to some conformational changes. Often the viscosity dependence is a proof for a conformational change upon the reaction (10, 32, 86). There have been many attempts to reveal the mechanism of how the solvent effects are mediated through the protein interior to the active site or to find structural explanations to the observed differences in internal viscosities. Five types of observations have been described so far in the literature: these five main ideas about the structural background of viscosity dependence are illustrated by a simplified model conformational change of two protein domains moving relative to each other on Figure 4.

i) Viscosity dependence is influenced by the amplitude of the conformational change (29), experiments in sugar glasses also support this finding: even though the viscosity is higher than 10^{15}cP, small-amplitude dynamics remain unchanged while large-amplitude dynamics are dampened (20, 21, 87) (Figure 4 A).

ii) Flexibility is also often showed to influence viscosity dependence. The Kostic group compared the rate of electron transfer within a rigid (covalently bound) and a more flexible (electrostatically bound) complex of cytochrome c and plastocyanin. The ET of the rigid complex was found insensitive to viscosity, while the more flexible complex showed viscosity dependence. They proposed that the more rigid a structure, the less sensitive it is to viscosity (30, 80). A similar conclusion was drawn from the dronpa photoswitching reaction (45), where the reaction of the more flexible mutant was more sensitive to the external viscosity (Figure 4 B).

iii) A hinge-like role was attributed to specific Gly residues in chymotrypsin and trypsin as these Gly hinges border specific loops which change conformation during the activation of these proteases. Based on molecular dynamics simulations, the dihedral angles of these Gly hinges rotate to a great extent during the activation of these enzymes (88-90), which supports the idea that they work as hinges. With mutagenesis studies it was observed that bulkier residues at the hinge position increase the internal viscosity during trypsin activation (79) (Figure 4 C).

iv) When labeling hemoglobin residues with NO spin labels, Steinhoff found (27) that the more buried a region in a protein, the less sensitive it is to the solvent viscosity. (Figure 4 D). This observation is also supported by molecular dynamics simulations, where the atomic fluctuations of the interior of myoglobin were found to be less sensitive to the viscosity of the solvent than fluctuations close to the surface of the protein (91).

v) Recently, the investigation of the structural background of internal friction of unfolded proteins has been published (14). With single molecule Förster resonance energy transfer and nanosecond fluorescence correlation spectroscopy Soranno et al were able to characterize the dynamics of the unfolded state of three proteins, namely small cold shock protein, intergrase and the C terminal segment of prothymosin α, by a reconfiguration time. The effect of internal friction on the dynamics was determined by the estimated reconfiguration time at zero solvent viscosity. They found that proteins have greater internal friction and consequently are less sensitive to viscosity in a more compact conformation, at the presence of low denaturant concentrations. They also deduced from chain length and amino acid composition analyses that nonspecific side chain and backbone interactions are the most probable causes of internal friction. Even

though the experiments were done on unfolded proteins, for illustration the findings are applied for a conformational change of a folded protein (Figure 4 E).

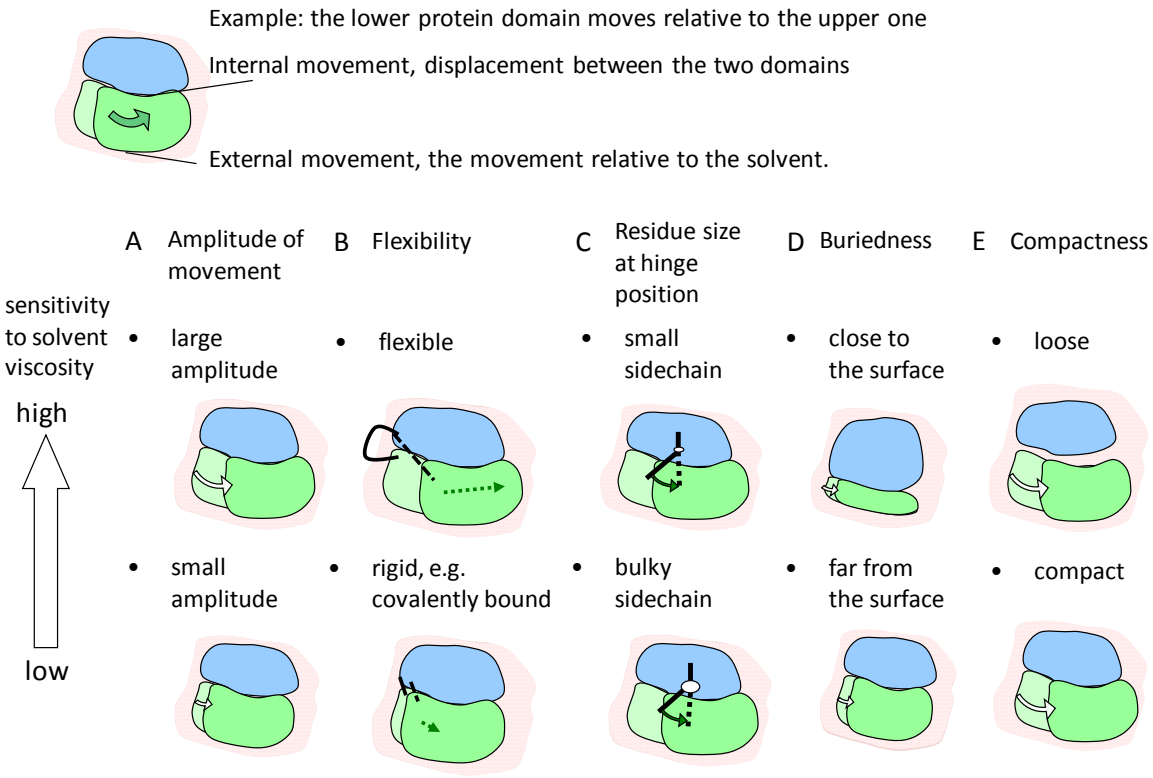

Figure 4 Structural background of viscosity dependence

Five main structural features have been found to affect the viscosity dependence of a conformational change; these are illustrated on a conformational change where two protein domains slide along each other (Fig 2 from (85), modified). A) The conformational changes with greater amplitude are more sensitive to viscosity (29) (20, 21, 87). B) The more flexible enzymes were found to be more sensitive to viscosity. (30, 80) (45) C) The bulkiness of a sidechain at a hinge region was found to play key role in viscosity dependence (79). D) The conformational change close to the surface of a protein is more sensitive to viscosity than at a buried region (27) (91). E) Proteins in a more compact state are less sensitive to viscosity (14).

1.7. Experimental approaches for measuring internal viscosity of enzyme reactions

Internal viscosity was introduced empirically and it characterizes the viscosity dependence of a reaction (See section 1.3 above). It is determined in an indirect way, by measuring the viscosity dependence of the reactions (Figure 3). For this measurement the viscosity of the reaction buffers is varied by the addition of viscogen cosolvents, e.g. glycerol, glucose, sucrose, maltose, PEGs of different molecular weights, ethanol, methanol. As the addition of cosolvent changes not only the viscosity but other features of the solution are also affected, the method has some drawbacks that have to be

considered in the planning and evaluation of the experiments. Dielectric properties, water activity, ionic strength, osmotic pressure are just some of the most important properties that may be affected by the extra cosolvent in the reaction buffer. These unwanted changes should be kept to a minimum or it should be tested if the changes are negligible in the specific experimental setup. A widely used method for testing if there are cosolvent specific effects interfering with the reaction is to compare different cosolvents in the same setup (15, 16, 29, 30, 40, 60, 66, 67). Cosolvents may perturb equilibria especially in folding/unfolding reactions (69) or affect the height of the activation energy barrier (86), but in most reactions of folded enzymes cosolvents are proved or supposed to be (22) inert in this sense. In a relatively small concentration range of cosolvents the unwanted effects might be negligible. However, it is especially a serious challenge to distinguish whether the viscosity dependence of the relaxation time of the reaction is linear or follows a power law, since it requires a large viscosity range (see Figure 3) and when a large viscosity range is investigated, the perturbation caused by the high concentration of the viscogen is difficult to estimate. Moreover, in aqueous solvents viscosity can hardly be reduced by additives, therefore the extrapolation of the rate constant to zero viscosity (see Figure 3) cannot be precisely predicted.

Computational methods have the advantage that solvent properties can be independently varied; changing solvent viscosity without affecting the chemical composition of solution is also possible. In molecular dynamics simulations the change in solvent viscosity is achieved by several methods, e.g. changing the solvent temperature independently of the protein temperature (91), increasing the mass parameter of the solvent molecules (92), or simply using implicit solvent with a damping constant (72, 93, 94). These *in silico* experiments can be useful in complementing *in vitro* studies and theoretical considerations.

1.8. Introduction to trypsin conformational change

Trypsin in the body is expressed as trypsinogen, its inactive, zymogen form. Trypsinogen activation is an enzymatic process when the N-terminal peptide of inactive enzyme is proteolytically cleaved by another protease. Upon this proteolytic cleavage a conformational change occurs, which transforms trypsin from an inactive zymogen conformation to its active form (Figure 5 A). The zymogen and the active forms are

stable conformations of trypsinogen and trypsin, respectively, and their atomic crystal structures are available (1TGN, 2PTN)(95, 96).

In vitro, the conformation of trypsin can be modulated by pH: at pH 11 trypsin is in zymogen conformation, at pH 8 it is in active conformation, which provides an excellent experimental system for studying the conformational change during activation. A single-step activation reaction can be initiated by a rapid jump in pH and the reaction can be followed by the change of the intrinsic tryptophan fluorescence in a stopped-flow apparatus (79, 97). Toth et al (79) were the first who characterized trypsin activation using this transient kinetic method originally developed for studies on chymotrypsin activation (98-100).

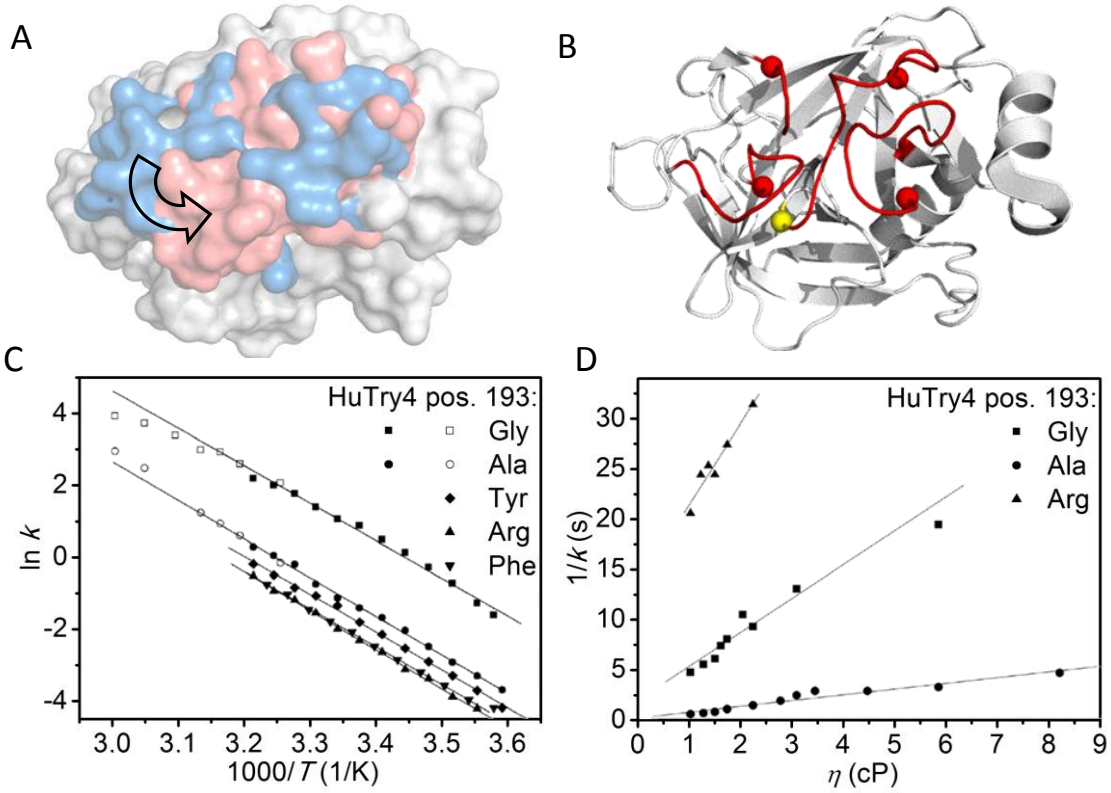

Figure 5 Trypsin activation: HuTry4

A) The overlaid atomic structures of bovine trypsin in active (2PTN) and zymogen (1TGN) conformation. During activation the activation domain moves from the zymogen (blue) to active (red) conformation. B) The active structure of bovine trypsin (2PTN). The four loops of the activation domain are shown in red (residues 16-19, 142-152, 184-194, 216-223). The Gly residues bordering these loops are shown as spheres, position 193 is in yellow. These Gly residues have been suggested to work as hinges during loop rearrangement (96). C) Arrhenius plots of HuTry4 activation for the different mutants at position 193. D) Viscosity dependence of the activation of HuTry4. Illustrations for A and B are done with PyMol (101), data for C and D are taken from (79).

It was found that trypsinogen activation is a domain rearrangement which occurs by the rotation of a separate domain - called activation domain - around five glycine hinges (residues 19, 142, 184, 193, 216, Figure 5 B) (91, 92). The role of the Gly hinges in the activation process and the proteolytic activity of trypsin were deeply investigated recently (102). Except for Gly193, the Ala mutations of these glycines dramatically reduce the proteolytic activity of trypsin. Although Gly193 is located next to the active site, its Ala mutation causes very little change in all enzymatic steps of the proteolysis (102). The conformation of trypsin is affected only slightly and locally upon the Gly-Ala exchange of this sidechain, which was also confirmed by molecular modeling (103).

Recently it was shown that activation slowed by replacing this Gly with Ala or bulkier sidechains (79) at position 193. While the slope of the Arrhenius plots remained parallel (Figure 5 C), the viscosity dependence of the reactions changed drastically (Figure 5 D), which implied that the mutations at this hinge position (Gly193) cause highly specific changes in the apparent internal viscosity parameter (σ) of activation without affecting the structural and activity properties of the protein.

Trypsin activation is thus an ideal model process for the investigation of the internal friction during enzymatic conformational changes, because it is a well defined single-step reaction between two conformers manifested by the rotation of a distinct domain around a few glycine hinges, and mutations at the hinge position 193 specifically affect internal viscosity. 193A and 193G mutants of human trypsin 4 (HuTry4) were chosen as model enzymes for this study.

2. Aims

The nature of internal friction is interesting from many aspects. We aimed to characterize the physical and structural background of the internal viscosity phenomenon. The following scientific questions were in the focus:

2.1. The physical background of internal friction was approached by investigating the temperature dependence of internal viscosity. Specifically, the temperature and viscosity dependence of the rate constant of HuTry4 activation were determined.

2.2. The relations of internal friction to the protein structural characteristics were approached by investigating a Gly-Ala exchange at an important hinge position. Specifically we determined how the exchange of Gly to Ala at position 193 in HuTry4 affects the internal viscosity during trypsinogen activation.

2.3. Finally, we aimed to construct a comprehensive model that explains our observations and relates internal viscosity to the well established parameters describing the energy landscape.

3. Methods

3.1 Transient kinetic measurements

The temperature and viscosity dependence of the conformational change during trypsin activation was characterized by transient kinetic methods: upon rapid mixing with a stopped-flow apparatus (Figure 6 A) a pH jump triggered the activation of the enzyme. This activation resulted in a measurable Trp fluorescence intensity change that was recorded for different viscosity and temperature conditions. A 20% fluorescence intensity increase was detected upon the reaction of both 193A and 193G HuTry4, this intensity change was fitted with exponential decays (Figure 6 B). There are altogether 5 Trp residues in HuTry4. One (or more) of them produce the detectable fluorescence change upon the pH induced activation (Figure 6 C).

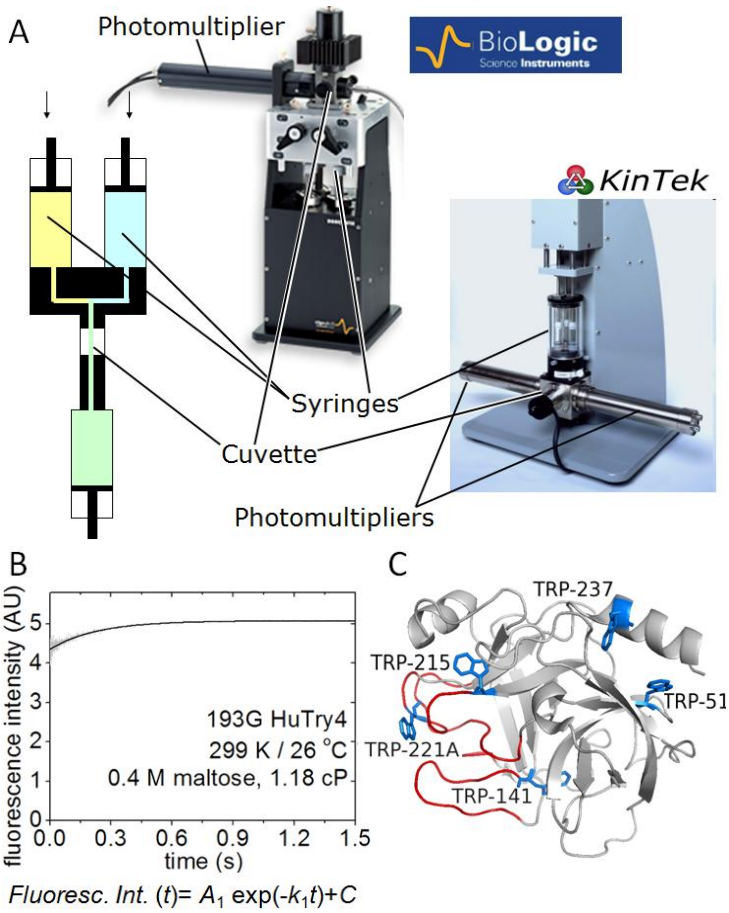

Figure 6 The conformational change upon trypsin activation produces a fluorescent signal increase.

A) The schematic representation of the rapid mixing with photographs of two different stopped-flow devices. Source of the photos: (104, 105) B) An example of the measured fluorescent signal transient reporting the conformational change from zymogen to active trypsin, the form of the fitted exponential decay is presented below the graph. C) Position of Trp residues in HuTry4. The activation domain is shown in red, the Trp residues are colored blue. Trp 221A, 215 and 141 are more likely to be involved in the signal as they are closer to the activation domain. The illustration was done with Pymol (101) based on the PDB structure 1H4W (106).

3.1.1. Technical details of the measurement setup

The stopped-flow apparatus (Figure 6 A) is a rapid (<ms) mixing device with a small (~5 ul) cuvette which allows the detection of fast reactions that are coupled to an optical signal. The optical signal, intrinsic Trp fluorescence (Figure 6 C, Figure 7 A, B)

reported about HuTry4 conformational change upon trypsin activation. For measuring this fluorescence change the Trp residues were excited by 297±2 nm wavelength light using a superquiet Hg-Xe lamp (150W, Hamatsu Photonics UK Ltd., Welwyn Garden City, UK), with a monochromator (Model 77250, Thermo Oriel Instruments, Stanford, USA) (Figure 7 C) and the emitted light was detected through a 340 interference filter (Comar Instruments, Cambridge, UK) (Figure 7 D) by the photomultiplier (PMT) set to 700V.

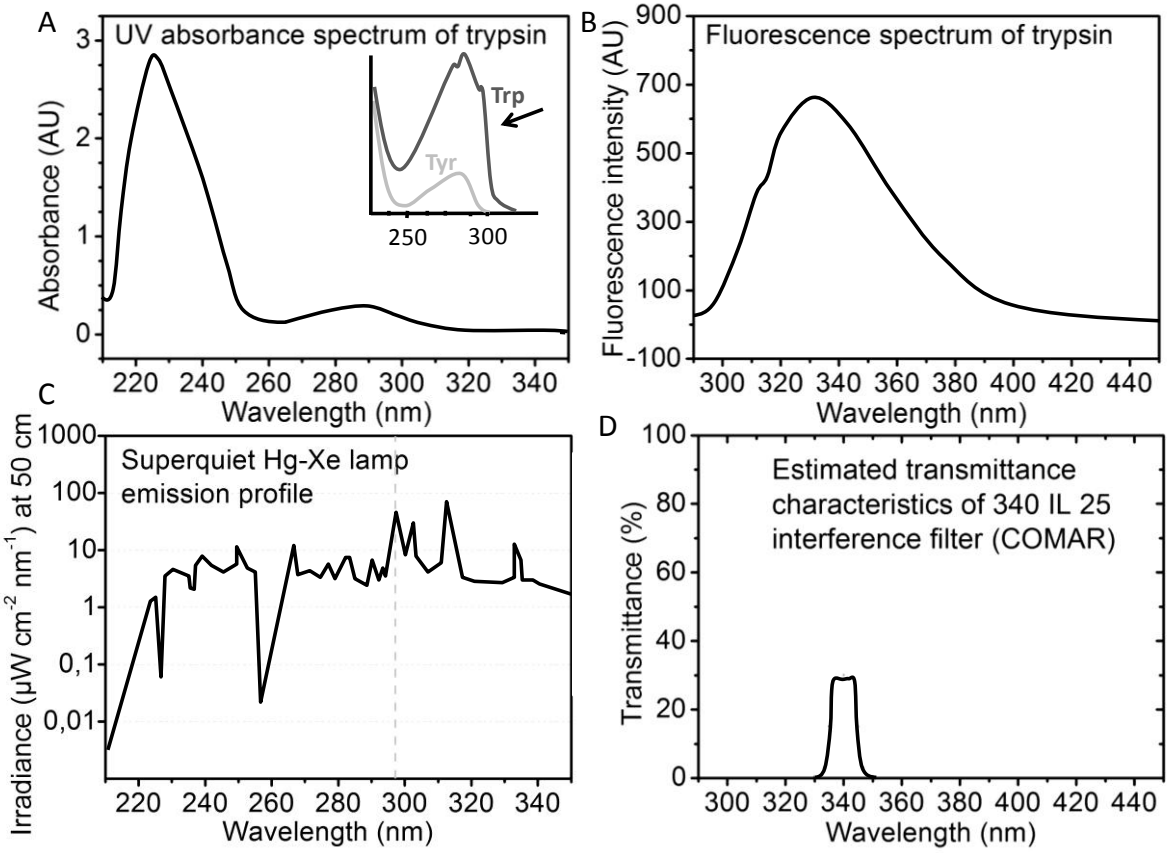

Figure 7 Optical signal detection

A) The UV absorption spectrum of trypsin (107). Inset: Trp can be selectively excited above 290 nm (108). B) The Trp residues dominate the fluorescence emission spectrum of trypsin (109). C) Super Quiet Mercury-Xenon Lamp profile from the Hamamatsu Catalogue (110). The 297 nm peak is shown by the solid grey line. D) Estimated transmission spectrum for 340 interference filter based on the technical data (111).

3.1.2. Preparing solutions for the measurements

Two solutions, solution A and solution C were prepared and loaded into the stopped flow apparatus, where their mixing in a 1:1 ratio resulted in a pH jump, which activated the enzyme, HuTry4. The contents of the solutions are listed in Table 2.

3.1.2.1. General preparation

As air bubbles, precipitates or impurities in the solvents may seriously affect the optical signal, solutions were always degasified after filtration by Millex® syringe-driven filter unit (Millipore, pore size: 0.22um). Degasification was done above measurement temperature with a water aspirator during continuous stirring or sonication. Solutions containing viscogen were always freshly prepared. Enzymes were kept in frozen aliquots, freezing-thawing cycles were kept to a minimum. The enzyme concentration after mixing was 1 μM, which gives a satisfactory signal-to-noise ratio. Above 30°C/303K fluorescence intensity drops, which was compensated with higher enzyme concentrations (2-3 uM). The following mixing parameters were applied with the stopped-flow apparatus (SF-2004, KinTek Corp. Austin, TX): mixing speed: 12 ml/s, mixing volume: 80 ul, estimated deadtime:1 ms, repetition: 5-7 repeats.

HIGH SALT VERSION I=182 mM		
	solution A	solution C
mixing ratio	1	1
buffer	50 mM HEPES pH 7.5	10 mM CABS pH 11
enzyme	-	2 uM HuTry4
salts	150 mM NaCl	150 mM NaCl
	5 mM $CaCl_2$	5 mM CaCl2
viscogen	0-1 M maltose	same as solution A

LOW SALT VERSION I=32mM		
	solution A	solution C
mixing ratio	1	1
buffer	HEPES:	2 mM CABS pH 11
	42 mM / 2-11 °C	
	52 mM / 14-23 °C	
	65 mM / 26-38 °C	
enzyme	-	2 uM HuTry4
salts	5 mM $CaCl_2$	5 mM $CaCl_2$
viscogen	0-1 M maltose, 0.1 M increments	same as solution A

solutions for mT-jump experiments I~32mM		
	solution A	solution C
mixing ratio	3	1
buffer	26 mM HEPES pH 7.3	4 mM CABS pH 11.7
salts	5 mM $CaCl_2$	5 mM $CaCl_2$
enzyme	-	4 uM HuTry4
viscogen	-	-

Table 2 Solutions used for the trypsin activation stopped-flow experiments. All reagents were produced by Sigma Aldrich Co (St. Louis, MO 63103).

3.1.2.2. Control of variables: considerations and implementation

pH

A pH jump was designed to induce the activation of trypsin, because at high pH the enzyme acquires the zymogen conformation which is transformed to the active form upon pH reduction.

Trypsin was diluted with a low buffer capacity pH 11 solution. CABS was chosen as buffer, because its pK value is 10.7. Upon mixing in a 1:1 ratio with a neutral, high buffer capacity HEPES solution, the pH of the mixture equilibrated at pH 8. The pH of the solutions was set with an electrode (Combination pH electrode, Radelkis, Budapest), the pH of the mixture was checked with pH test strip (PANPEHA Cat.no. Z134147, Whatman, Aldrich).

BOX 3 Challenges in setting the correct pH

Above 0.3 M maltose concentrations we observed that the buffering capacity of HEPES decreased. We researched the literature for an explanation.

According to an ultrasonic spectrometry study some disaccharides form complexes with alkaline-earth metal ions (112). We hypothesize that Ca^{2+} – maltose interactions might be responsible for making the solution more alkaline than expected. However, the anomaly was only observed in the low-salt buffer, even though HEPES and Ca^{2+} concentrations were identical to those in the high-salt buffer.

Temperature

Measurements were carried out in the 275–311 K temperature range with 3 K increments. The temperature was controlled with ±0.1 K accuracy with the following setup: The syringes and the cuvette were tempered in a waterbath controlled by a thermostate (Polyscience, Model 9000). The exact temperature of the cuvette was constantly monitored by a direcly attached thermometer (Testo 950).

Ionic strength

The pKa values of buffers change with temperature, resulting in change of the ionic strength. Although there are exceptions (7), change ionic strength may affect protein conformational changes (113) or enzymatic activity (114), therefore the ionic strength was controlled by two different methods. The first series of data was generated in solutions with high salt concentration (150mM NaCl), this way the absolute change in ionic strength due to the buffer was relatively low compared to the constantly high ionic strength due to salts. Zoltán Simon conducted the measurements in this high-buffer solution.

The second series of data was measured in low salt concentration, and the dissociation of the buffer with temperature was compensated: the HEPES concentration was slightly modified depending on the measuring temperature to keep the ionic strength change within ±10%: at 275–287 K 65 mM, at 290–299 K 52 mM, at 302–311 K 42 mM was the concentration of HEPES. A web service (115) was used for calculating the ionic strength. HEPES was chosen because its pK value is close to the measurement pH 8, and varies relatively little with temperature compared to other buffers, e.g. it is 2 times less temperature-sensitive than TRIS.

Viscosity

The ideal viscogen would be an intact cosolute that only modifies the viscosity of the solution but leaves the other variables, i.e. water content, dielectric constant unaffected. This ideal viscogen has preferably low molecular weight as experiments indicate that the effect of large cosolutes on molecular-scale movements is weaker than expected from their effect on the measurable bulk viscosity, which phenomenon is often referred to as the difference in macro- and microviscosity (50, 116).

Maltose was chosen as cosolvent, as it is relatively small, and the ratio of viscosity change and dielectric constant change is the greatest among simple saccharides. For comparison, in Table 3 water content, dielectric properties and viscosities are collected for some popular viscogens. Maltose concentration in the solutions varied from 0 to 1 M with 0.1 M increments resulting in viscosities between 0.6 cP and 6 cP.

viscogen	viscogen concentration (M)	water concentration (M)	dielectric constant	viscosity (cP)	temperature (°C)
pure water	0	55.4	80.37	1.0	20
	0	55.4	78.54	0.89	25
D-glucose	2M	42.79	69.7	2.89	25
D-fructose	2M	42.93	71.1	2.69	25
D-maltose	**1M**	**43.77**	**69.6**	**3.12**	**25**
D-sucrose	1M	43.6	71.1	2.80	25
glycerol	40% wt	36.1	68.76	3.65	20
	30% wt	41.28	71.77	2.50	20
D-xylose	1M	50.21	74.1	1.41	25
D-galactose	1M	49.33	77.3	1.57	25

Table 3 Properties of different viscogen solutions (117-119)

3.1.3. Determining the viscosity of solutions.

The viscosity of the solutions was measured by Zoltán Simon with an Ostwald viscometer in which the studied solution flows through a capillary. Flow-through times were collected for solutions of 50 mM HEPES, with or without 150 mM NaCl, containing

0.1 M–1 M maltose in water at 279.5, 283, 288, 293, 298, 303, 308 and 313 K, respectively. Temperature was controlled by a sensitive water circulator (Heto CBN 8-30/HMT 200, Jouan Nordic). Density of the solutions was interpolated from literature data (0 M and 1 M maltose (118)) and measurement data (0 M, 0.3 M, 0.6 M and 1 M maltose solutions at 279, 293 and 311 K). Each measurement was repeated twice. A third experiment was performed in case a difference larger than 5% occurred between the flow-through times. (The shortest and longest averaged flow-through times were 103 and 898 seconds, for pure water at 313 K and 1 M maltose at 279.5 K, respectively.) The absolute viscosity of the solutions was calculated based on the following relationship:

$$\eta_x = \eta_r \frac{\rho_x t_x}{\rho_r t_r} \qquad \text{Eq 4}$$

, where absolute viscosity (η) is proportional to the density (ρ) of the solution and the flow-through time (t). The studied and the reference solution (pure water), are indexed by an x or r, respectively.

The final viscosity data are summarized in Supplementary table 5 (Section A2.). In order to determine the viscosity in the stopped-flow measurements, an empirical interpolation function was constructed and fitted to the viscosity data:

$$\eta(T,[\text{maltose}]) = \left(A[\text{maltose}]^3 + B[\text{maltose}]^2 + C[\text{maltose}] + D\right)\exp\left(\frac{E_\eta}{k_B(T-T_0)}\right) \qquad \text{Eq 5}$$

where the viscosity, η is a VTF like function (120) of temperature, T, and a polynomial function of maltose concentration, [maltose]. The fitted parameters are summarized in Table 4. The measured viscosity values and the fitted surface are plotted on Figure 8 for illustration.

Fitting parameters	type of solution	
	50mM HEPES; 0–1 M maltose	50mM HEPES; 150 mM NaCl; 0–1 M maltose
A (cP M^{-3})	0.133 ± 0.054	0.174 ± 0.057
B (cP M^{-2})	0.0155± 0.065	-0.0722 ± 0.045
C (cP M^{-1})	0.107 ± 0.038	0.105 ± 0.035
D (cP)	0.107 ± 0.027	0.0686 ± 0.020
E_η (kJ mol^{-1})	1.23 ± 0.28	1.70 ± 0.37
T_0 (K)	225 ± 7	215 ± 8

Table 4 Fitting parameters for Eq 5: surface fitted to the viscosity of solutions by gnuplot software(121) (Table 1 from (138))

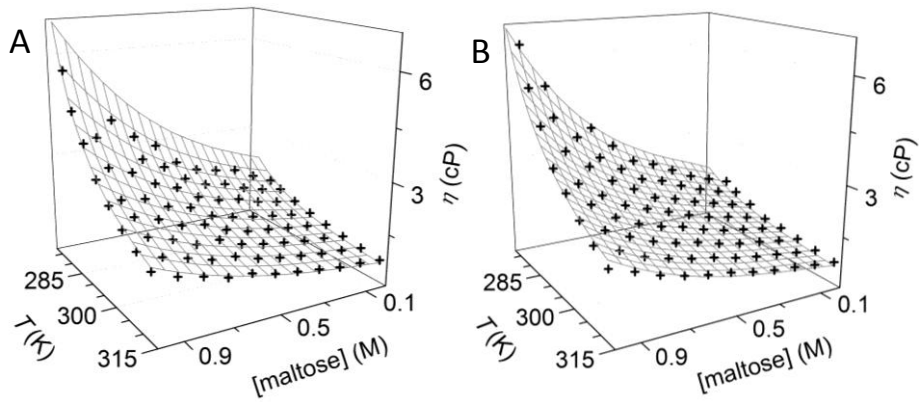

Figure 8 Viscosity of maltose solutions

The viscosity of maltose solutions was measured from 0–1 M with an increment of 0.1 M at eight different temperatures between 279.5 and 311 K. The data were fitted with a surface based on Eq 5. A) The maltose solutions also contain 50 mM HEPES. B) The maltose solutions also contain 50 mM HEPES and 150 mM NaCl. (Fig S1 and S2 from (138))

3.2. Human trypsin 4 constructs, expression of the enzymes

Briefly, the HuTry4 gene was amplified from a human cDNA library, mutations 193A and 193G were introduced by megaprimer mutagenesis. HuTry4 protein constructs were expressed in E. coli cells in inclusion body, which was later renatured in a reducing environment. Following ion-exchange purification, enterokinase activation and affinity purification HuTry4 193A and 193G were stored at -80 ^{o}C. I worked with the readily expressed and purified proteins that had been characterized and investigated in a series of publications (79, 106, 122, 123). A more detailed description of the protocol for their production is presented in the Appendix (Section A.7.).

3.3. Temperature jump experiments

The HuTry4 193G activation experiments were extended to higher temperatures without the viscogen. A temperature-jump technique, originally developed in our lab (124), was used to avoid keeping the enzyme at high temperatures for minutes in the reservoir syringes, as this would cause denaturation. The stopped flow apparatus (Bio-logic SFM 300) was equipped with an mT-jump accessory (Figure 9). In this setup the temperatures of the cuvette, the premix solutions and the reservoir syringes were all controlled independently with the combination of 3 Peltier elements and a water circulator. The mT-jump experiments were done between 303 and 333 K with 5 K

increments (at 30, 35, 40, 45, 50, 55, 60 °C degrees) without any added maltose. Buffer conditions were analogous to the previously described transient kinetic measurements.

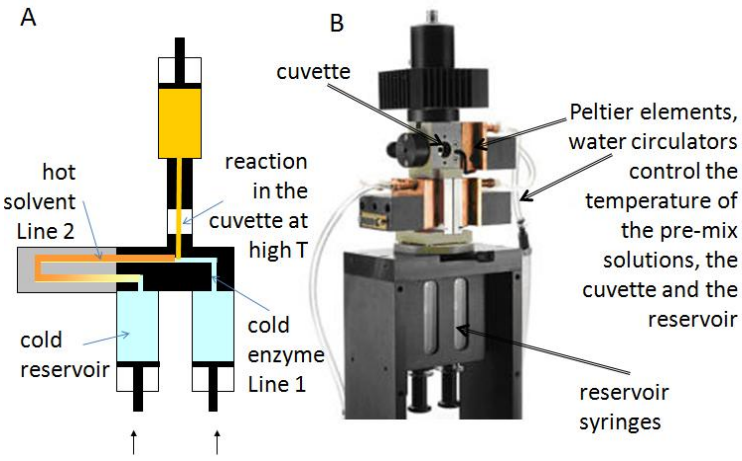

Figure 9 Illustration for the mT-jump apparatus

A) Schematic view of the mixing setup: the cold enzyme is mixed with hot solvent, so the reaction can be monitored for a short time above denaturation temperature. B) The photo of the mT-jump accessory for the Bio-logic SFM300 stopped flow apparatus copied from its website (105).

3.3.1 Temperature control of mT-jump experiments

Reservoir syringes were cooled by a water circulator (HMT 200 and CBN 8-30, Heto) to 11 °C. The cuvette and the pre-mix volumes of both solutions were independently controlled by 3 Peltier elements. The Peltier elements were also cooled by the water circulator. As fluorescence is temperature sensitive, it is important to avoid temperature shifts during the measurement, so the rapid mixing should result in a solution with a temperature exactly equal to the temperature of the cuvette. Therefore the temperature of the pre-mix loops (Line 1 and Line 2) with solution A and C are very critical and had to be optimized prior to the experiments. After mixing in a 3:1 ratio, theoretically, the temperature of the mixture will be the weighted average of the temperatures of the pre-mix solutions. However, this had to be checked and temperature settings had to be slightly adjusted to the conditions present. During calibration the temperature shifts in the cuvette were monitored with 80 uM NATA (N-Acetyl-L-tryptophanamide) in 50mM HEPES buffer (Figure 10). The temperature of the enzyme containing solution C in pre-

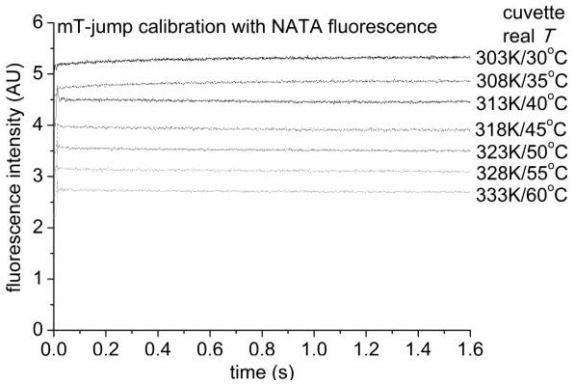

Figure 10 mT-jump calibration with NATA fluorescence

The structure of NATA with the transient fluorescent traces at the different measurement temperatures with the settings in Table 5. The constant fluorescent signal indicates that there is no significant temperature shift in the cuvette after the rapid mixing of solutions.

mix line 1 was kept constant at 25 °C, to avoid denaturation prior to the measurement. The temperature of solution A in the pre-mix line 2 and the cuvette were adjusted with Peltier elements, the settings in Table 5 were found to control the temperature correctly in the mT-jump apparatus. Room temperature was 25-27 °C, the water circulator was set to 11 °C.

Solution C – Line 1	Solution A – Line 2		Cuvette	
FIXED (°C)	Peltier setup (°C)	real (°C)	Peltier setup (°C)	real (°C)
25	35	35	29.7	30
25	40.9	40.9	35.2	35.4
25	48.5	48.5	40.1	40.1
25	54.1	54.1	46.3	44.5
25	60.1	60.2	52.1	50.0
25	68.6	68.7	57.9	55.2
25	74.8	75	63.3	60

Table 5 Temperature settings for mT-jump measurements

3.3.2. Ionic strength for mT-jump experiments

HEPES concentration was adjusted to the higher temperature conditions: with the web service, Buffercalc (115), we calculated that ionic strength of pH 7.5, 38mM HEPES solution at 40-60 °C is close to the ionic strength of the previous measurements (e.g. 25 °C, 52 mM, pH 8). We changed the mixing ratio to 3:1, so the concentrations of solutions had to be adjusted to give the identical composition after mixing. (see Table 2)

3.3.3. Viscosity of the mT-jump experiments

The viscosity values at each temperature (in Table 6) were estimated by extrapolating from the viscosity measurements described in section 3.3.1. Eq 5 and Table 4.

Temperature (K)	viscosity (cP)
303	0.71
308	0.63
313	0.57
318	0.52
323	0.48
328	0.45
333	0.42

Table 6 Estimated viscosity values in the mT-jump experiments

3.4. Viscosity dependence of ATP-N binding in myosin

Dictyostelium myosin II motor domain is stabilized in the closed state by γ-Amido-ATP (ATP-N) binding (125, 126). The fluorescence of the Trp residue W501, located at the end of the relay helix close to the converter region is a relevant reporter of this binding event. The effect of increased viscosity on this binding was investigated at four different temperatures (10, 16, 20, 25 ^{o}C – 283, 289, 293, 298 K). The measurement was done in standard assay buffer and maltose was used as viscogen (4mM $MgCl_2$, 20mM HEPES, 40mM NaCl, pH 7.3,+/- 1 M maltose). The myosin construct contained a single Trp at position 501 (127, 128).

Trp fluorescence was detected (as described above in Section 3.3.1) upon a rapid mixing in the stopped-flow apparatus (Bio-logic SFM 300). Final concentrations in the cuvette after mixing were: 2.25uM W501 myosin II motor domain, 4mM ATP-N (γ-Amido-ATP), 0 or 0.5 M maltose. The technical details of the mixing are the following: 25x25 ul solutions were mixed at a 7 ml/s speed and the recording was done for 4 s with 300 us integrations with a PMT set to 600 V. The estimated deadtime is 250 us.

Viscosities were assumed to be similar to those measured for trypsin experiments in HEPES buffer. In the table below for each measurement the corresponding viscosity values can be found:

temperature (K)	maltose concentration (M)	viscosity (cP)
283	0	1.41
289	0	1.05
293	0	0.94
298	0	0.82
283	0.5	2.38
289	0.5	1.78
293	0.5	1.59
298	0.5	1.39

Table 7 Viscosity values calculated for the assay buffer used in the ATP-N binding experiment with W501 myosin

3.5. Analyzing transient kinetic fluorescence traces

Fluorescence intensity was detected by a photomultiplier and the output of the photomultiplier was recorded. The magnitude of the signal depends on the

measurement settings (e.g. high voltage of the photomultiplier, protein concentration, temperature effects on fluorescence), therefore it was only used as a general control and in case of discrepancies, the equipment was double checked or solutions were replaced. The time course of the signal was analyzed in detail.

All trypsinogen activation measurements were repeated 5–7 times, and exponential functions were fitted to the averaged transient traces by the KinTek software (KinTek Corporation, 7604 Sandia Loop, Suite C, Austin, TX 78735). Example traces can be found on Figure 6. The fluorescence intensity change generally fitted a single exponential, which indicates that trypsinogen activation is a single-step reaction. We also know that it is irreversible under the given experimental conditions. Sometimes a fast (5-10x faster), small-amplitude (less than 15% of the total intensity) second phase was also observed, the mechanism of which remained unsolved[1]. As the small-amplitude phase did not show any viscosity-dependence, it was neglected in the subsequent analysis of the rate constants.

The observed rate constants versus temperature and viscosity data were fitted by the gnuplot software (121), using the least squares method. To optimize the fitting, a transformation of the general form of the viscosity and temperature dependence of the relaxation time

$$k(T,\eta) = \frac{A}{\eta + \sigma_0 \exp\left(\frac{\Delta E_\sigma}{k_B T}\right)} \exp\left(-\frac{\Delta E_a}{k_B T}\right) \qquad \text{Eq 6}$$

[1] Speculations about the nature of the second phase: i) The zymogen structure of HuTry4 has not been crystallized yet, but from other crystallized trypsinogens and trypsin-related research we know that the loops in the activation domain have several different conformations in the zymogen state (Gombos 2008), therefore it is possible that a fast reorganization of the zymogen loops preceeds the activation step. ii) The autolysis of trypsin might occur even at extreme conditions, e.g. above pH 10 in solution C. Autolysis results in an inhomogeneous population, which can modify or result in a second phase. The storage of the enzyme or the incubation time prior to measurement (which varied from minutes to an hour), might have affected this second phase. iii) The after-mix pH was set with a pH strip, which is less accurate than an electrode, this pH inaccuracy could have resulted in deviations. iv) The 193A mutant was more likely to show the second phase than the 193G mutant, (85% 193A, 50% 193G) so the appearance of the second phase might be related to loop flexibility or specific conformations.

to the modified form

$$k(T,\eta) = \frac{A_{300}}{\eta + \sigma_{300}\exp\left(\frac{\Delta E_\sigma}{k_B}\left(\frac{1}{T} - \frac{1}{300\mathrm{K}}\right)\right)} \exp\left(-\frac{\Delta E_{SUM} - \Delta E_\sigma}{k_B}\left(\frac{1}{T} - \frac{1}{300\mathrm{K}}\right)\right) \qquad \text{Eq 7}$$

was necessary.

By using Eq 7 the fitting is optimized for data around 300 K and the correlation of the two energy values (ΔE_σ and ΔE_a) is minimized. The original parameters of Eq 6 can be calculated from the fitting parameters:

$$A = A_{300}\exp\left(\frac{\Delta E_{SUM} - \Delta E_\sigma}{k_B 300\mathrm{K}}\right) \qquad \text{Eq 8}$$

$$\sigma_0 = \sigma_{300}\exp\left(-\frac{\Delta E_\sigma}{k_B 300\mathrm{K}}\right) \qquad \text{Eq 9}$$

$$\Delta E_a = \Delta E_{SUM} - \Delta E_\sigma \qquad \text{Eq 10}$$

4. Results

4.1. General overview of the fluorescent transient kinetic data

Trypsin activation triggered by a pH jump was followed by recording the fluorescence transients. The fluorescent signal change is dominated by a single exponential decay phase, which allows the calculation of the rate constant of the trypsin activation reaction. We found that both temperature and viscosity affected the rate constant of the reaction and the Gly to Ala switch at position 193 in HuTry4 slowed the reaction approximately 10 times (Figure 11). Fluorescence intensity and the amplitude of the signal systematically decreased by increasing temperature, other tendencies concerning the amplitude of the signal have not been discovered.

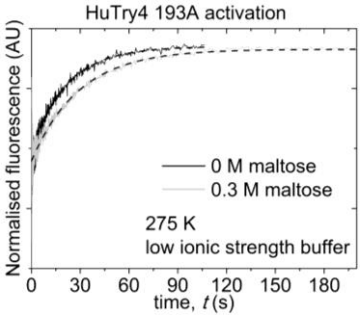

Figure 11 Timecourse of the fluorescent signal: effect of maltose

Typical single fluorescence transients are shown to illustrate the effect of viscosity on trypsin activation. The fluorescence change upon the activation of HuTry4 193A is shown at 275 K in low-salt buffer, without any viscogen (black) and with added maltose (grey). The dashed line is the fitted exponential decay curve.

The rate constants were calculated by fitting the average traces at each condition (13 different temperatures, 6-11 different maltose concentrations, 2 different ionic strengths) and are presented in the Appendix (Section A1). For illustration, the data for 193G HuTry4 in low-salt buffer are plotted on Figure 12 A, the rest of the data, i.e. rate constant vs viscosity and temperature plots of 193A, and 193G high-salt measurements are shown in the Appendix (Section A1), next to their corresponding tables. To reveal the pattern of 3D data (measured rate constant versus the controlled viscosity and temperature), the viscosity dependence and the temperature dependence of the rate constant was investigated separately (Figure 12 B and C, respectively). The relaxation time (i.e. reciprocal of the rate constant) depends linearly on viscosity, the rate constant has classical, Arrhenius-like temperature dependence.

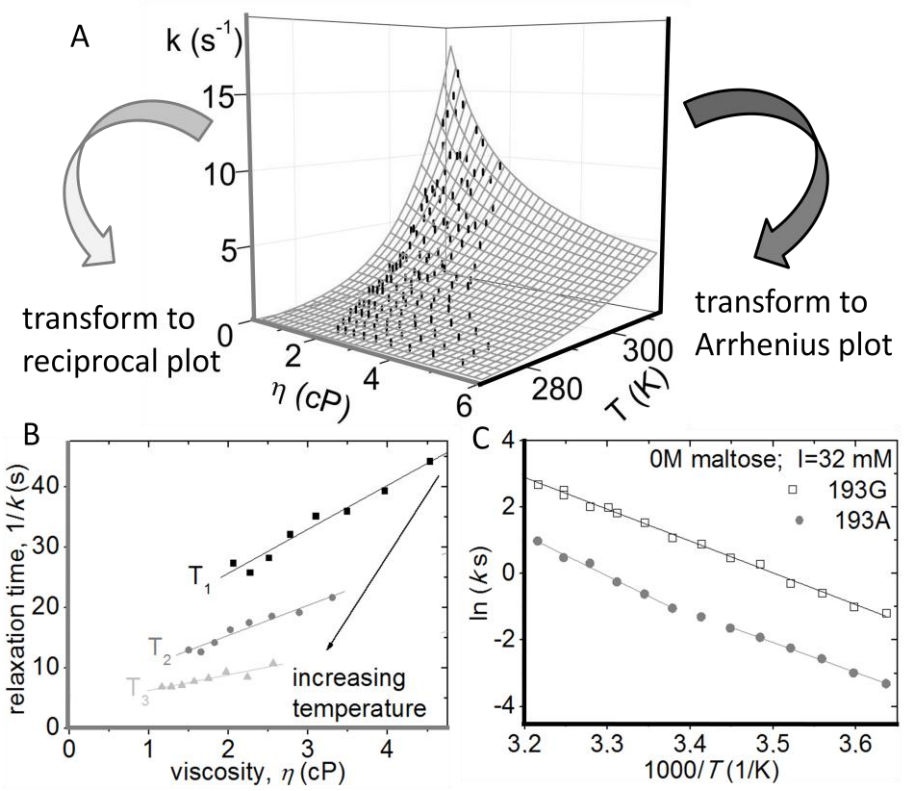

Figure 12 The pattern of the 3D data can be recognised when variables are separated

A) The measured rate constants for 193G HuTry4 are plotted against both viscosity and temperature. The fitted surface is based on Eq 13 (see Section 4.4.)(Fig 2B in (138)) B) Viscosity-dependence of the relaxation time. Representative data from measurements with 193A HuTry4 in low-salt buffer, at 275, 283 and 287K. C) The temperature-dependence of rate constants in buffer without viscogen.

4.2. Arrhenius plots

The temperature dependence data produce classical Arrhenius plots (Figure 12 C), which are parallel in case of the two trypsin mutants. As classical Arrhenius plots are constructed from data with identical buffer conditions, with the change in temperature, the viscosity of the buffer also changes. Therefore the Arrhenius plots are biased by the temperature dependence of viscosity (Figure 13 A). With interpolation, our systematic data allow the calculation of the rate constants at different temperatures at constant viscosity. Practically, in this iso-viscous, interpolated data varying maltose concentration balances the change in viscosity caused by temperature. The iso-viscous Arrhenius plots constructed from the interpolated data have a slightly reduced slope compared to the traditional Arrhenius plots, but the plots are still parallel for the two mutants (Figure 13 B).

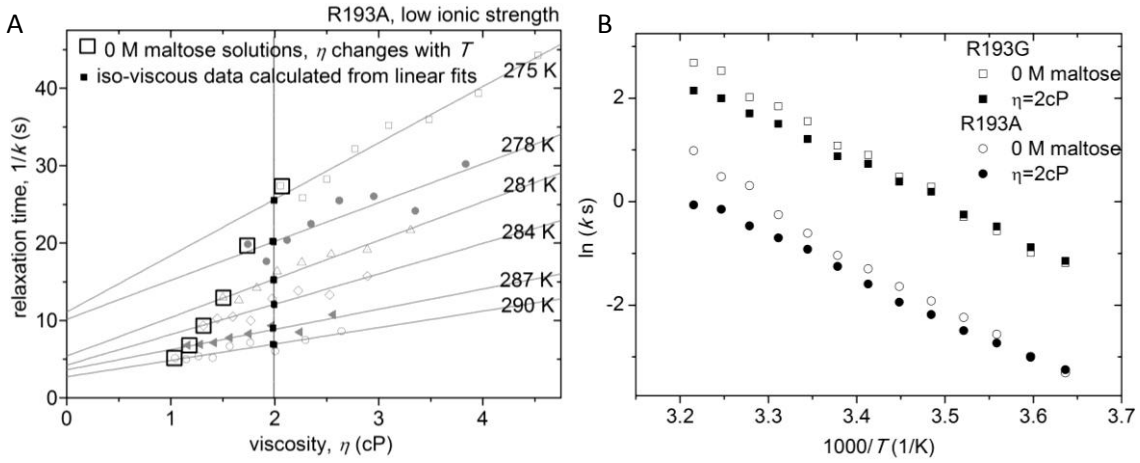

Figure 13 Constructing an Arrhenius plot in iso-viscous solution

A) The viscosity dependence of the rate constant measured at 275-290 K, for 193A mutant in low ionic strength buffer (analogous to Figure 12 B). The framed data points were collected in buffer without added viscogen, where viscosity changed with temperature. From the linear fits to isothermal data, rate constants can be calculated for 2cP viscosity solvents (black squares on the η=2 cP line). B) The temperature dependence of these iso-viscous rate constants (solid symbols) is compared to the traditional Arrhenius plot (open symbols) for 193G (squares) and 193A (circles) HuTry4 mutants in low ionic strength buffer.

4.3. Viscosity dependence of the rate constant and internal viscosity

4.3.1. The temperature dependence of internal viscosity is Arrhenius-like

Representative data illustrate (Figure 12 B, Figure 13 A and Figure 16) that the relaxation time (reciprocal of the rate constant) linearly depends on viscosity. Therefore Eq 11, first suggested by Ansari (8) (Eq 2 in Introduction)

$$k(T,\eta) = \frac{A}{\sigma + \eta} \exp\left(-\frac{\Delta E_a}{k_B T}\right) \qquad \text{Eq 11}$$

was fitted to the viscosity dependence of the isothermal rate constants and an internal viscosity value (σ) was calculated for each temperature from the linear fits. From 193G HuTry4, low ionic strength data (Figure 14) we concluded that an Arrhenius-type exponential function fits the temperature-dependence of internal viscosity:

$$\sigma(T) = \sigma_0 \exp\left(\frac{\Delta E_\sigma}{k_B T}\right) \qquad \text{Eq 12}$$

where the characteristic energy ΔE_σ (the activation energy of internal friction) describes the temperature dependence of the internal viscosity and σ_0 is a temperature independent prefactor.

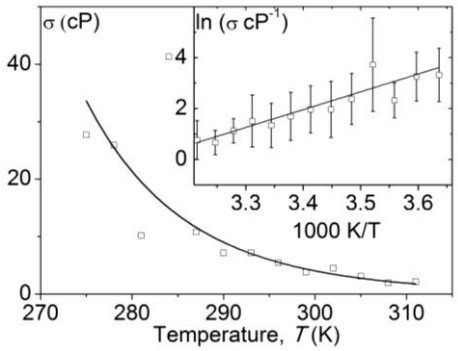

Figure 14 Temperature dependence of the calculated internal viscosity values

The internal viscosity values for 193G low-ionic-strength data are plotted against temperature. An Arrhenius-like exponential function (Eq 12) fits the data. Inset: linearisation reveals the exponential temperature dependence.

4.3.2. Effect of ionic strength on internal viscosity

To see the effect of ionic strength on internal viscosity, the data for 193G HuTry4 in low-salt and high-salt buffers was compared (Figure 15). Although there are fewer data points, and therefore a higher uncertainty in the high-ionic-strength data, the calculated internal viscosities are clearly different from low-ionic-strength data and fitting Eq 12 gives much weaker temperature dependence (Figure 15, inset).

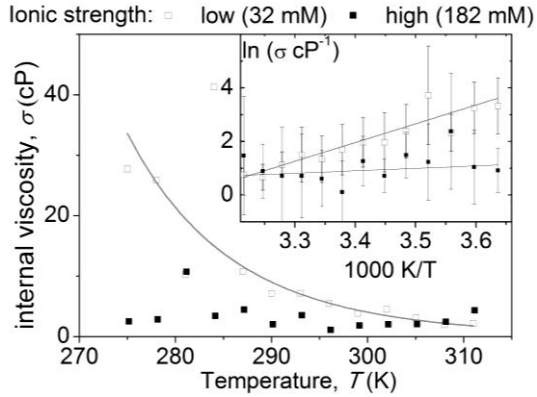

Figure 15 Effect of ionic strength on internal viscosity.

Calculated internal viscosity values for 193G mutant at each temperature in solutions with high (solid) and low (open) ionic strength. The data from measurements with high ionic strength are less accurate as they originate from fewer measurements, but a clear difference in tendency is shown by the linear fits in the inset.

4.3.3. The Gly to Ala mutation at position 193 in Human Trypsin 4 increases the viscosity-sensitivity of the trypsinogen activation step

The above presented results of the 193G mutant shed light on the temperature dependence of internal viscosity and the sensitivity of data to ionic strength. In order to reveal the effect of a Gly-Ala change in the hinge region of the domain movement to the

internal viscosity of trypsin activation, these results will now be compared to measurements with a different HuTry4 mutant, 193A. The relaxation time vs. viscosity plots (Figure 16) show that the slopes of the fitted lines are greater for 193A HuTry4, therefore it is more sensitive to viscosity than 193G HuTry4 both in high and low ionic strength environment.

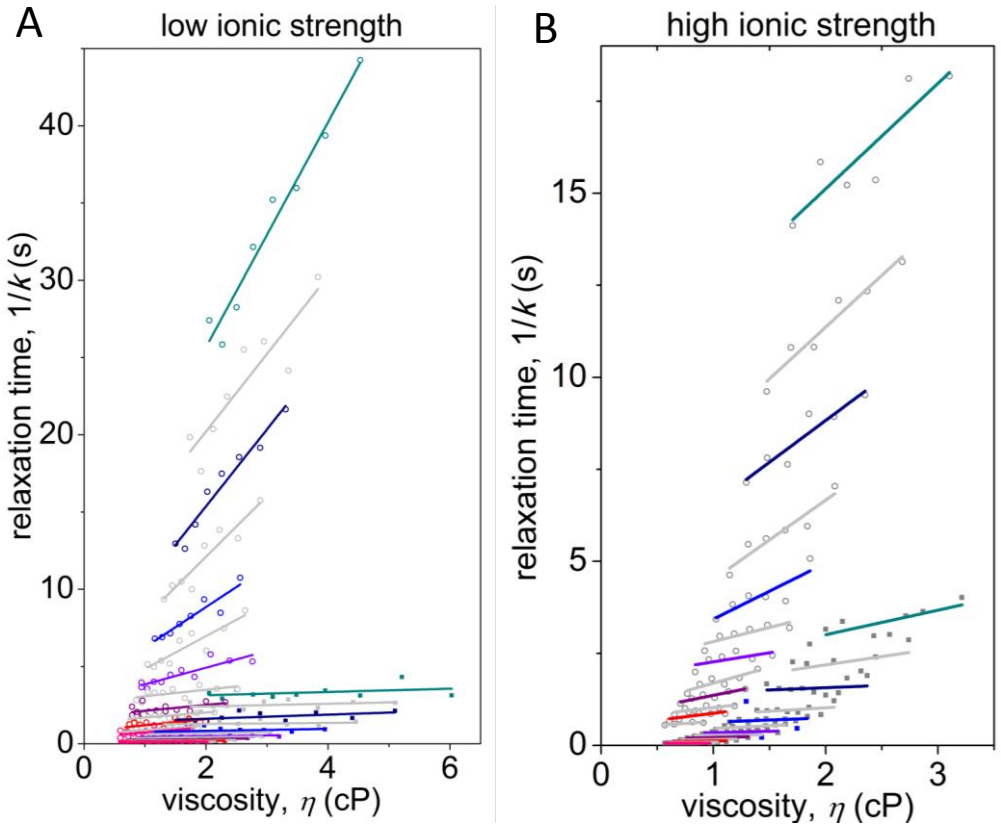

Figure 16 Effect of mutation on the viscosity dependence of the relaxation time

Relaxation times vs viscosity data are plotted for 193G (solid squares) and 193A (open circles) in A) low-salt environment B) high-salt environment. Isothermal data are represented by the same color (2, 8, 14, 20, 26, 32, 38 ^{o}C are in cyan, navy, blue, violet, purple, red and magenta, respectively). Only every second different measurement temperature is colored for clarity. Lines are linear fits to the isothermal relaxation time vs. viscosity data. From the fitted linear equations, internal viscosity can be calculated for each temperature based on Eq 11.

4.3.4. Effect of Gly to Ala mutation at position 193 in Human Trypsin 4 on internal viscosity

The internal viscosities of the two mutants were compared in both low-salt and high-salt conditions (Figure 17 A and B, respectively). A marked difference is visible between 193A mutant and the 193G mutant in low-salt conditions, as below 20 ^{o}C internal viscosity of 193G has strong temperature dependence while the values for 193A are nearly constant. Nevertheless, above 20 ^{o}C both mutants have identical internal

viscosities and relatively strong temperature dependence (Figure 17 A). In high-salt conditions the two mutants have very similar, nearly temperature-independent internal viscosities (Figure 17 B), though the values for 193A are slightly lower. The Arrhenius-like temperature dependence of internal viscosity, i.e. Eq 12, holds for every condition within measurement error.

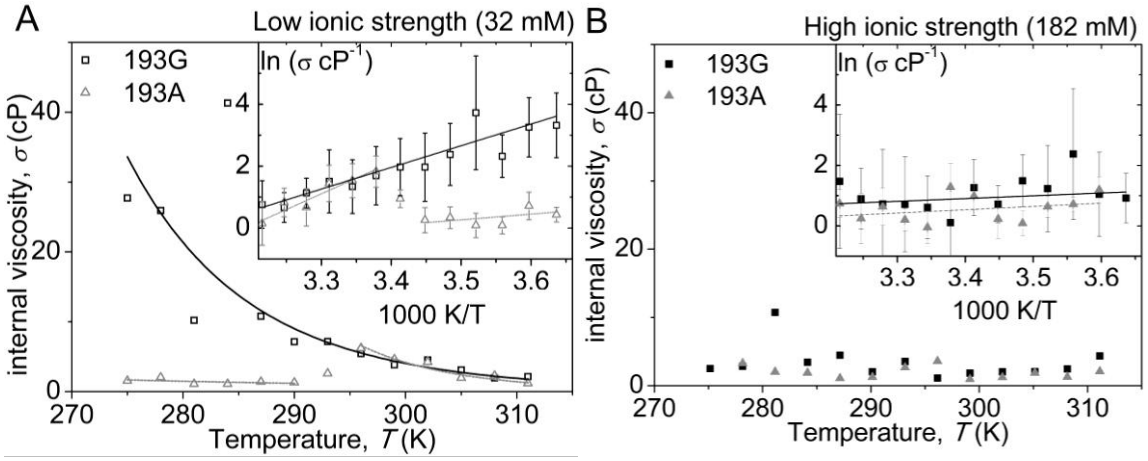

Figure 17 Effect of Gly/Ala switch at position 193 on the internal viscosity of trypsin activation

Calculated internal viscosities from the isothermal viscosity-dependence data on Figure 16 for 193G (black) and 193A (grey). Inset: logarithmic scale, with error bars. Lines are linear fits to the data based on Eq 12. A) Low-salt environment. B) High-salt environment.

4.4. Global fit to the temperature and viscosity dependence of the rate constants

After the sequential viscosity and temperature dependence analyses we obtained a bivariate surface fit for the 3D measurement data (Figure 12 A). The original bivariate function (Eq 11) for the viscosity and temperature dependence of the rate constants was extended with the temperature dependence of internal viscosity (Eq 12). Plugging Eq 12 into Eq 11 resulted in:

$$k(T,\eta) = \frac{A}{\eta + \sigma_0 \exp\left(\frac{\Delta E_\sigma}{k_B T}\right)} \exp\left(-\frac{\Delta E_a}{k_B T}\right) \qquad \text{Eq 13}$$

By fitting this equation to all measurement conditions in 3D, we can derive more accurate exponential or pre-exponential parameters and internal viscosity values than from the 2D extraction of the data (Table 8).

parameter ±SE	193G I=32 mM	193A below 293 K I=32 mM	193A above 293 K I=32 mM	193G I=182 mM	193A I=182 mM
Fitting parameters					
ΔE_σ (kJ mol^{-1})	43.8±11.5	16.1±17.8	77.2±30.1	0 ± 10.5	2.4 ± 6.8
ΔE_{SUM} (kJ mol^{-1})	77.1±2.7	67.7 ± 10.9	97.2 ±10.0	70.0 ± 2.8	60.4 ± 3.6
σ_{300} (cP) at 300 K	3.97±0.83	0.940±0.420	3.62±1.22	3.48±1.96	1.17±0.24
A_{300} (cP s^{-1})	3.11±0.15	-0.099±0.18	0.85± 0.25	3.19±0.44	0.30±0.11
Calculated values					
ΔE_a (kJ mol^{-1})	33.3	51.6	20.0	73.7	58.0
σ_0 (cP)	9.4×10^{-8}	1.5×10^{-3}	1.3×10^{-13}	3.5	1.2
A (cP s^{-1})	1.4×10^{7}	8.64×10^{8}	7.07×10^{3}	1.62×10^{14}	1.69×10^{10}

Table 8 Parameters of the fitted surface in the (T, η) parameter space for all measurement conditions. (Eq 13)

4.5. Fitting results for alternative theories

In the Introduction (Section 1.4) we mentioned alternative theories for the viscosity dependence of reactions. We also fitted Eq 3, the exponential viscosity dependence equation first suggested by Beece (7) to our data:

$$k(T,\eta) = \frac{A}{\eta^p} \exp\left(\frac{-\Delta E_a}{k_B T}\right) \qquad \text{Eq 14}$$

Similarly to internal friction, parameter p, the exponent for the alternative viscosity dependence relationship was calculated at every temperature by fitting a power function to the isothermal rate constants (Figure 3 in introduction). The exponent p was found to depend on temperature (Figure 18), based on the plot, the temperature dependence of p was estimated to be linear, so the final form of the fitted alternative surface is:

$$k(T,\eta) = \frac{A}{\eta_0}\left(\frac{\eta}{\eta_0}\right)^{-[p_0 + a_p T]} e^{-\Delta E_a/(RT)} \qquad \text{Eq 15}$$

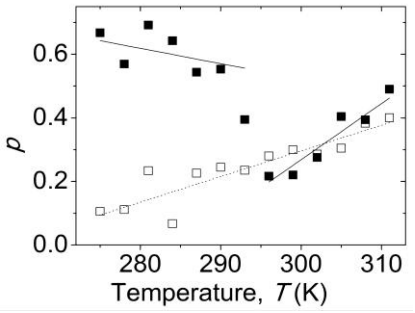

Figure 18 Temperature dependence of p from Eq 15

Isothermal fits of Eq 14 provided *p* values for every temperature. The plotted data for 193A (solid squares, ■) and 193G (open squares, □) are derived from the measurements in low-salt buffer. Lines are linear fits to the data. The temperature dependence of exponent *p* was therefore approximated with a linear function.

This alternative theory was only fitted to experiments done in buffers with low ionic strength, as the higher ionic strength data were less reliable due to the fewer data points. The final parameters of the fitted temperature and viscosity dependence of the rate constant are summarized in Table 9.

low ionic strength data	parameter	193G	193A below 293 K	193A above 293 K
Eq 15	**ΔE_a (kJ/mol)**	56.3	48.7	65.9
	A (cP/s)	2.66×10^{10}	1.33×10^{8}	1.41×10^{11}
	p_0	-2.12	1.97	-5.02
	a_p (1/K)	8.06×10^{-3}	-4.82×10^{-3}	1.76×10^{-2}
	p at 300 K	0.296	0.522	0.269

Table 9 Fitting parameters for the alternative surface with a power function

4.6. mT-jump results

We extended our measurements with 193G HuTry4 in low-salt buffer above denaturation temperature, where the viscosity of the solutions is relatively lower. Our aim was to distinguish between the alternative viscosity-dependence theories, based on how they fit the experimental data in this lower viscosity range. We managed to measure the rate constant of activation up to 60 °C/333 K. Above this temperature, denaturation of the protein was faster than its activation. Transient kinetic traces of the measurements were fitted with single exponential decays (Figure 19 A). While the rate constant of activation increased, the amplitude of the signal decreased with increasing temperature due to the temperature dependence of fluorescence. The fitted surfaces (Table 8 and Table 9) to the 193G low-salt data at ambient temperature were extrapolated to this high temperature region in order to see how well the mT-jump data fit the predicted values (Figure 19 B). The cross-section of the surfaces along the curve

for 0M maltose solutions (Figure 19 C) shows that although the mT-jump data are slightly closer to the internal friction model, they do not significantly distinguish between the surfaces predicted from Eq 13 and Eq 15.

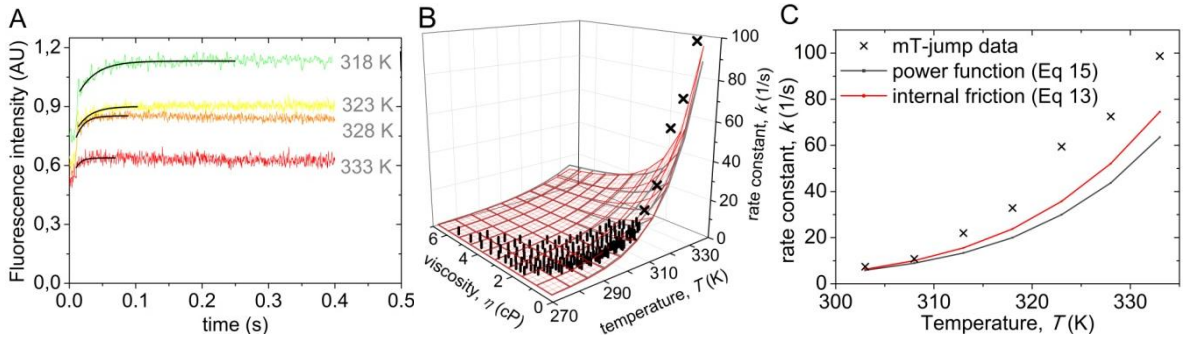

Figure 19 mT-jump data slightly deviate from both fitted surfaces

A) Averaged fluorescence transients (colored lines) of the mT-jump measurements at 318, 323, 328 and 333 K with the fitted exponential decays (black lines). B) Rate constants of 193G HuTry4 in low-salt buffer are plotted against both viscosity and temperature. Surfaces based on Eq 15 (dark grey) and Eq 13 (red) are fitted to the measurement data at ambient temperatures (black rods). The mT-jump data (black × marks) slightly deviate from the predicted values. C) The rate constants of the mT-jump data are plotted against temperature. The lines indicate the corresponding predictions of the two fitted surfaces shown on B.

4.7. Viscosity dependence of ATP-N binding to Dictyostelium myosin motor domain

In order to see the effect of viscosity on a different enzymatic conformational change, the viscosity dependence of a nucleotide binding by the motor enzyme myosin was investigated. Dictyostelium myosin II motor domain is stabilized in the closed state by γ-Amido-ATP (ATP-N) (125, 126). The fluorescence of the Trp residue W501, located at the end of the relay helix close to the converter region is a relevant reporter of this ATP-N binding event (Figure 20 A). Upon mixing ATP-N and myosin II W501 motor domain a fast (k_3=600/s) fluorescence decrease is observed, followed by a two-phase fluorescence increase (k_1=30/s; k_2=3/s) (Figure 20 A). The fluorescent traces were fitted with a triple exponential function:

$$Fluorescence(t) = A_1 \exp(-k_1 t) + A_2 \exp(-k_2 t) + A_3 \exp(-k_3 t) + slope \cdot t + offset \qquad \text{Eq 16}$$

The viscosity dependence of the fitting parameters – summarized in the Appendix (Section A3) – was analyzed. The fitted, apparent rate constants of ATP-N binding to myosin do not show any viscosity dependence (Figure 20 B), whereas the fitted amplitudes significantly change with viscosity (Figure 20 C).

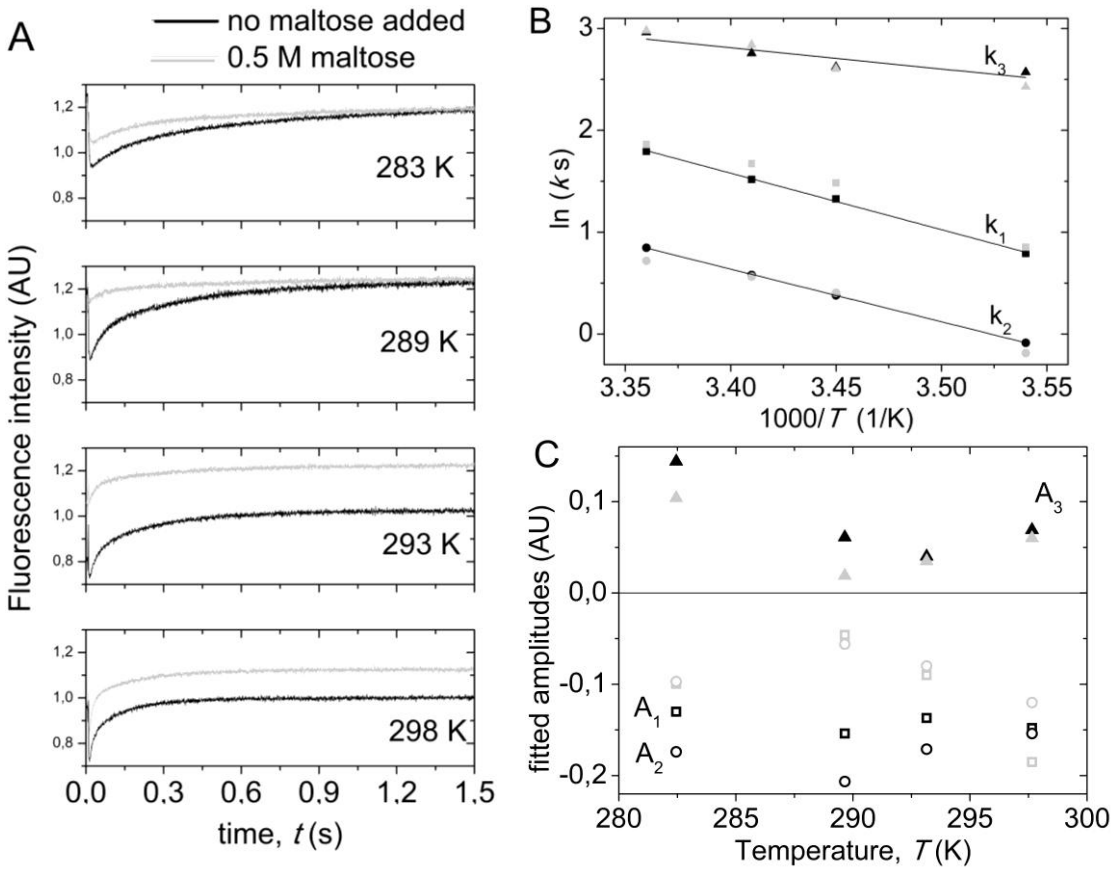

Figure 20 Increased viscosity does not affect the apparent rate constants of ATP-N binding

A) Transient kinetic traces with (gray) and without (black) 0.5 M maltose at four different temperatures (283, 289, 293, 298 K). B) On the Arrhenius plots the three apparent rate constants (k_1, k_2, k_3) are almost identical in the assay buffer (black) to those in the 70% more viscous buffer with maltose (gray). C) The fitted amplitudes change with increasing viscosity.

From the fitted, apparent rate constants the theoretical equilibrium constant and rate constants were calculated based on the 3-step model (Eq 17) presented below. Briefly, a fast binding step with a rate constant k_3 is followed by an equilibrium of two different bound states (k_{fast}+ and k_{fast}– are the forward and reverse rate constants with an equilibrium constant K). A stabilized state is formed as a last step, with a rate constant k_{slow}. This last state is considered stable as the hydrolysis of ATP-N is very slow (2-3x10^{-4}/s (126)).

$$\text{myo} + \text{ATPN} \xrightarrow{k_3} \text{myoATPN} \underset{k_{fast}-}{\overset{k_{fast}+}{\rightleftharpoons}} \text{myo}_A\text{ATPN}^* \xrightarrow{k_{slow}} \text{myo}_B\text{ATPN}^* \qquad \text{Eq 17}$$

For estimating the rate contstants k_{slow}, k_{fast}+ and k_{fast}– and the equilibrium constant K the following relationships were used:

$K = A_1/A_2$ Eq 18

$k_{fast}+ = k_1 \cdot A_1/(A_1+A_2)$ Eq 19

$k_{fast}- = k_1 - k_{fast}+ = k_1 \cdot A_2/(A_1+A_2)$ Eq 20

$k_{slow} = k_2 \cdot (K+1)/K$ Eq 21

The effect of increased viscosity on the calculated theoretical rate constants is illustrated on Arrhenius plots with/without added viscogen. The equilibrium constant, K is affected by viscosity (Figure 21 A) in a temperature-dependent manner. The fast forward rate constant, $k_{fast}+$ is accelerated by increased viscosity (Figure 21 D), while the fast reverse rate constant $k_{fast}-$ and the slow step k_{slow} are unaffected by the 70% increase in viscosity (Figure 21 C and B, respectively).

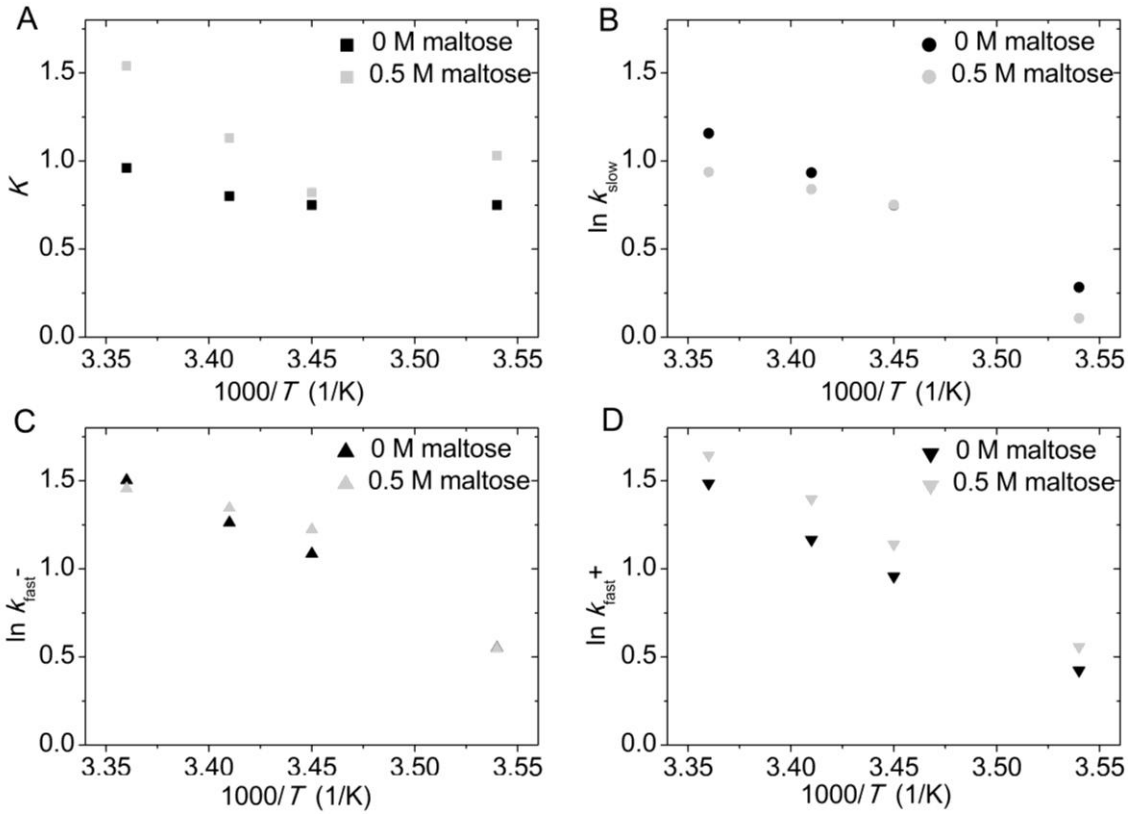

Figure 21 Effect of viscosity on the Arrhenius plots of the equilibrium constant and rate constants

A) The equilibrium constant, K and the logarithm of B) the slow rate constant , k_{slow} C) fast reverse rate constant, k_{fast}^- D) the fast forward rate constant, k_{fast}^+ are plotted against the reciprocal of temperature in assay buffer with 0.5 M maltose (grey symbols) or assay buffer without maltose (black symbols).

5. Discussion

5.1. Comparison of our data to previously published data on the same trypsin mutants.

5.1.1. Arrhenius plots of both mutants are parallel

As it was found earlier (79), the classical Arrhenius plots of 193G and 193A determined in a buffer without added viscogen are linear and parallel to each other. Our measured rate constants are slightly higher, trypsin activation was found to be 1.5 - 3 times faster than reported previously, but the slope of the Arrhenius plots remained unaffected (Figure 22 A). The activation energies that can be calculated from the Arrhenius plots are very close to each other (Figure 22 B).

5.1.2. Viscosity dependence of the rate constants compared to previous measurements

As we already saw on the Arrhenius plots, the relaxation times measured by Toth et al are 1.5-3 times longer. When we compare the viscosity dependence of the relaxation times (1/k or τ) at 293K, it is visible that the longer relaxation times reported by Toth et al produce seemingly steeper viscosity dependence, especially in 193G HuTry4 (Figure 22 C,D). The internal viscosity values calculated from the viscosity dependence data at 293 K in three different buffer conditions are between 0.27-7.5 cP (Figure 22 E). Both the mutation and the buffer conditions influence its value.

Thus we observed that our data slightly differ from the previously published similar measurements. However, we believe that the observed difference is more superficial and less fundamental as the slope of the Arrhenius plots is constant and only the viscosity dependence data are affected. As we described in the Results Section 4.3.2 that ionic strength significantly influences the viscosity dependence, we attribute the difference from previously published data mainly to the difference in the composition of solutions used: the previously published data were buffered with Tricine instead of HEPES, and 10 times more CABS, 2 times more $CaCl_2$ were used (79).

This observation that the solution composition and measurement conditions may play a crucial role further emphasizes the importance of controlling buffer conditions. As we took extra care in the optimization for our measurements described in detail in Methods Section 3.1.2.2, we expect to have minimized unspecific buffer-related effects.

Any tendency, or difference observed in our experimental results should therefore be related to the characteristics of the proteins.

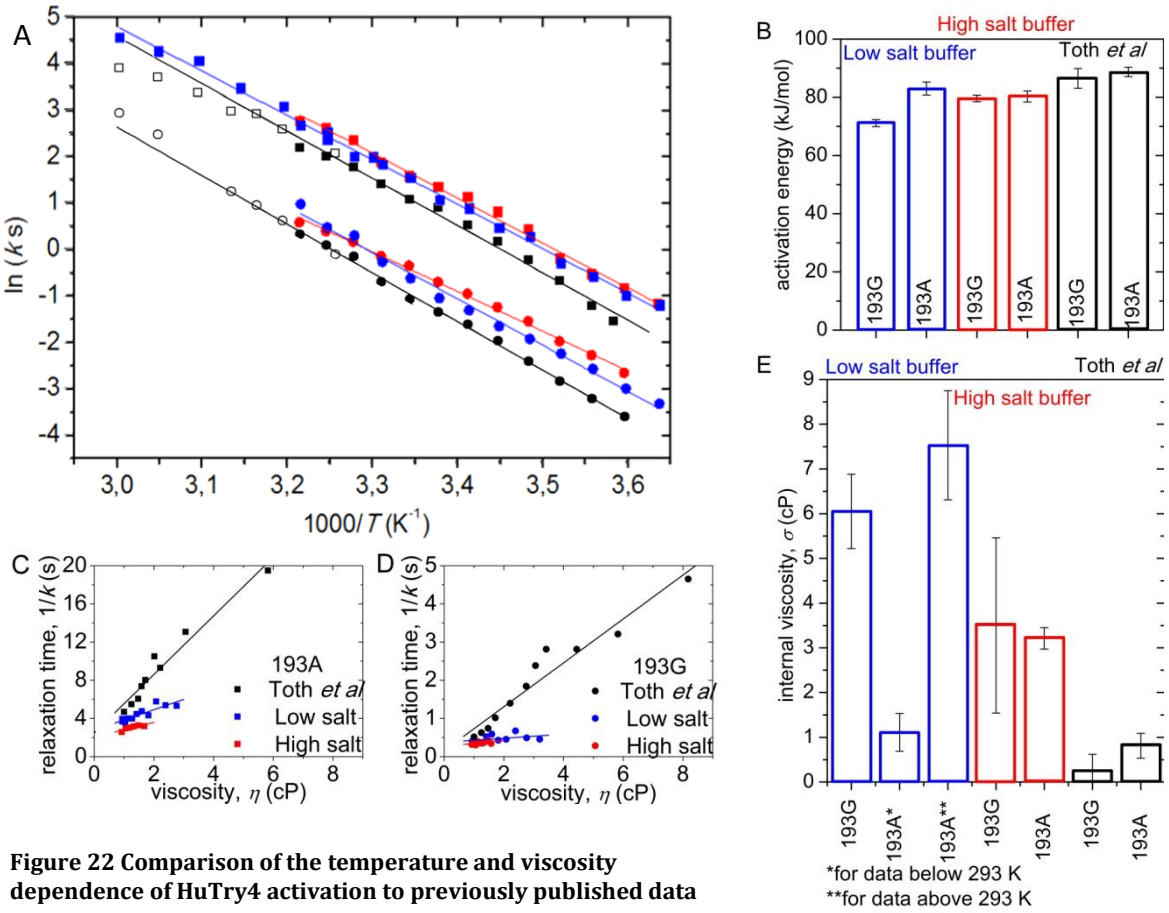

Figure 22 Comparison of the temperature and viscosity dependence of HuTry4 activation to previously published data

A) Arrhenius plots for 193A (circles) and 193G (squares) in high ionic strength (red), and low ionic strength (blue) buffers are compared to data from literature (79) (black). None of the buffers contain additional viscogen. B) Activation energies calculated from the Arrhenius plots. The viscosity dependence of the relaxation time of HuTry4 C) 193G and D) 193A at 20 °C/293 K in high (red) and low (blue) ionic strength conditions are compared to previously published data (79) (black). Lines are linear fits based on Eq 11 . E) Calculated internal viscosity values (from Table 8) for both mutants in three different buffer conditions: low-salt (blue), high-salt (red) and literature data (black) by Toth et al (79). As the 193A mutant has a phase transition at 293 K, the internal viscosity value for 293 K was extrapolated in two ways: from data below and above 293 K.

5.2. Comparison of our data to other viscosity-dependence data on enzyme reactions or protein conformational changes

In the introduction I made an attempt to mention briefly all viscosity dependence experiments from the literature (Section 1.5 Table 1). From these measurements those that investigate both the effect of temperature and viscosity are most relevant to our results. Table 10 below collects these publications where both temperature and viscosity dependence data are presented in some way. From these publications, four

important sets of data (in bold) originate from systematic temperature and viscosity dependence measurements and are therefore comparable to our results.

Type of reaction studied	range of viscosity (cP)	range of temperature (K)
photoinduced electron transfer between Zn cytochrome c and Cu plastocyanin (10, 83**) by Ivkovic-Jensen et al**	**0.8-790**	**260-308**
photoinduced electron transfer between Zn cyt c_6 and cyt f (31)	0-60	283, 293, 313
electron transfer between cytochrome f and plastocyanin (129)	1-3	293, 300
proton and hydride tunneling in light-activated protochlorophyllide oxidoreductase (40)	1-10	298-323
horseradish peroxidase phosphorescence quenching (63) by Khajehpour et al	**0.9-12**	**278-298**
hemoglobin bound NO spin label (27) by Steinhoff et al	**1-10000**	**276-315**
Trp phosphorescence lifetime of 4 different proteins (65)	~1-100	253-333
lysosyme Trp isotope exchange (67)	1-6.3	288, 293, 299
cytochrome C folding from a compact configuration (68) by Pabit et al	**0.7-6**	**290, 293, 298, 303**
O_2 and CO binding to myoglobin and protoheme (7)	~1-100000	180-340
CO binding to ferrous microperoxidase 11 (17)	~7cP- 700	253-313
CO binding to myoglobin (22)	~1-10^{10}	63-290
carboxypeptidase A hydrolysis rate (52)	~7-90	283-308
H^+ ATPase (60)	1-3	293, 308, 313

Table 10 Studies investigating both viscosity and temperature dependence of reactions (Table 2 from (85), extended)

These four viscosity and temperature dependence measurements span a wide range of viscosities and the studied reactions vary from ns-scale to ms-scale reactions (Figure 23 A): ms-range: phosphorescence quenching by Khajehpour (63), μs range: electron transfer reaction by Ivkovic-Jensen (10), and folding by Pabit (68) ns range: NO spin label by Steinhoff (27). Since the authors of these publications did not discuss in detail either the internal viscosity parameter or its temperature dependence, in order to compare these measurements to our data, we fitted Eq 2 (Eq 11) to the experimental data extracted from the published figures of the publications:

$$k(T,\eta) = \frac{A}{\sigma + \eta} \exp\left(-\frac{\Delta E_a}{k_B T} \right) \qquad \text{Eq 22}$$

This linear viscosity dependence of the relaxation time is valid for most of the data, except for very high (above 25 cP) viscosities, so we calculated the internal viscosity for these four types of reactions for several temperatures (Figure 23 B). The calculations are presented in more detail in the Appendix (Section A4, Supplementary Figure 4). Interestingly, these calculated internal viscosity values show very similar temperature dependence to our data: the logarithm of internal viscosity linearly changes with the reciprocal of temperature (Figure 23 B), there is only a slight deviation from linearity in the electron transfer data by Ivkovic-Jensen et al. (Figure 23 B).

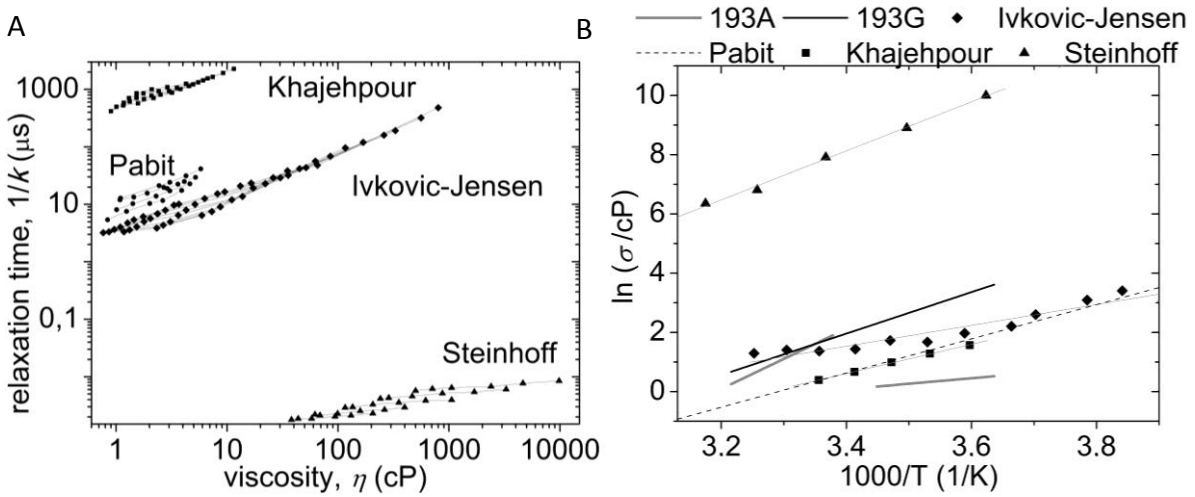

Figure 23 Temperature dependence of internal viscosity in the literature

A) Relaxation time vs viscosity data in the literature. Grey lines connect isothermal data. ms-range: phosphorescence quenching by Khajehpour (63) (squares), µs range: electron transfer reaction by Ivkovic-Jensen (10) (diamonds),and folding by Pabit (68)(circles) ns range: hemoglobin dynamics by Steinhoff (27) (triangles) B) Internal viscosity values were calculated for each temperature from the published data using Eq 2/Eq 11/Eq 22. Grey lines are linear fits to the data. For the folding reaction by Pabit the function for the temperature dependence of internal viscosity (dashed line) was calculated from published fitting parameters (see below Section 5.4.1 Model#1), as not all raw data were available. The details of the calculations are included in the Appendix. For comparison, the internal viscosities of the 193G and 193A HuTry4 are illustrated as bold black and grey lines, respectively.

Moreover, the internal viscosity data not only share the Arrhenius-like temperature-dependence, but are also similar in value to each other. There is only one exception, the internal viscosities calculated for the NO spin label dynamics in hemoglobin, but those data are less reliable and can only be considered as estimates for the upper limit of internal viscosity (see Supplementary Figure 4 C). The similarity in internal viscosity values is especially remarkable as the rate of reactions differs by magnitudes from each other. In conclusion, the analysis of published viscosity dependence data from the literature also support our observation about the Arrhenius-like temperature dependence of internal viscosity (Eq 12, Eq 23).

5.3. The temperature dependence of internal viscosity is Arrhenius-like

We already demonstrated (Section 4.3.1) that internal viscosity has an Arrhenius-like temperature dependence, which suggests that it can be associated with an energy barrier (Eq 12)

$$\sigma(T) = \sigma_0 \exp\left(\frac{\Delta E_\sigma}{k_B T}\right) \qquad \text{Eq 23}$$

, where σ_0 is a temperature independent internal viscosity parameter and ΔE_σ is a characteristic activation energy parameter of internal friction. This finding is further supported by the above described analysis of viscosity dependence results from independent publications (Figure 23). Moreover, a mathematically identical relationship - with a different interpretation, Model #1 below - was described for the temperature and viscosity dependence of cytochrome c folding from a collapsed state (68), and for the folding/unfolding rates of Trp Cage (72).

Theoretically, the relationship found for the temperature dependence of internal viscosity (Eq 12, Eq 23) is in analogy to the behavior of the viscosity of liquids, which also originates from microscopic barrier-crossing events (130), and is often characterized by the empirical Vogel-Tammann-Fulcher relationship (120):

$$\eta(T) = A_{VTF} \exp\left(\frac{E_\eta}{k_B (T - T_0)}\right) \qquad \text{Eq 24}$$

, where T_0 is the ideal glass transition temperature, A_{VTF} is a temperature-independent constant, E_η is a parameter with energy dimensions. For illustration of the similarity, the internal viscosity values are compared to the viscosity of pure solvent (Figure 24).

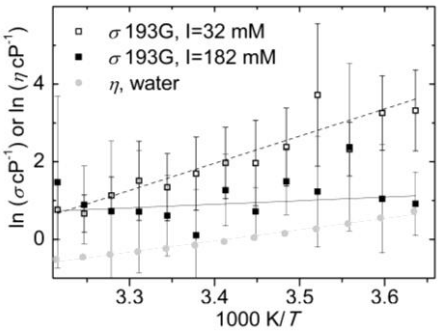

Figure 24 Temperature dependence of internal viscosity of 193G trypsin activation compared to the viscosity of the solvent.

The logarithm of internal viscosity of 193G in low (open sqares) and high (solid squares) ionic strength conditions and the viscosity of the low-salt buffer without maltose (grey circles) are plotted against the reciprocal temperature. Lines are linear fits to the data.

The experimental results, which fit to Eq 23 and demonstrate that internal viscosity has an Arrhenius-like temperature dependence, indicate that internal friction is related to a characteristic energy barrier. How can we reconcile this energy barrier with the energy landscape? What is its relationship to the activation energy barrier? In the next sections several theoretical models explaining the viscosity dependence of reactions and its possible energetic background will be described in detail.

5.4. Models for explaining the observations – preliminary models

The observations described in the Results section come from strictly controlled, systematic measurements, which would be even more valuable if we were able to generalize them. A theoretical model that explains the findings and can make predictions for future experiments is therefore a very important requirement for a greater impact within the scientific community. In this chapter I describe the evolution of our model, with preliminary models and dead-ends.

The important observations that have to be consistent with the theoretical model are the followings:

1. The Arrhenius plots of the activation of 193A and 193G HuTry4 mutants are parallel, so the activation energy barriers are equal. (Results Section 4.1. Figure 12 C, Results Section 4.2. Figure 13 B, Discussion Section 5.1.1. Figure 22 A)

2. There is a phase transition at 293K in the Ala hinge mutant, 193A. (Results Section 4.3.4. Figure 17)

3. There is an energy value associated with internal viscosity. (Eq 12/Eq 23)

4. Altogether there are two energy values associated with the reaction (ΔE_a and ΔE_σ), the sum of these two energies is constant, while their ratio depends on measurement conditions. (Eq 13, Table 8 in Results Section 4.4.)

5. The faster, supposedly more flexible Gly hinge mutant, 193G HuTry4 is more sensitive to viscosity and consequently has higher apparent internal viscosity than 193A HuTry4. (Figure 17)

5.4.1. Model #1

Pabit and Hagen also used mathematically equivalent forms of Eq 13 to describe the folding of cyt c from a collapsed state (68). The mathematical transformation of their formulae to our nomenclature is presented in the Appendix (Section A4). They used a two-step reaction scheme for explaining the single reaction step that they observed (Figure 25): a viscosity-dependent step was followed by a viscosity-independent internal rearrangement. Based on (131) they suggested that the relaxation time of the folding of a polymer chain consists of two components, $\tau = \tau_s(\eta) + \tau_{int}$, where $\tau_s(\eta)$ is a relaxation time associated with solvent-damped motion of the polymer, whereas τ_{int} reflects the

dynamics apparently controlled by some viscogen independent, “internal” friction. Both components are supposed to have Arrhenius type temperature dependences (Figure 25 C). Theoretically, the timecourse of a two-step reaction does not fit a single exponential, but in practice this might not be apparent due to noise in the observed signal so therefore their reasoning is defensible. To learn more about the mechanism of viscosity dependence, however, ideally a single, viscosity-dependent reaction step should be investigated.

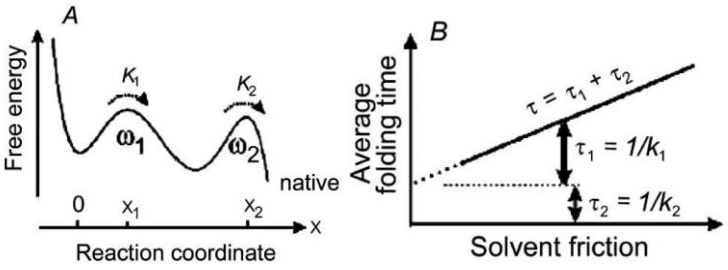

C

$$k_1 = 1/\tau_1 = \omega_0\,\omega_1/\,2\pi\gamma_1\,\exp(-\Delta G_1/k_BT)$$

$$k_2 = 1/\tau_2 = \omega_0\,\omega_2\,/\,2\pi\gamma_2\,\exp(-\Delta G_2/k_BT)$$

$$\tau = 1/\,k_1 + 1/\,k_2 = \tau_1 + \tau_2$$

Figure 25 Two-step model for explaining viscosity dependence of folding

A) Energy landscape of the two-step folding reaction, where the first step is a viscosity-dependent larger conformational change, and the second step is an internal conformational change, where internal viscosity dominates as this step is independent of solvent viscosity. ((69) Fig 4A) B) The observed viscosity dependence of the relaxation time of the two-step reaction. ((69) Fig 4B) C) The relationships between the respective rate constants, k_1, k_2, relaxation times τ_1, τ_2 and reaction friction coefficients γ_1, γ_2, energy barriers, ΔG_1, ΔG_2, curvatures ω_1, ω_2. The figures and the equations are copied from the review by Hagen (69).

5.4.2. Model #2 – mechanistic model

We started out with a mechanistic picture of the protein conformational change. We modeled the conformational change of a protein in the solvent mechanistically, in hope for an insight into the mechanism of how the viscosity of the solvent influences a protein conformational change. Our assumption was that during the conformational change in the enzyme internal rearrangements and movements relative to the solvent take place parallel, at the same time. The internal rearrangements are affected by internal viscosity (σ) while the movements relative to the solvent are slowed down by solvent viscosity (η). To model this situation we constructed a very simple, mechanistic model consisting of a cylindrical object that rotates in an oily cylinder, which is surrounded by water (Figure 26 A). The object is in contact with the oily phase, but the rotation of the object is affected by both the viscosities of the oily phase and the water. In this model the oily phase represents the internal medium in the protein, the water represents the solvent. Viscosities of the oily phase and the water phase are σ_M and η, respectively. From an

analytical calculation we get a surprisingly simple formula, the weighted harmonic mean of the two viscosities is proportional to the relaxation time of the movement:

$$\tau = 1/k \sim 1/\left(\frac{A}{\sigma_M} + \frac{1-A}{\eta}\right) \qquad \text{Eq 25}$$

It is especially interesting that the internal friction model (Eq 2) calculates with the weighted arithmetic mean, $\tau = 1/k \sim A\sigma + B\eta$, and in the alternative, power-dependence model (Eq 3) the weighted geometric mean is applied, if $\sigma=\eta_0$, $\tau = 1/k \approx \eta^p \sigma^{1-p}$. Therefore our mechanistic model with rotation in two different solutions nicely complements this series of arithmetic-geometric-harmonic means (Figure 26 B,C,D).

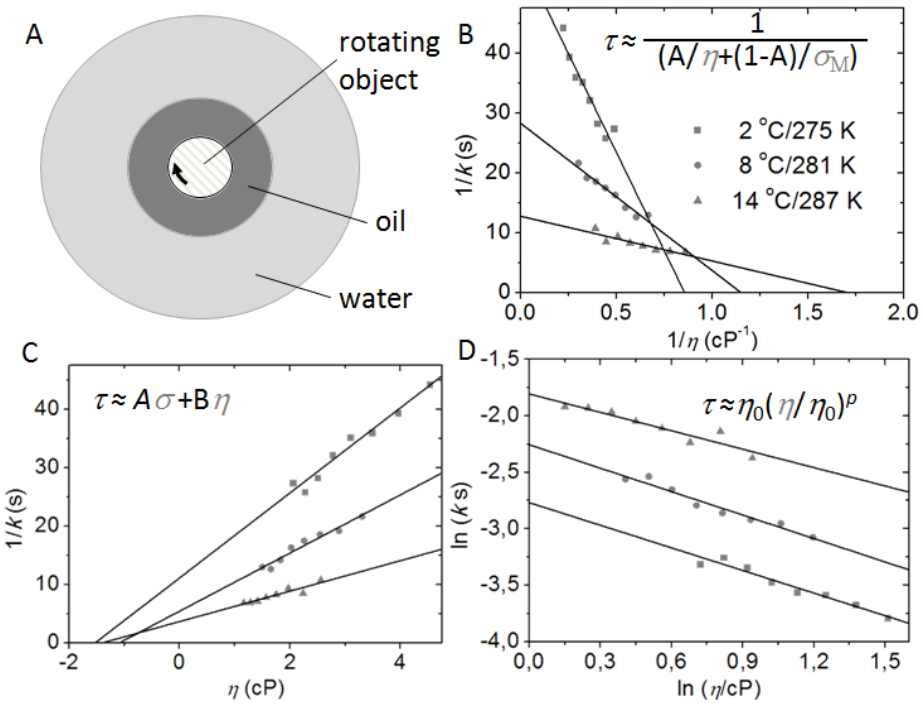

Figure 26 Modeling the viscosity dependence of enzyme conformational change

A) The mechanistic model: a cylindrical object rotates in an oily cylinder, surrounded by water. B) Based on this model the relaxation time is a linear function of the reciprocal of solvent viscosity, which is illustrated with data measured at three different temperatures with 193A HuTry4. For comparison, the same data are plotted according to C) the classical internal viscosity model (Eq 22, Eq 11, Eq 2) and D) the exponential p model (Eq 14, Eq 3).

When the temperature dependence of internal viscosity σ_M derived from this mechanistic model is observed we see interesting phenomena: the value of this 'mechanistic internal friction' (σ_M) is negative, and while the difference between the

mutants is kept, the previously observed (see Results Section 4.3.2. Figure 15) difference between high-salt and low-salt data does not appear in this parameter (Figure 27 A, B). The phase transition is observable in both buffers for the 193A HuTry4.

After this short analysis the mechanistic model was not considered any further. The negative σ_M values (Figure 27 A,B) and its prediction that below a certain solvent viscosity the relaxation time is negative (Figure 27 C) were found too extreme and difficult to interpret.

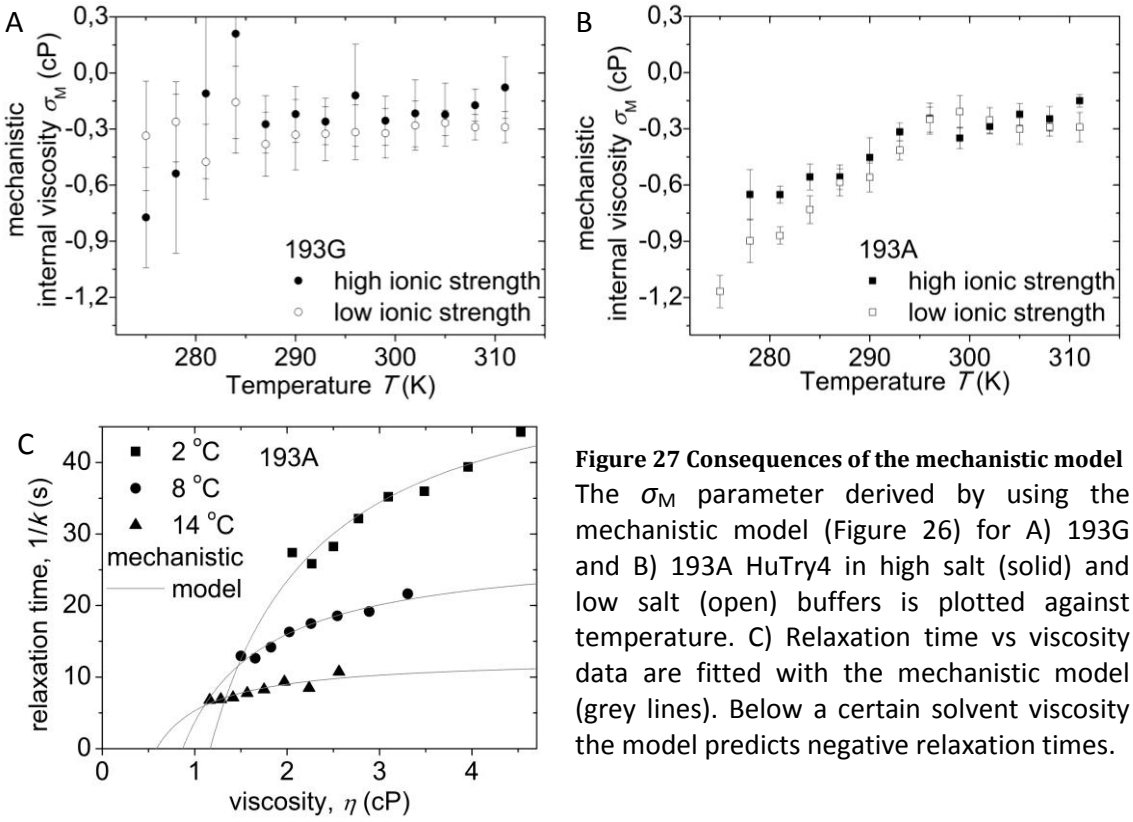

Figure 27 Consequences of the mechanistic model
The σ_M parameter derived by using the mechanistic model (Figure 26) for A) 193G and B) 193A HuTry4 in high salt (solid) and low salt (open) buffers is plotted against temperature. C) Relaxation time vs viscosity data are fitted with the mechanistic model (grey lines). Below a certain solvent viscosity the model predicts negative relaxation times.

5.4.3. Model #3

In the next round of models the two energy values found in Eq 13, the temperature and viscosity dependence of the rate constant,

$$k(T,\eta) = \frac{A}{\eta + \sigma_0 \exp\left(\frac{\Delta E_\sigma}{k_B T}\right)} \exp\left(-\frac{\Delta E_a}{k_B T}\right) \qquad \text{Eq 26}$$

were interpreted in a way that ΔE_a reflects the height of the energy barrier, and ΔE_σ is characteristic of friction, the 'surface' of the energy landscape. We envisioned a scenario where the characteristics of the 'surface' and the height of the energy landscape

coincidentally compensate each other, which results in apparently parallel Arrhenius plots (Figure 28).

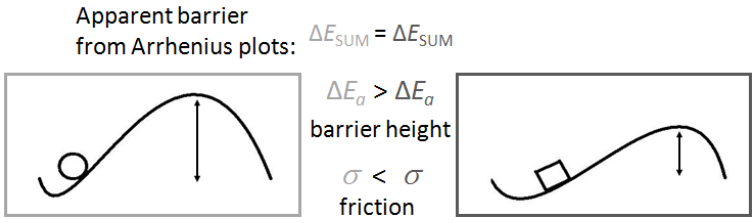

Figure 28 Preliminary illustration for explaining the parallel Arrhenius plots

The apparent energy barrier, calculated from the Arrhenius plots is a combination of the actual height of the energy barrier and the effect of friction along the reaction coordinate. This way it is possible to measure parallel Arrhenius plots for reactions with different actual barrier heights. In this example the ball on the left encounters smaller friction (σ) and has to overcome a greater energy barrier (ΔE_a) than the block on the right. This way the apparent energy barriers (ΔE_{SUM}) will be the same for both of them.

Following this line of thought we constructed several models of the possible energy landscape trying to explain the observations, some examples of energy landscapes that once seemed to be promising are illustrated on Figure 29. For a start we envisioned a saddle like energy barrier (Figure 29 A,B). The surface of the barrier is drawn rough, to illustrate friction (Figure 29 C,D,E,F). The energy landscape for 193G (Figure 29 C) shows that a single energy barrier (ΔE_a in Table 8) and some type of temperature-dependent viscosity (σ, shown as roughness) is involved during the activation. The energy landscape model for 193A had to account for the phase change observed at 293K/20 °C for the 193A low-ionic strength data (Table 8). Our first approach was that if a phase change occurs, at some point the system has to exist at least in two different states. There may be two different zymogen ground states (Figure 29 D) or two different routes towards the active state i.e. two different transition states (Figure 29 E). The temperature change would shift the equilibria between the two states, which results in the observable phase change. As we determined that ΔE_a is greater for T<293K (Table 8), the energy landscape with two zymogen ground states (Figure 29 D) is more likely than the one with two different transition states (Figure 29 E). Even though the energy landscape with two zymogen ground states (Figure 29 D) can explain the energy barrier height change observed for 193A HuTry4, it does not account for the observed change in internal viscosity (σ_{300} and ΔE_σ in Table 8). Therefore a similar model with inhomogeneous friction was also envisioned (Figure 29 F).

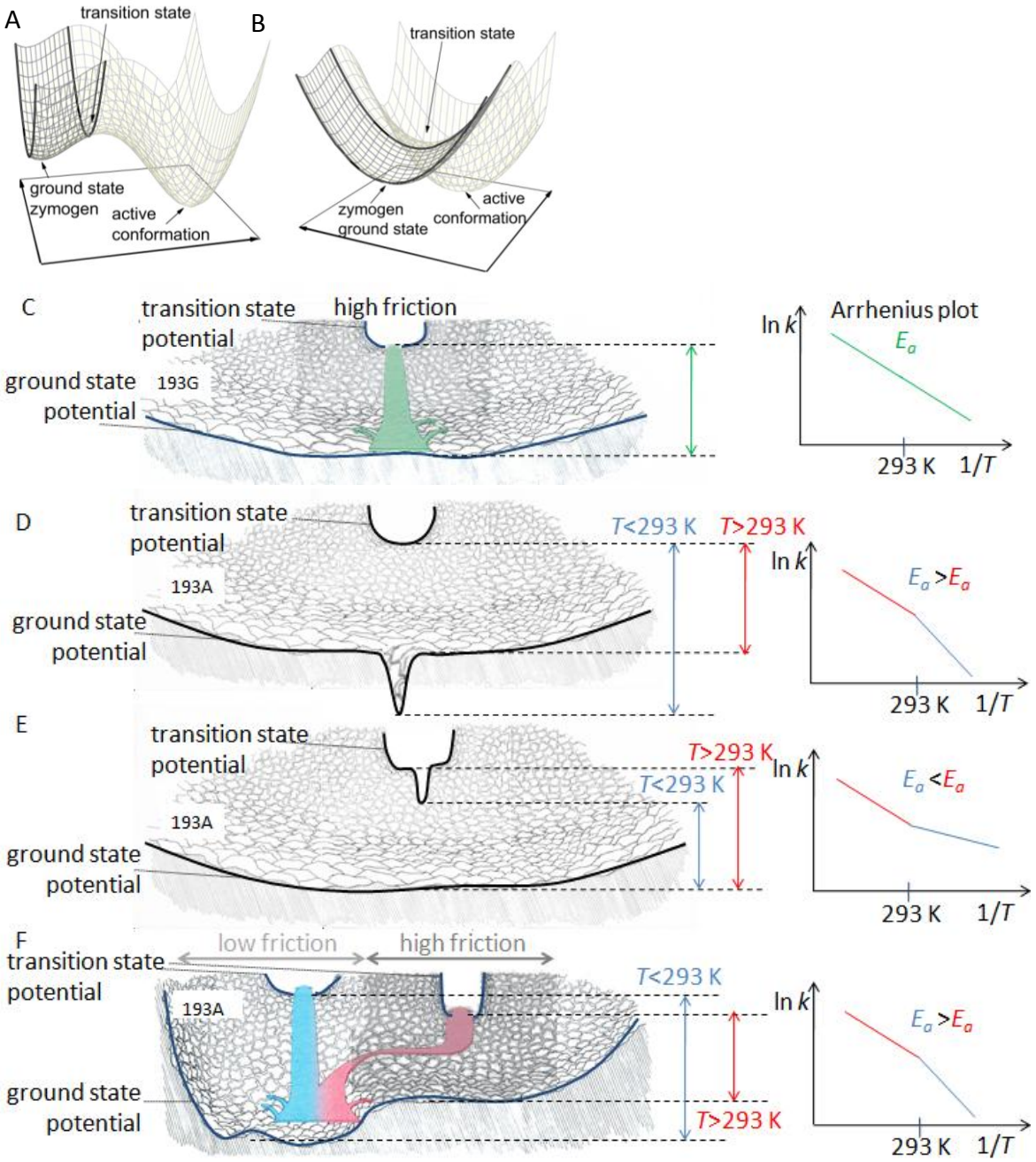

Figure 29 Imaginary energy landscapes

A)-B) A saddle-like energy barrier for a single 2D reaction coordinate provides the basis of our models. The saddle is illustrated by the wireframe plot A) from the side and B) from the front. All illustrations below depict the darker area of the saddle, the 'uphill' part from the zymogen conformation to the transition state. C) A simple energy landscape for the activation of 193G HuTry4: the rough surface illustrates friction, the green arrow represents the main flux from the ground state to the transition state. D), E), F) are modified versions of the energy landscape adapted to the phase transition observed in 193A at 293 K, which implies that 193A HuTry4 has two different states, two different energy barriers. If there is a lower energy, lower entropy state either in the ground state (D) or in the transition state (E), a phase transition is visible on the Arrhenius plots, which are shown on the right. At colder temperatures (blue) the lower energy state is occupied while at higher temperatures (red) the higher entropy state is more probable, so activation energies vary accordingly. F) A model incorporating differences in friction into the phase transition. Below 20 ^{o}C the blue route is preferred, above 20 ^{o}C the main flux is via the red route. We envisioned that friction, illustrated as roughness also has a role in directing the flux. (Drawings by Tamás Cserna)

However, provided that this model with inhomogenous friction describes the observations, the role of friction in directing the flux is still not understood and its generalization would be problematic. Moreover, a thought experiment revealed that the model with inhomogeneous friction (Figure 29 F) can easily be contradictory: if the enzyme chooses the higher energy barrier due to friction below 20 °C, on the way back, without friction, the enzyme could return through the lower energy barrier, which leads to a perpetuum mobile. For the above listed reasons the various energy landscape models (Figure 29), proved to be inefficient or self-contradictory for describing our observations. Consequently, we could not explain our experimental observations with a single reaction coordinate.

5.4.4. Model #4

Two, perpendicular reaction coordinates have already been used by Zwanzig (132) for explaining the viscosity dependence of ligand escape from enzymes (7). In his elegant, easily conceivable model the ligand moved through a fluctuating bottleneck (Figure 30) based on the model of Agmon and Hopfield (133). The escape rate is proportional to the size of the bottleneck, which is a quadratic function of its radius. The radius of the bottleneck obeys a simple Langevin equation (a quadratic function assuming that the greater the bottleneck, the faster its relaxation to closed state). The two perpendicular, independent reaction coordinates are characterized by two functions: i) the rate of escape as a function of the size of the bottleneck, ii) the size of the bottleneck as a function of time. If the radius of the bottleneck is assumed to relax by a rate inversely proportional to viscosity, the viscosity dependence of the rate of the escape can be calculated as: $k \propto \eta^{-0.5}$

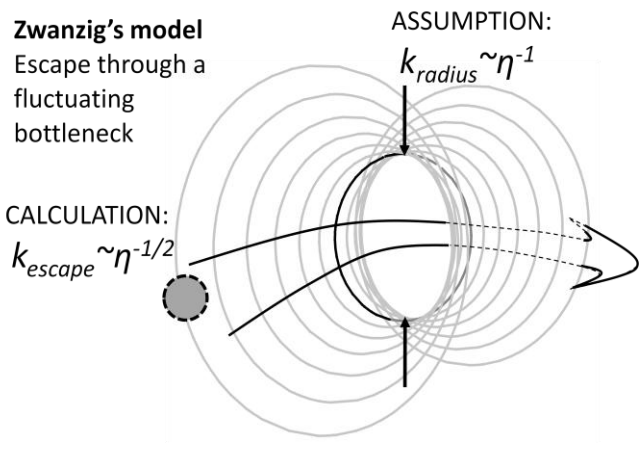

Figure 30 Fluctuating bottleneck in Zwanzig's model

The viscosity dependence of the rate of escape in Zwanzig's model is derived from three assumptions: the fluctuation of the radius of the hole i) is described by a Langevin potential ii) is inversely proportional to solvent viscosity iii) the escape rate is proportional to the square of the radius. Analytical calculations lead to the result that the rate of escape is a power function of solvent viscosity.

This model is based on several assumptions and is a calculation for a very specific case, but it is related to the empirical observation of Beece (7), where the rate constant is a power function of viscosity (Eq 3, Eq 14):

$$k(T,\eta) = \frac{A}{\eta^{p}} \exp\left(\frac{-\Delta E_{a}}{k_{B}T}\right) \qquad \text{Eq 27}$$

We already illustrated (Figure 3) that it requires very wide range of viscosity data, preferably low viscosity data, to distinguish the exponential viscosity dependence (Eq 27) from the linear dependence (Eq 22). Our mT-jump data were measured in relatively low viscosity buffers, but due to the measurement uncertainties the data are not conclusive in differentiating the two different viscosity dependence theories (Figure 19). To our knowledge, no systematic study has been performed to discriminate between Eq 27 and Eq 22 in a close to physiological range of temperatures and viscosities. This indecisive nature of the experimental data was already recognized in several works where authors analyzed their data by applying different alternative fitting functions (10, 11, 18, 30, 31, 40, 80, 134). We also fitted Eq 27 to our data and found that similarly to internal viscosity η, exponent p is also temperature dependent (Figure 18), it is also sensitive to Gly-Ala exchange at position 193 and shows a phase transition at 293 K.

This power-law dependence (Eq 27) was explained frequently in qualitative ways, e.g. suggesting that the effect of solvent viscosity is transferred by the protein or that solvent composition is modified around the protein (7, 22, 27). The concepts of macro and microviscosity - the viscosity of the bulk solvent and around the protein, respectively - are often mentioned, which refer to the observation that viscosity in the solution may be heterogeneous. Others gave more quantitative explanations to the power-law dependence: Yedgar et al. established an empirical relationship between exponent p and the molecular weight of the cosolvent (16). Another related and frequently cited theory is the frequency-dependent friction (135), which is based on the idea that the reduced one dimensional reaction coordinate entails memory effects causing nonlinear dependence of friction on solvent viscosity. These examples illustrate that exponent p is difficult to interpret. To our knowledge Zwanzig's model has not been generalized, therefore our observations about exponent p, its temperature dependence and its change upon a Gly-Ala change in HuTry4 are not discussed further.

5.5. The ultimate model with fundamentally new concepts - Model #5

In our model with elastically coupled reaction coordinates we combine and relate flexibility, roughness of the energy landscape and friction. The primary driving force that created this model was that we could not believe that the observed parallel Arrhenius plots (Figure 22) were just a coincidence. It seemed unlikely that internal viscosity and the energy barrier would combine in such a special way that they create a seemingly identical energy barrier (Figure 28). This new model proves that the energy barriers are really identical and these identical energy landscapes can produce very different viscosity dependence and internal viscosity values. Our new model is consistent with our observations (see beginning of this section (5.4.)) and uses two parallel, elastically coupled reaction coordinates as a single reaction coordinate was insufficient to describe all observations (Figure 29).

The model was also inspired by an important idea from the folding literature. It is widely accepted that the energy landscape has a hierarchical structure (1, 2)(Figure 1). An early study for calculating the absolute value for roughness of the energy landscape was a study on cyt c folding (68): they calculated the absolute value for energy landscape roughness from temperature and viscosity dependence data based on a theoretical calculation about the effect of energy landscape roughness on the diffusional constant (136). Recently, also internal friction was connected to the roughness of the energy landscape (11). More specifically, based on the same theoretical basis (136), the measured internal viscosity difference between two spectrin domain mutants during folding was hypothesized to arise from the difference in the roughness of their energy landscapes (11), even though in the latter study temperature dependence was not investigated. Following the line of thought of these two papers, in our model the height of roughness of the energy landscape was identified with ΔE_σ, the activation energy for internal friction, in the temperature dependence of internal viscosity (Eq 12, Eq 23).

$$\sigma(T) = \sigma_0 \exp\left(\frac{\Delta E_\sigma}{k_B T}\right) \qquad \text{Eq 28}$$

For the effect of roughness on the effective diffusional coefficient two historical formulae are well-known. For periodic roughness the effective diffusional coefficient (D^*) has an Arrhenius like temperature dependence (137):

$$D^* \propto \exp(-2\varepsilon / k_B T) \quad \text{Eq 29}$$

where 2ε is the height of the roughness. For non periodic roughness where fluctuations in the potential have Gaussian distribution with a root mean square of ε, the diffusional constant depends on temperature in a non-Arrhenius fashion (136):

$$D^* = \exp\left[-(\varepsilon / k_B T)^2\right] \quad \text{Eq 30}$$

, where D* is the effective diffusional coefficient, D is the diffusional coefficient, ε is the root mean squared roughness. The latter formula (Eq 30) is slightly misleading because the dramatic slowing effect is mainly due to the assumption about Gaussian distribution of barrier heights, which allows infinitely high energy barriers with very low probability. Therefore in our model with rough energy landscape we always assume Arrhenius-like temperature dependence.

5.5.1. The mathematical and/or physical basics

The basis of our model is a theoretical calculation with two parallel, elastically coupled reaction coordinates (Figure 31 A). The common, net movement, what an external observer would observe can be numerically modeled if we apply external forces to the two coordinates. Effects of viscosity on the system were studied by changing the friction coefficient along the coordinates. For the description of both viscosity and temperature dependence of the system, the numerical simulations produce a relationship (Figure 31 B) where the height of roughness is partitioned to two energy components. Note that this is very similar to our observation, we also observed two energy components in the temperature and viscosity dependence of the rate constant (Eq 13). The partitioning depends on the strength of the coupling between the two coordinates (Figure 31 C). The effect of partitioning is illustrated by the apparent, common energy landscape of the parallel reaction coordinates (Figure 31 D). Depending on the flexibility of coupling either the height of roughness stays high or the friction along the reaction coordinate increases. In conclusion, if we relate these calculations to our observations, in an elastically coupled system, some part of the rough energy barrier will increase the as 'activation energy' of internal friction for the movement.

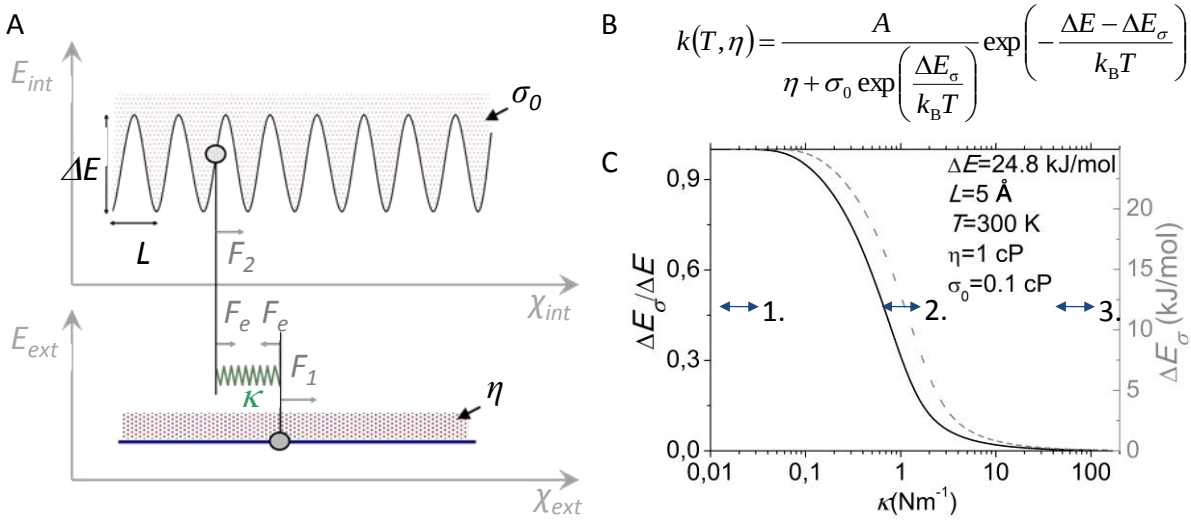

D

κ region coupling strength	**1. flexible κ<<ΔE/L²**	**2. intermediate κ≈ΔE/L²**	**3. rigid κ>>ΔE/L²**
ΔE_σ	~25 kJ/mol	~12 kJ/mol	~0 kJ/mol
σ_{300K}	2200 cP	15 cP	0.1 cP
$\Delta E_A=\Delta E-\Delta E_\sigma$	~0 kJ/mol	~12 kJ/mol	~25 kJ/mol
apparent energy landscape of the common reaction coordinate		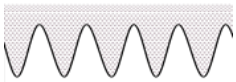	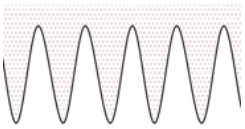

Figure 31 The model with two elastically coupled reaction coordinates

A) Two parallel reaction coordinates (χ_{int} and χ_{ext}) are coupled to each other elastically. The strength of the coupling is characterized by the spring constant κ, the viscosity along the reaction coordinates is characterized by σ_0 and η, and there is a harmonic, rough potential with height ΔE and width L along one of the coordinates. The common, net movement, what an external observer would observe can be numerically modeled if we apply two external forces, F_1 and F_2 to the two coordinates and we assume that due to the coupling the imaginary spring exerts force F_e on both coordinates. (Fig 7 in (138), modified) B) The numerical calculations produce the result that the energy barrier of the observed net movement is partitioned to two components. C) An example on how the energy barrier partitioning depends on the coupling strength if the reaction takes place at 300 K, and we assume that the height of the energy barrier, ΔE is 10 k_BT=25 kJ/mol, the width of the rougness, L is 5 Å and the viscosities along the reaction coordinates are σ_0=1cP and η=1 cP. As κ increases, the ratio of $E_\sigma/\Delta E$ decreases (left axis). On the right axis the corresponding values of E_σ are also plotted. Three distinct regions of κ values are marked. D) For the three different κ regions the observed net energy landscapes are characterized and illustrated based on the calculation results from C. σ_{300K} is the observed internal friction at 300 K.

5.5.2. The energy landscape for trypsinogen activation

Based on the above described model with two elastically coupled reaction coordinates, we envisioned the energy landscape of the activation of trypsin mutants in a way that depending on the flexibility of the enzyme different hierarchical levels of the

roughness of the energy landscape appear as energy barriers or as 'activation energy' of internal friction (Figure 32). We are aware of the speculative nature of these energy landscape representations, therefore they are meant to be rather thought-provoking illustrations.

From the fitting parameters for both mutants in high and low ionic strength conditions in Table 8, a consensus energy landscape was estimated for HuTry4 activation (Figure 32 C). The overall height of the energy landscape i.e. the slope of the Arrhenius plots varies between 70-80 kJ/mol, depending on solution conditions and mutation (Figure 22), therefore the height of the consensus energy landscape is shown as 75 kJ/mol (Figure 32). Where the temperature dependence of internal viscosity is high (193G and 193A above 293K, in low ionic strength buffer), the average of ΔE_σ is 60 kJ/mol, which is associated with the 1st level of roughness on the energy barrier. The lower values of ΔE_σ (high ionic strength buffer and 193A below 293K) are very inaccurate, for the illustration we estimated that the height of the 2nd level of roughness is 10 kJ/mol.

This consensus energy landscape has three different hierarchical levels, and depending on the conditions and the type of measurement, different apparent energy landscapes are observed. While Arrhenius plots will always result in 75 kJ/mol activation energy barrier height, viscosity-dependence measurements will result in different values for internal viscosity, depending on the flexibility. For completely rigid coupling, internal viscosity would be constant at all temperatures (Figure 32 D). For intermediate coupling, where the movements along the reaction coordinate can be separated by a distance measurable to the width of the 2nd level of roughness, this 2nd level of roughness will be associated with internal viscosity (Figure 32 E). This is a likely scenario for 193A HuTry4 in low ionic strength buffers, below 293 K. For loose coupling, where the separation of the reaction coordinates can be as great as the width of the 1st level of roughness, the temperature dependence of internal viscosity will further increase (Figure 32 F). This is what we see for 193G HuTry4 in low ionic strength buffer.

Consequently, the model with elastically coupled reaction coordinates resolved the question of how we should interpret the two energy values and the parallel Arrhenius plots. A more detailed analysis of the model revealed that it has other interesting consequences as well: i) it resolves the contradiction with previous literature

findings by explaining how the more flexible enzyme is less sensitive to viscosity. ii) it is consistent with the picture that the rate constant of the more rigid enzyme is lower than that of the more flexible one. In the next sections I briefly describe these important characteristics and consequences in more detail.

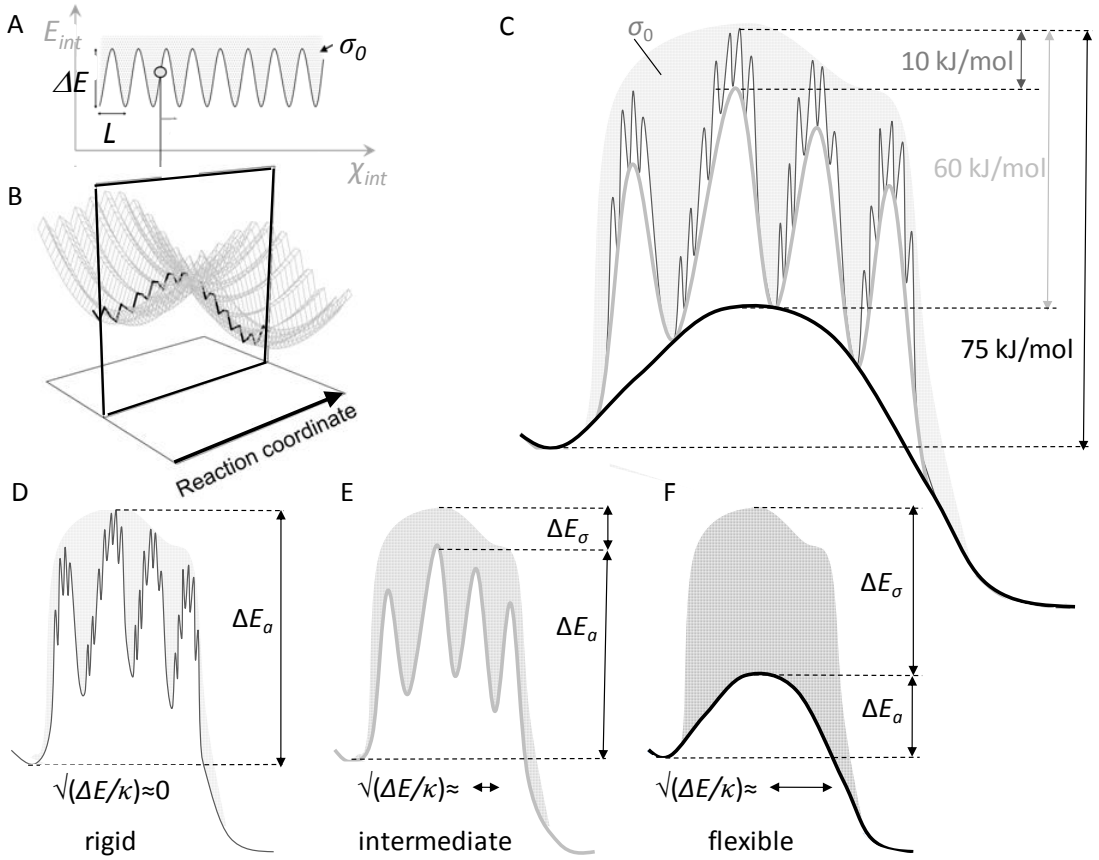

Figure 32 Schematic representation of the hierarchical structure of the energy barrier

A) For the simplified illustration of the model of elastically coupled reaction coordinates the traditional depiction of a single-coordinate energy landscape can be used, provided that we include a note on the elasticity of the coupling. The internal reaction coordinate from the model on Figure 31 is shown here as a reminder. B) To relate this new model to the preliminary models, roughness is integrated into the saddle-like energy barrier from Figure 29. The cross section of the saddle is shown on C-F. C) The hierarchical structure of the energy landscape for HuTry4 activation, energy values are estimated from the fitting parameters in Table 8. D-F) Apparent energy landscapes depending on the flexibility defined by arrows along the reaction coordinate. The length of the arrow shows the possible separation of the two reaction coordinates. D) Rigid coupling, none of the roughness is transformed to internal viscosity, ΔE_σ=0, the whole height of the energy barrier appears as ΔE_a. E) A moderately elastic coupling, where the small-scale roughness results in internal viscosity, e.g. 193A HuTry4, low ionic strength, T<293 K. F) Very flexible coupling, where all roughness is partitioned to the internal viscosity part, e.g. 193G HuTry4 in low ionic strength buffer.

5.5.3. Flexibility and internal viscosity

So far in the literature it was found that the more rigid structures are less sensitive to viscosity (see Introduction Section 1.6. Figure 4). In contrast to this, our observation was that the supposedly more flexible trypsin with Gly hinge was less sensitive to viscosity. The contradiction may lie in the vague concept of flexibility. Below, I describe how our model can resolve this contradiction by defining flexibility.

In the literature of viscosity-dependence and internal viscosity, flexibility is defined in different ways. Our assumption about the flexibility of the two mutants, i.e. 193G HuTry4 is more flexible than 193A HuTry4, is based on the fact that the backbone rotational angles of the Gly residues are more free to move than those of any other residues. This was also confirmed by short molecular dynamics simulations of the two trypsin mutants. The details of the simulations can be found in the Appendix (Section A5), where the difference in flexibility is illustrated with Ramachandran plots of the 193Ala and 193Gly residues (Supplementary Figure 5). Other examples of flexibility describe the phenomenon by other measures: i) an electrostatic complex of a pair of metalloproteins (Cytochrome c and plastocyanin or cytochrome c and cytochrome b5) is considered more flexible than the covalently bound complex of the same proteins (30, 80) ii) multiexponential fluorescence lifetime decays and lower quantum yields were considered as signs of flexibility in case of the photocromic fluorescent protein, dronpa (45). These different observations, i.e. the variations in dihedral angles, the variation in bonding between domains and the multiexponential timecourse of decay all lead to the same assumption that flexibility varies between the objects under examination. However, flexibility has not been quantified or defined any further.

We already mentioned in the introduction that there is consensus in the literature that the increased amplitude of the movement will cause greater sensitivity to viscosity (Figure 4 and (20, 21, 29, 87)). How does this fit with the above mentioned flexibility descriptions? i) In case of the covalent vs. electrostatic complex, it is reasonable to assume that flexibility involves a greater-amplitude conformational change. Kostic and coworkers also mention that the viscosity-dependence observed for the more flexible, electrostatic complex is probably due to a conformational change that is not allowed in the rigid, covalent complex (30). ii) The multi exponential decay for the fluorescent protein, dronpa means that there are some new, different routes for decay

compared to the non-mutant with single exponential decay. If some of these new routes involve conformational changes with greater amplitudes, consistently with literature, the flexible dronpa mutant will be more sensitive to viscosity due to the increased amplitude of movement. Therefore it seems that in these cases, flexibility can be defined by the amplitude of movement and viscosity dependence of the reactions will agree with the observations about the effect of amplitude change on viscosity dependence.

Our description about more flexible dihedral angles does not contain any assumption on the change in amplitude of movement, which can explain the different viscosity dependence results. The model with two elastically coupled reaction coordinates defines flexibility as a measure of coupling between the parallel movements within the enzyme-solvent system. A strong or rigid coupling means that the conformational change happens at the same time on each "venue" (e.g. both inside the protein and at the protein-solvent interface), while a weak or flexible coupling means that the two movements may be partially sequential because of the elastic property of the hinge and/or the moving domain (138). There is no assumption on any change in the path or amplitude of the movement upon a change in flexibility.

These two different definitions of flexibility are illustrated on Figure 33, similarly to Figure 4 in the Introduction (Section 1.6). Flexibility v.1 is the measure of the amplitude of the movement, whereas flexibility v.2 is the measure of coupling between two different sites, where movement occurs. In conclusion, the greater amplitude movements (flexibility v.1) are more sensitive to solvent viscosity while the elastically coupled movements (flexibility v.2) are less sensitive to viscosity.

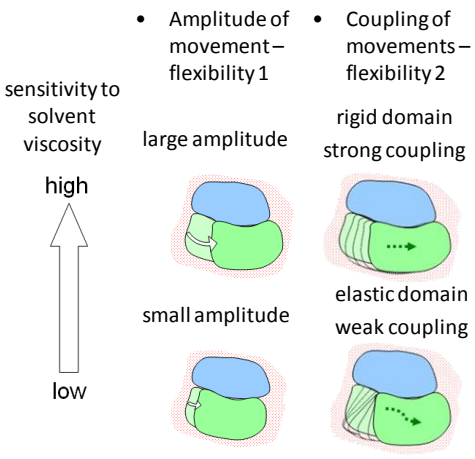

Figure 33 Definitions of flexibility: amplitude of the movement or coupling between two movements

The two different types of flexibility are illustrated on two protein domains sliding along each other (see Figure 4). Based on the first definition of flexibility, in the more flexible enzyme, the displacement of the lower domain (indicated by the arrows) is greater. In the second definition of flexibility, when the lower domain is elastic, the internal displacement and the external movement are decoupled, in this example the internal displacement precedes the external movement.

5.5.4. Flexibility, internal viscosity and rate of reactions

In the original assumption by Kramers (Eq 1), which has been simplified and adapted to enzyme reactions by Ansari (Eq 2), internal viscosity is assumed to influence the preexponential term in the Arrhenius equation:

$$k(T,\eta) = \frac{A}{\sigma + \eta} \exp\left(\frac{-\Delta E_a}{k_B T}\right) \qquad \text{Eq 31}$$

This has been interpreted for trypsin activation in a way that, as the Arrhenius plots were parallel (Figure 12 C and Figure 22) and the difference between the mutants was visible in the preexponential, so the mutants were assumed to have different internal viscosities. This produced a consistent image that the preexponential term depended on internal viscosity and higher internal viscosity was responsible for slowing down the reaction rate.

With our model this situation changes: internal viscosity was found to be related to an energy barrier (Eq 28, Eq 23, Eq 12), therefore we derive it from the roughness of the energy landscape. This way internal viscosity practically became a new 'embodiment' of the energy barrier; as the value of σ is substantial in the denominator, its energy component (ΔE_σ) will affect the slope of the Arrhenius plot, together with ΔE_a.

$$k(T,\eta) = \frac{A}{\eta + \sigma_0 \exp\left(\frac{\Delta E_\sigma}{k_B T}\right)} \exp\left(-\frac{\Delta E_a}{k_B T}\right) \qquad \text{Eq 32}$$

It seems that viscosity dependence measurements revealed that the energy barrier consists of two parts: one part is the traditional barrier, the other part is responsible for friction, but this distinction remains hidden when only the temperature dependence is investigated (Figure 32). It is now more challenging to assign the 10 times slower rate of the more rigid 193A HuTry4 to internal viscosity. Especially as we found that the faster 193G HuTry4 has higher internal viscosity (Figure 17).

Fortunately, the observation that the faster enzyme has higher internal viscosity is also consistent with the model with elastically coupled reaction coordinates. From analytical calculations (see BOX 4 for details) it is apparent that if we assume identical conditions and only change the coupling between the reaction coordinates, the more elastic, more flexible enzyme will always be faster. The two extremities, completely rigid coupling, and completely flexible coupling can be calculated arithmetically. The calculations provide the viscosity dependence of the rates of the infinitely rigid and the

infinitely elastic coupling. From the formulae it is visible that for identical energy landscapes and external conditions the rigid enzyme will always be slower than the flexible enzyme:

$$k_{\text{rigid}} \propto \frac{1}{(\eta+\sigma_0)c\exp\left(\frac{\Delta E}{k_B T}\right)} < k_{\text{flex}} \propto \frac{1}{\eta+\sigma_0 c\exp\left(\frac{\Delta E}{k_B T}\right)} \qquad \text{Eq 33}$$

From this relationship it is also apparent that an elastic enzyme will have higher internal viscosity than a rigidly coupled enzyme if other conditions remain unchanged. Therefore the model is consistent with the observation that the more rigid 193A HuTry4 is slower and has lower internal viscosity.

BOX 4 Analytical calculation of the relaxation time as a function of the height of roughness and friction along the reaction coordinates (Appendix from (138))

To determine the effective friction coefficient of the coupled system (Figure 31 A), we apply two constant external forces (F1 and F2) to the two reaction coordinates, and calculate their average speed (which is necessarily the same for both of them). When the coupling is very rigid ($\kappa L^2 >> \Delta E$), i.e., when the expansion of the spring to distance L requires much more energy than climbing an energy barrier, the two reaction coordinates can be considered as a single one with an effective friction coefficient $\gamma_{\text{eff}} = \gamma_{\text{ext}} + \gamma_{\text{int}}$ moving in the superposition of the two energy landscapes with barriers of height ΔE. Their average speed is thus:

$$v_{\text{rigid}} = \frac{F_1+F_2}{(\gamma_{\text{ext}}+\gamma_{\text{int}})c\exp\left(\frac{\Delta E}{k_B T}\right)} \qquad \text{Eq 34}$$

where c is a geometrical factor and it is approximately $k_B T/(\pi\Delta E)$ for sinusoidal potentials (136, 137).

For a very flexible coupling ($\kappa L^2 << \Delta E$) the two coordinates will be separated long apart, and the elastic element will exert an essentially constant elastic force (F_e) on both of them (with opposite signs). Their speed can thus be written as:

$$v_{\text{flex}} = \frac{F_1 - F_e}{\gamma_{\text{ext}}} \qquad \text{Eq 35} \qquad\qquad v_{\text{flex}} = \frac{F_2 + F_e}{\gamma_{\text{int}} c\exp\left(\frac{\Delta E}{k_B T}\right)} \qquad \text{Eq 36}$$

The solution of this system of equations gives:

$$v_{\text{flex}} = \frac{F_1+F_2}{\gamma_{\text{ext}}+\gamma_{\text{int}} c\exp\left(\frac{\Delta E}{k_B T}\right)} \qquad \text{Eq 37}$$

indicating that the barriers of the internal reaction coordinates is translated into the activation energy of the internal friction, resulting in an effective friction coefficient $\gamma_{\text{eff}} = \gamma_{\text{ext}} + \gamma_{\text{int}}\, c\exp(\Delta E/(k_B T))$ for the coupled system.

5.5.5. Limitations of the model

Our model provides the simplest explanation to our observations in many aspects. For example, unlike the models with single reaction coordinates (Figure 29) this model does not use any assumption about the homogeneity or heterogeneity of friction or roughness along the energy landscape. Even though our model elegantly fits the observations it remains phenomenological as without quantifying the flexibility or coupling strength within the enzymes we are not able to make predictions or characterize the structure of the roughness along the reaction coordinate. However, the

rationality of the model is strengthened by the fact that if we assume κ=1 Nm^{-1} with nm-scale protein movements and a roughness of ΔE=10 k_BT we get a Young modulus of 1 GPa, which is a reasonable value for an average protein (139). Moreover, from the observed 10-times difference between 193A and 193G HuTry4 reaction rates we estimate that the roughness is minimum 2.3 k_BT (see Appendix, Section A6 for more detailed calculation).

5.6. Viscosity dependence of Dictyostelium myosin ATP-N binding is very weak.

There are few data on the viscosity dependence measurements on myosin. Chase et al investigated the viscosity dependence on the contraction of skinned muscle fibers (48). They found that the rate of isometric tension development and shortening velocity are affected by viscosity and their conclusion was that the crossbridge diffusion is rate limiting. Later they continued their research on purified proteins and found (51) that the sliding speed of actin filaments in an in vitro motility assay decreases with viscosity. When solvent drag or osmolality were excluded as possible reasons for the slowing, it was suggested that viscosity acts directly on the myosin head. The ATPase activity of HMM in solution however was practically unaffected by viscosity below 10 cP. Only above 10 cP was a marked slowing observed.

Our observation that the ATP-N binding to the myosin head is not sensitive to viscosity in the region 0.5-2.5 cP correlates with the finding that ATPase activity of HMM was not affected by viscosity below 10 cP. From the HuTry4 data and the model with elastically coupled reaction coordinates we learnt that it is possible that in case of flexible, elastically coupled movements, high internal friction, and weak viscosity dependence are observed. This implicates that in myosin the conformational changes at the nucleotide binding site, switch 1 and switch 2 and the lever movement might be able to uncouple. This possible uncoupling is mentioned in the myosin literature from a different point of view: Davis and Epstein (140) after measuring the temperature-dependence of reverse and forward rate of tension generation concluded that 'local unfolded tertiary and/or secondary structure of the actomyosin cross-bridge mediates the power stroke'. They also provided a more detailed thermodynamic model for the power-stroke (141). The partial unfolding found by Davis and Epstein and the

potentially uncoupled movements deduced from the viscosity-insensitivity nicely complement each other. This coincidence is very promising and proves that there is potential in viscosity-dependence data.

5.7. Latest findings in the folding literature

Internal viscosity is gaining more and more interest in the field of protein dynamics. Even though folding is a supposedly different conformational change, we already saw that the observations about the temperature and viscosity dependence of cyt c folding from a compact state (68) were identical to our observations about the temperature and viscosity dependence of trypsin activation (Discussion Sections 5.2 and 5.4.1.). Previously (11) the viscosity dependence of slow and fast folding spectrin domains was investigated. The slow folding variants were less sensitive to viscosity; therefore the slow folding was associated with high internal viscosity. This internal viscosity was attributed to roughness in the energy landscape and was found to arise from frustration in the folding mechanism due to misdockings. Recently (12), the slowing effects of internal viscosity and the height of the energy barrier have been separated in the same spectrin variants: by elegant mutations folding was accelerated 40x, but the viscosity-dependence profile remained unchanged. Wensley et al derived that the mutations decreased the energy barrier i.e. the energy of the transition state, but the frustrated type of folding mechanism remained unchanged, thus internal viscosity was responsible for a 5x slowing. Another interesting study on the same spectrin domains revealed that in the two-step folding, the relaxation time of the second step is proportional to viscosity, while the first step is significantly less sensitive to viscosity (13). This way internal friction could be localized along the reaction coordinate: it was attributed to the first energy barrier, i.e. transition state of folding.

Unfortunately, without the temperature-dependence data for spectrin domains it is difficult to relate the observations to any quantitative model of the energy landscape at the moment. These data would be valuable as spectrin domains are also relatively little and fold relatively fast in a one-step or two-step reaction, therefore the observations and the theoretical consequences are likely to be relevant to enzyme reactions as well.

6. Conclusion and perspectives

This work was centered around three specific questions, i) What can we learn about the physical background of the empirically introduced internal friction parameter by measuring its temperature dependence? ii) What can we learn about the relationship of internal friction and the structural properties of enzymes? iii) How can we model the observed viscosity and temperature dependence of reactions, how can we relate internal viscosity and the well known parameters of the energy landscape?

We found that internal viscosity has an Arrhenius like temperature dependence, which suggests that similarly to the viscosity of liquids or other friction it is related to barrier crossing events. By re-analyzing earlier literature on viscosity and temperature dependence, we found that our observations about the temperature dependence of internal viscosity are also true for other reactions on very different timescales. Based on the observation that the more flexible enzyme had higher internal viscosity while the overall energy barrier calculated from the Arrhenius plot remained unchanged, we constructed a model with elastically coupled reaction coordinates that related the hierarchical roughness of the energy landscape, flexibility and internal friction of enzymes. Moreover, the model resolved two apparent contradictions: i) We distinguished flexibility as a greater amplitude movement from flexibility as elasticity and explained why they react to viscosity in opposite ways. ii) Our model explains why in case of identical energy barriers the more flexible enzyme with greater internal viscosity is faster.

Future plans of the project include the detailed computational modeling of the in vitro experiments and the behavior of the hypothesized hierarchical energy landscape. As a first approach, numerical simulations on the model with elastically coupled reaction coordinates can extend our understanding on the dynamics of reactions on rough, hierarchical surfaces. Another approach is to do molecular dynamics simulations on the same HuTry4 enzyme, the viscosity dependence of the fluctuations within the protein will be measurable and the effect of Gly to Ala exchange can also be tested, this way the whole in vitro experiment can be repeated in silico.

Another, currently running project is related to the fluctuating bottleneck model, which can account for the power dependence of the rate constant on viscosity. As this model was constructed for ligand escape by Zwanzig, it would be interesting to construct a

conclusive, comprehensive model with similar perpendicular reaction coordinates for a more general conformational change that could account for our observations, i.e. the temperature dependence of exponent *p* and its sensitivity to mutation.

An unexpected result of the model with elastically coupled reaction coordinates is that viscosity dependence data can be a valuable tool to detect the strength of the coupling between the conformational changes within an enzyme. Measurements with the viscosity dependence of myosin nucleotide binding nicely correlate with the hypothesis from the literature that movements might be uncoupled during the enzymatic cycle of myosin. Myosin is a well studied system in our lab and there are several Trp mutants available that report on the conformational change at different sites. Examples in Dictyostelium myosin 2 include W239 at switch 1 loop, W586, W416 at the actin binding cleft, W501 at the lever arm. Myosins with two Trp residues could therefore be the first candidates for testing coupling.

Summary

In protein dynamics the protein internal forces, especially internal friction recently became the focus of interest. In this thesis the physical and structural background of the empirically introduced internal viscosity parameter is approached by measuring its temperature dependence and the effect of mutation on its value. More specifically, the temperature dependence of internal viscosity was determined by measuring systematically the viscosity (0.6-6 cP) and temperature (275-313K) dependence of human trypsin 4 (HuTry4) activation upon a pH jump by transient kinetic methods, using maltose as viscogen. HuTry4 activation is a conformational change when four loops bordered by Gly residues rearrange by rotation, therefore a hinge-like role is attributed to the bordering Gly residues. The structural background of internal friction is approached by determining the effect of a Gly-Ala exchange at the hinge position 193 on the internal viscosity of HuTry4 activation. Internal viscosity was found to have an Arrhenius-like temperature-dependence, which suggests that an energy barrier is associated with the internal friction phenomenon. Moreover, while the Gly-Ala exchange slowed HuTry4 activation, it decreased both the value and the temperature dependence of internal viscosity during activation. Based on the results we constructed a coherent energy landscape model for HuTry4 activation, which attributes the roughness of the energy landscape to internal friction. Our model with two elastically coupled reaction coordinates explains why increased flexibility can lead to an increase in internal viscosity.

Összefoglalás

Az utóbbi években a fehérje dinamikai kutatások fókuszába kerültek a fehérjékben fellépő belső erők, különösen a belső súrlódás. Ezen tézis az eredetileg empirikusan bevezetett belső viszkozitás paraméter fizikai és szerkezeti hátterét a hőmérsékletfüggésén keresztül valamint mutációs analízissel vizsgálja. A belső viszkozitás hőmérsékletfüggését a humán tripszin 4 (HuTry4) enzim aktivációjának szisztematikus viszkozitás- és hőmérsékletfüggéséből határoztuk meg (0,6-6 cP és 275-313 K tartományon) tranziens kinetikai módszerrel, mely során az aktivációt pH ugrással váltottuk ki, a viszkozitás szabályozására pedig maltózt használtunk. A HuTry4 aktiváció olyan konformációváltozás, mely során négy, glicinekkel határolt hurok átrendeződik, átforog, ezért a határoló glicineknek csukló-szerű szerepet tulajdonítanak. A belső súrlódás szerkezeti hátterének vizsgálatakor a 193-as csukló pozícióban történt glicin-alanin cserét vizsgáltuk, hogyan hat a csere a HuTry4 aktiváció belső viszkozitására. A belső viszkozitást Arrhenius-szerű hőmérsékletfüggés jellemzi, tehát feltételezhetjük, hogy valamiféle energiagáttal összefüggő jelenségről van szó. Ezenkívül kimutattuk, hogy bár a glicin-alanin csere lassítja a HuTry4 aktivációt, a folyamat belső viszkozitása és annak hőmérsékletfüggése is csökken. Az eredményeink alapján modelleztük a HuTry4 aktiváció energiagátjának hierarchikus szerkezetét, melyben a belső súrlódást kis energiagátak okozzák. A modellben két, egymással elasztikusan kapcsolt koordinátát használtunk, melyek jól magyarázzák miért nő a belső viszkozitás, ha növeljük a flexibilitást.

Appendix

A.1. Measured rate constants

Supplementary table 1

HuTry4 193A

low ionic strength buffer

k: rate constant, s^{-1}

T: temperature, K

M: [maltose], M

T(K)	M	k ()
275	0	0.0365
275	0.1	0.0387
275	0.2	0.0354
275	0.3	0.0311
275	0.4	0.0284
275	0.5	0.0278
275	0.6	0.0254
275	0.7	0.0226
278	0	0.0504
278	0.1	0.0567
278	0.2	0.0491
278	0.3	0.0445
278	0.4	0.0392
278	0.5	0.0384
278	0.6	0.0414
278	0.7	0.0331
281	0	0.0772
281	0.1	0.0792
281	0.2	0.0705
281	0.3	0.0613
281	0.4	0.0572
281	0.5	0.0539
281	0.6	0.0522
281	0.7	0.0462
284	0	0.107
284	0.1	0.0977
284	0.2	0.0952
284	0.3	0.1
284	0.4	0.078
284	0.5	0.0722
284	0.6	0.0752
284	0.7	0.0635
287	0	0.147
287	0.1	0.145
287	0.2	0.14
287	0.3	0.129
287	0.4	0.121
287	0.5	0.107
287	0.6	0.118
287	0.7	0.0931
290	0	0.194
290	0.1	0.201
290	0.2	0.186
290	0.3	0.193
290	0.4	0.15
290	0.5	0.14
290	0.6	0.166
290	0.7	0.134
290	0.8	0.116
293	0	0.253
293	0	0.273
293	0.1	0.281
293	0.2	0.25
293	0.3	0.251
293	0.4	0.224
293	0.5	0.21
293	0.6	0.231
293	0.7	0.173
293	0.8	0.186
293	0.9	0.188
296	0	0.354
296	0.1	0.373
296	0.2	0.3
296	0.3	0.303
296	0.4	0.304
296	0.5	0.283
296	0.6	0.34
296	0.7	0.263
296	0.8	0.281
296	0.9	0.283
299	0	0.418
299	0	0.543
299	0.1	0.554
299	0.1	0.488
299	0.2	0.526
299	0.2	0.359
299	0.3	0.483
299	0.4	0.466
299	0.5	0.477
299	0.5	0.415
299	0.6	0.457
299	0.7	0.47
299	0.8	0.365
299	0.9	0.372
302	0	0.778
302	0.1	0.611
302	0.2	0.655
302	0.3	0.532
302	0.4	0.501
302	0.5	0.549
302	0.5	0.484
302	0.6	0.618
302	0.7	0.57
302	0.8	0.508
302	0.9	0.494
305	0	1.366
305	0.1	1.083
305	0.1	0.804
305	0.2	0.716
305	0.2	0.742
305	0.3	0.819
305	0.4	0.73
305	0.5	1.046
305	0.5	0.864
305	0.6	1.012
305	0.7	0.607
305	0.8	0.619
305	0.8	0.633
305	0.9	0.696
308	0	1.623
308	0.1	1.541
308	0.2	1.082
308	0.3	0.988
308	0.4	0.984
308	0.5	1.267
308	0.5	0.993
308	0.6	1.139
308	0.7	0.963
308	0.8	0.915
308	0.8	0.897
308	0.9	0.916
308	0.9	0.995
311	0	2.678
311	0	1.177
311	0.1	1.575
311	0.1	1.582
311	0.2	2.142
311	0.2	1.351
311	0.3	1.517
311	0.4	1.620
311	0.5	1.236
311	0.5	2.046
311	0.6	0.845
311	0.7	1.442
311	0.8	1.134
311	0.8	1.145
311	0.9	1.001

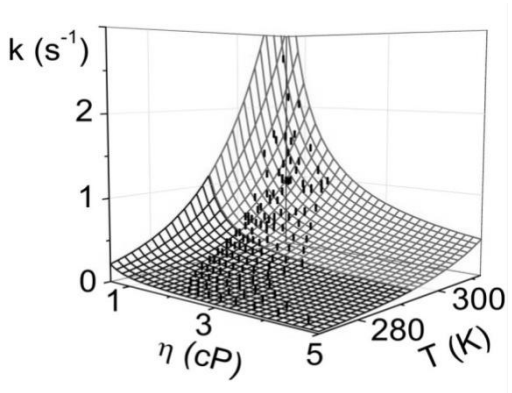

Supplementary Figure 1 Rate constant vs temperature and viscosity for HuTry4 193A in low ionic strength buffer (Fig 2C from (138))

Supplementary table 2

HuTry4 193G

low ionic strength buffer

k: rate constant, s^{-1}

T: temperature, K

M: [maltose], M

T	M	k
275	0.0	0.306
275	0.1	0.343
275	0.2	0.286
275	0.3	0.315
275	0.4	0.330
275	0.5	0.316
275	0.6	0.291
275	0.7	0.321
275	0.8	0.232
275	0.9	0.320
278	0.0	0.372
278	0.1	0.484
278	0.2	0.415
278	0.3	0.411
278	0.4	0.455
278	0.5	0.368
278	0.6	0.350
278	0.7	0.432
278	0.8	0.372
278	0.9	0.379
281	0.0	0.567
281	0.1	0.793
281	0.2	0.685
281	0.3	0.682
281	0.4	0.601
281	0.5	0.466
281	0.6	0.511
281	0.7	0.674
281	0.8	0.497
281	0.9	0.602
281	1.0	0.471
284	0.0	0.745
284	0.1	0.805
284	0.2	0.928
284	0.3	0.916
284	0.4	0.710
284	0.5	0.694
284	0.6	0.781
284	0.7	0.625
284	0.8	0.806
284	0.9	0.887
284	1.0	0.709
287	0.0	1.338
287	0.1	1.491
287	0.2	1.502
287	0.3	1.555
287	0.4	1.129
287	0.5	0.846
287	0.6	1.046
287	0.7	1.124
287	0.8	1.140
287	0.9	1.282
287	1.0	1.078
290	0.0	1.614
290	0.1	1.555
290	0.2	2.014
290	0.3	2.053
290	0.4	1.561
290	0.5	1.044
290	0.6	1.496
290	0.7	1.370
290	0.8	1.331
290	0.9	1.517
293	0.0	2.465
293	0.1	2.399
293	0.2	2.605
293	0.3	2.850
293	0.4	1.920
293	0.5	1.695
293	0.6	2.328
293	0.7	2.200
293	0.8	1.481
293	0.9	2.033
293	1.0	2.184
296	0.0	2.957
296	0.1	3.118
296	0.2	2.987
296	0.3	3.953
296	0.4	2.063
296	0.5	1.798
296	0.6	3.029
296	0.7	2.130
296	0.8	2.708
296	0.9	2.265
296	1.0	2.210
299	0.0	4.735
299	0.1	4.921
299	0.2	4.527
299	0.3	3.022
299	0.4	4.156
299	0.5	3.156
299	0.6	5.066
299	0.7	2.616
299	0.8	3.344
299	0.9	4.350
299	1.0	2.780
302	0.0	6.305
302	0.1	5.516
302	0.2	6.954
302	0.3	6.079
302	0.4	5.208
302	0.5	3.106
302	0.6	5.441
302	0.7	4.264
302	0.8	5.141
302	0.9	5.139
302	1.0	4.100
305	0.0	7.541
305	0.1	7.294
305	0.2	8.032
305	0.3	6.821
305	0.4	7.559
305	0.5	4.936
305	0.6	7.220
305	0.7	6.406
305	0.8	5.845
305	0.9	5.203
305	1.0	5.447
308	0.0	12.579
308	0.1	8.826
308	0.2	13.298
308	0.3	10.111
308	0.5	10.101
308	0.6	8.123
308	0.7	8.032
308	0.8	8.889
308	0.9	9.025
308	1.0	6.427
311	0.0	14.641
311	0.1	13.298
311	0.2	16.367
311	0.3	10.010
311	0.4	13.986
311	0.5	9.814
311	0.6	7.174
311	0.7	12.063
311	0.8	11.123
311	0.9	8.306
311	1.0	9.434

mT-		jump
303	0.0	7.435
308	0.0	10.806
313	0.0	21.992
318	0.0	32.865
323	0.0	59.455
328	0.0	72.548
333	0.0	98.722

Supplementary table 3

HuTry4 193G

high ionic strength buffer

k: rate constant, s^{-1}

T: temperature, K

M: [maltose], M

M	T	k
0	275.15	0.317
0	278.15	0.441
0	281.15	0.599
0	284.15	0.837
0	287.15	1.581
0	290.15	2.295
0	293.15	3.142
0	296.15	3.902
0	299.15	4.943
0	302.15	6.681
0	305.15	10.67
0	308.15	13.96
0	311.15	16.28
0.2	275.15	0.332
0.2	278.15	0.547
0.2	281.15	0.693
0.2	284.15	1.100
0.2	287.15	1.378
0.2	290.15	2.028
0.2	293.15	2.795
0.2	296.15	4.545
0.2	299.15	5.794
0.2	302.15	9.179
0.2	305.15	10.070
0.2	308.15	12.030
0.2	311.15	15.220
0.3	275.15	0.275
0.3	278.15	0.417
0.3	281.15	0.701
0.3	284.15	0.966
0.3	287.15	1.395
0.3	290.15	1.885
0.3	293.15	2.748
0.3	296.15	3.834
0.3	299.15	4.541
0.3	302.15	5.473
0.3	305.15	7.769
0.3	308.15	12.230
0.3	311.15	17.230
0.4	272.15	0.189
0.4	275.15	0.249
0.4	278.15	0.349
0.4	281.15	0.528
0.4	284.15	0.826
0.4	287.15	1.270
0.4	290.15	1.742
0.4	293.15	2.390
0.4	296.15	2.801
0.4	299.15	4.015
0.4	302.15	5.268
0.4	305.15	7.544
0.4	308.15	10.570
0.4	311.15	13.080
0.05	275.15	0.297
0.05	278.15	0.450
0.05	281.15	0.646
0.05	284.15	1.045
0.05	287.15	1.410
0.05	290.15	1.869
0.05	293.15	2.689
0.05	296.15	3.304
0.05	299.15	4.534
0.05	302.15	6.250
0.05	305.15	9.337
0.05	308.15	12.100
0.05	311.15	16.870
0.15	275.15	0.336
0.15	278.15	0.434
0.15	281.15	0.646
0.15	284.15	1.034
0.15	287.15	1.442
0.15	290.15	2.174
0.15	293.15	2.529
0.15	296.15	3.384
0.15	299.15	4.675
0.15	302.15	5.822
0.15	305.15	6.117
0.15	308.15	10.71
0.15	311.15	15.14
0.25	275.15	0.284
0.25	278.15	0.495
0.25	281.15	0.733
0.25	284.15	1.113
0.25	287.15	1.592
0.25	290.15	2.032
0.25	293.15	2.739
0.25	296.15	3.150
0.25	299.15	4.502
0.25	302.15	6.878
0.25	305.15	9.336
0.25	308.15	10.510
0.25	311.15	18.190
0.1	279.15	0.3635
0.1	281.15	0.659
0.1	284.15	1.0605
0.1	287.15	1.576
0.1	290.15	1.945
0.1	293.15	3.277
0.1	296.15	3.845
0.1	299.15	5.507
0.1	302.15	7.547
0.1	305.15	10.102
0.1	308.15	14.069
0.1	311.15	19.363
0.35	284.15	1.197
0.35	287.15	1.512
0.35	290.15	1.802
0.35	293.15	2.498
0.35	296.15	3.146
0.35	299.15	3.703
0.35	302.15	5.106
0.35	305.15	7.205
0.35	308.15	12.353
0.35	311.15	21.669
0.45	290.15	2.169
0.45	293.15	2.921
0.45	296.15	4.588
0.45	299.15	4.840
0.45	302.15	7.236
0.45	305.15	9.775
0.45	308.15	12.130
0.45	311.15	15.730

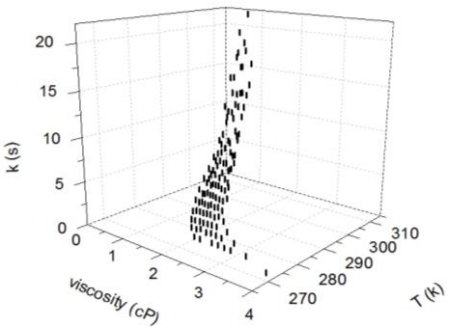

Supplementary Figure 2 Rate constant vs temperature and viscosity for HuTry4 193G in high ionic strength buffer

Supplementary table 4

HuTry4 193A

high ionic strength buffer

k: rate constant, s^{-1}

T: temperature, K

M: [maltose], M

M	T	k
0	278.15	0.0708
0	281.15	0.104
0	284.15	0.140
0	287.15	0.216
0	290.15	0.292
0	293.15	0.389
0	296.15	0.502
0	299.15	0.711
0	302.15	0.878
0	305.15	1.194
0	308.15	1.497
0	311.15	1.813
0.2	278.15	0.0657
0.2	281.15	0.0924
0.2	284.15	0.131
0.2	287.15	0.178
0.2	290.15	0.246
0.2	293.15	0.330
0.2	296.15	0.415
0.2	299.15	0.551
0.2	302.15	0.726
0.2	305.15	1.063
0.2	308.15	1.100
0.3	278.15	0.0651
0.3	281.15	0.0827
0.3	284.15	0.111
0.3	287.15	0.171
0.3	290.15	0.248
0.3	293.15	0.317
0.3	296.15	0.390
0.3	299.15	0.602
0.3	302.15	0.772
0.3	305.15	0.924
0.3	308.15	1.147
0.3	311.15	1.582
0.4	278.15	0.0552
0.4	281.15	0.081
0.4	284.15	0.112
0.4	287.15	0.168
0.4	290.15	0.255
0.4	293.15	0.306
0.4	296.15	0.425
0.4	299.15	0.544
0.4	302.15	0.684
0.4	305.15	0.982
0.4	308.15	1.165
0.4	311.15	1.625
0.5	278.15	0.055
0.5	281.15	0.0761
0.5	284.15	0.105
0.5	287.15	0.142
0.5	290.15	0.197
0.5	293.15	0.313
0.5	296.15	0.409
0.5	299.15	0.482
0.5	302.15	0.654
0.5	305.15	0.933
0.5	308.15	1.160
0.1	278.15	0.0631
0.1	281.15	0.0925
0.1	284.15	0.128
0.1	287.15	0.183
0.1	290.15	0.261
0.1	293.15	0.337
0.1	296.15	0.429
0.1	299.15	0.601
0.1	302.15	0.786
0.1	305.15	0.994
0.1	308.15	1.418
0.1	311.15	1.731

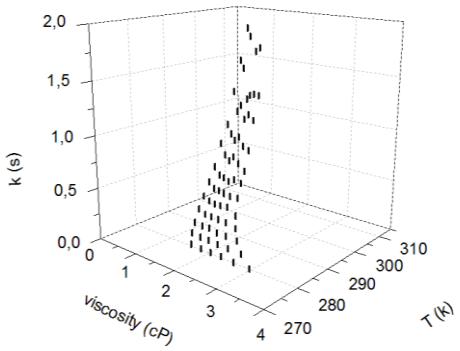

Supplementary Figure 3 Rate constant vs temperature and viscosity for HuTry4 193A in high ionic strength buffer

A.2. Raw data of viscosity measurements

T	Viscosity (cP) of solutions with 50mM HEPES, 150 mM NaCl, varying maltose										
(^{o}C)	[maltose] M										
	0	0,1	0,2	0,3	0,4	0,5	0,6	0,7	0,8	0,9	1
6,5	1,52	1,71	1,92	2,22	2,52	2,73	3,31	3,95	-	5,34	6,57
10	1,31	1,44	1,63	1,86	2,13	2,30	2,72	3,17	3,88	4,54	5,45
15	1,12	1,24	1,40	1,57	1,78	1,94	2,32	2,68	3,21	3,75	4,55
20	0,89	1,07	1,21	1,33	1,52	1,75	1,96	2,18	2,60	3,04	3,57
25	0,86	0,97	1,08	1,18	1,35	1,55	1,69	1,90	2,21	2,70	3,13
30	0,78	0,87	0,97	1,06	1,19	1,37	1,49	1,67	1,94	2,26	2,65
35	0,72	0,79	0,88	0,96	1,07	1,23	1,33	1,49	1,68	2,00	2,26
40	0,65	0,72	0,80	0,86	0,97	1,11	1,20	1,33	1,49	1,74	1,97
	Viscosity (cP) of solutions with 50mM HEPES and varying maltose										
T	[maltose] M										
(^{o}C)	0	0,1	0,2	0,3	0,4	0,5	0,6	0,7	0,8	0,9	1
6,5	1,45	1,71	2,01	2,11	2,24	2,57	3,20	3,58	4,16		5,72
10	1,31	1,42	1,58	1,82	1,92	2,21	2,68	3,02	3,97	3,85	4,69
15	1,14	1,25	1,36	1,57	1,66	1,87	2,28	2,51	2,95	3,18	3,97
20	1,00	1,08	1,16	1,27	1,38	1,55	1,92	2,07	2,42	2,50	3,19
25	0,89	0,98	1,05	1,14	1,22	1,40	1,68	1,78	2,09	2,28	2,71
30	0,80	0,87	0,93	1,02	1,12	1,25	1,52	1,53	1,80	2,01	2,34
35	0,72	0,79	0,83	0,92	1,01	1,14	1,34	1,40	1,59	1,76	2,05
40	0,65	0,72	0,75	0,83	0,93	1,02	1,19	1,23	1,41	1,56	1,85

Supplementary table 5 Viscosity measurement data

A.3. ATP-N binding to myosin

The fluorescent traces of ATP-N binding to myosin 2 motor domain were fitted with the following triple exponential equation:

$$Fluorescence(t) = A_1 \exp(-k_1 t) + A_2 \exp(-k_2 t) + A_3 \exp(-k_3 t) + slope \cdot t + offset \qquad \text{Eq 38}$$

where each of the three phases is characterized by an amplitude A and a corresponding rate constant *k*. The *slope* and *offset* parameters correct for the baseline of the fitting.

The resulting fitting parameters are presented in Supplementary table 6.

T (K)	[maltose] (M)	η (cP)	A_1	k_1	A_2	k_2	A_3	k_3	*slope*	*offset*
282.45	0	1.41	-0.13	6.2	-0.174	0.821	0.144	372	0.0020	1.24
282.45	0.5	2.38	-0.0996	7.13	-0.097	0.649	0.104	267	0.0020	1.24
289.65	0	1.05	-0.154	21.2	-0.2065	2.4	0.061	420	0.0020	1.23
289.65	0.5	1.78	-0.046	30.5	-0.056	2.55	0.019	403	0.0020	1.24
293.15	0	0.94	-0.137	32.9	-0.171	3.81	0.04	570	0.0014	1.022
293.15	0.5	1.59	-0.09	47.1	-0.08	3.66	0.035	693	0.0020	1.218
297.65	0	0.82	-0.148	62.3	-0.154	7.04	0.069	917	0.0020	0.997
297.65	0.5	1.39	-0.185	72.6	-0.12	5.25	0.06	953	0.0015	1.151

Supplementary table 6 Fitting parameters for the ATP-N binding of myosin

A.4. Calculating internal friction from published data

For the cyt c folding reaction from a compact state, the following fitting data have been published by Pabit et al (68):

$$\tau_s(T, \eta_s) = A\eta_s \exp(\Delta H/k_B T) \qquad \Delta H = 19 \pm 7 \text{ kJ/mol} \qquad A \approx 1.88 \text{ ns/(mPa s)} \qquad \text{Eq 39}$$

$$\tau_{int}(T) = B \exp(\Delta E/k_B T) \qquad \Delta E = 67 \pm 16 \text{ kJ/mol} \qquad B \approx 8.31 \times 10^{-18} \text{ s} \qquad \text{Eq 40}$$

Note that the original nomenclature is presented above, which differs from the nomenclature used throughout this thesis. The above described fitting parameters relate to our parameters and the concept of internal friction used throughout the thesis by

$$1/k(T,\eta) = \tau_s(\eta) + \tau_{int} = (\eta/A)e^{\Delta E_a/(RT)} + (\sigma_0/A)e^{(\Delta E_a + \Delta E_\sigma)/(RT)} \qquad \text{Eq 41}$$

The temperature dependence of internal friction presented throughout the thesis can be derived from the published fitting parameters to cyt c folding data and calculated as

$$\sigma(T) = \sigma_0 \exp\left(\frac{\Delta E_\sigma}{k_B T}\right) = B/A \exp\left(\frac{\Delta E - \Delta H}{k_B T}\right) \qquad \text{Eq 42}$$

(on the left side of the equation the nomenclature of this thesis, on the right side nomenclature from the publication by Pabit et al is used)

This equation gives the following function: $\ln(\sigma \text{ cP}^{-1}) = \ln(4.42*10^{-9}) + 5773 \text{ K}/T$, which is presented on Figure 23 in Discussion Section 5.2.

For other data internal viscosity was calculated from fitting the viscosity dependence of the published rate constants (Supplementary Figure 4). There are some extremely high viscosity data where deviation is found from linearity e.g. electron transfer reaction above 25 cP, which data were excluded from the calculations (Supplementary Figure 4 B). The NO spin label dynamics were measured in an extremely wide range of viscosities from 0-10000 cP (Supplementary Figure 4 C), the viscosity dependence deviates from linearity as early as above 500 cP, so the exclusion of any data would have been rather arbitrary, therefore all data were included in the linear fit. Consequently, the resulting internal viscosity values have to be considered rather an upper limit to internal viscosity. The nonlinear viscosity dependence might be an inherent characteristic of the system, but it can be equally likely that other properties of the solvent, e.g. dielectric

constant, water content, etc… also influence the rate constant, causing deviation from linear viscosity dependence.

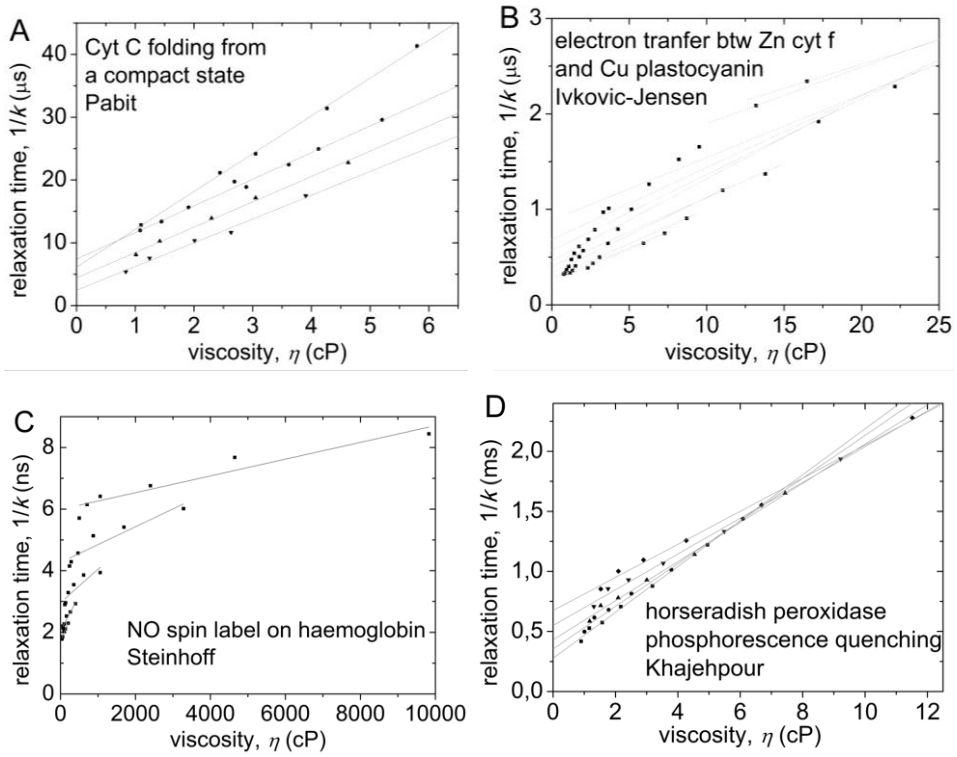

Supplementary Figure 4 Viscosity dependence of reactions in the literature

The relaxation time vs viscosity data were collected for four systematic measurements. The grey lines represent linear fits to the isothermal data (rate constants collected at identical temperature and changing viscosity) Internal viscosity was calculated from the fits. A) Cyt c folding, only the data with glycerol are available B) electron transfer reaction, only data with viscosity below 25 cP are illustrated for clarity C) dynamics of a hemoglobin-bound NO spin label D) phosphorescence quenching in horseradish peroxidase.

A.5. Molecular dynamics simulations of trypsin 193G and 193A variants

From the public database the crystal structures 1TGB and 2PTN (bovine trypsinogen and trypsin, respectively) were prepared for molecular dynamics simulation: hydrogens were added, His protonation was calculated for a neutral pH and position 193 was either kept as Gly or changed to Ala. Cl^- ions were added to neutralize any charge. The simulations were run in explicit water. The scripts for the heating, preliminary energy minimization and the simulation in equilibrated states can be found below (BOX 5).

The Ramachandran plots for residue 193 show that the Gly residue occupies a greater area on the Ramachandran plot both in the active (2PTN, Supplementary Figure 5 A) and in the zymogen (1TGB, Supplementary Figure 5 B) structure. This observation indicates that Gly is more flexible than Ala.

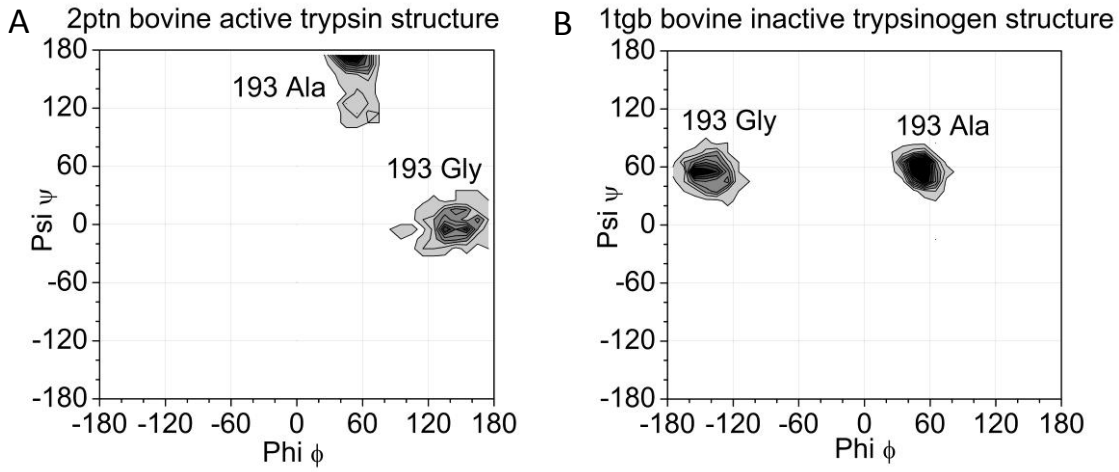

Supplementary Figure 5 Flexibility of residue 193

Ramachandran plots (142) for position 193 are derived from MD simulations of the A) active and B) zymogen forms of bovine trypsin, PDB ID 2PTN and 1TGB, respectively. The contour plots show the distribution of the dihedral angles during the molecular dynamics simulation. Position 193 is either Gly or Ala as indicated by the labels.

BOX 5: Collection of scripts used for MD simulations

Heating script: 10ps MD with restriction on protein

```
 &cntrl
  imin   = 0,  //molecular dynamics are run
  irest  = 0,  ntx = 1,  //not restart,
  ntb    = 1, //uses constant volume periodic boundaries
  cut    = 12, //value for the non-bonded cut off (Angstrom)
  ntr    = 1, //uses position restraints based on the GROUP input (here the original pdb
structure)
  ntc    = 2,  ntf  = 2, //SHAKE should be turned on and used to constrain bonds involving
hydrogen
  tempi  = 0.0,  temp0  = 300.0, // heating from 0K to 300K
  ntt    = 3,  gamma_ln = 1.0, //Langevin thermostat, L. dynamics collision frequency
  nstlim = 5000, dt = 0.002 //5000 steps, 2 fs time step
  ntpr = 100, ntwx = 100, ntwr = 1000 //Write to the output file (NTPR) every 100 steps, to
the trajectory file (NTWX) every 100 steps and write a restart file (NTWR), in case our job
crashes and we want to restart it, every 1,000 steps.
 /
Keep protein fixed with weak restraints
10.0     //force constant of 10 kcal mol-1 angstrom-2
RES 1 223  //all residues
END
END
```

min1:**initial minimisation water + Cl ions**

```
 &cntrl
  imin   = 1, //minimization
  maxcyc = 100, //100 steps
  ncyc   = 50, //50 steps in steepest descent algorithm, other 50 is conjugate gradient
method
  ntb    = 1, //uses constant volume periodic boundaries
  ntr    = 1, //uses position restraints based on the GROUP input (here the original pdb
structure)
  cut    = 12 //value for the non-bonded cut off (Angstrom)
 /
Hold the protein fixed
500.0  //force constant of 500 kcal mol-1 angstrom-2
RES 16 245 //all residues fixed
END
END
```

min2: **initial minimisation whole system**

```
 &cntrl
  imin   = 1,   //minimization
  maxcyc = 500, //500 steps
  ncyc   = 250, /250 steps in steepest descent algorithm, other 250 is conjugate gradient
method
  ntb    = 1,   //uses constant volume periodic boundaries
  ntr    = 0,  //no position restraints
  cut    = 12  //value for the non-bonded cut off (Angstrom)
 /
```

simulation in equilibrium 1: MD with no restriction on protein

```
 &cntrl
  imin   = 0, //molecular dynamics are run
  irest  = 1,  ntx = 5, //restart a simulation
  ntb    = 1,  //uses constant volume periodic boundaries
  cut    = 12,  //value for the non-bonded cut off (Angstrom)
  ntc    = 2,  ntf  = 2,  //SHAKE should be turned on and used to constrain bonds involving
hydrogen
  tempi  = 300.0,  temp0  = 300.0, //constant temperature, 300K
  ntt    = 3,  gamma_ln = 1.0, //Langevin thermostat, L. dynamics collision frequency
  nstlim = 100000, dt = 0.002 //100000 steps, 2 fs time step
  ntpr = 100, ntwx = 100, ntwr = 1000 //Write to the output file (NTPR) every 100 steps, to
the trajectory file (NTWX) every 100 steps and write a restart file (NTWR), in case our job
crashes and we want to restart it, every 1,000 steps.
 /
```

A.6. Rate of reactions and flexibity

Here we present a theoretical calculation for the height of roughness within the energy landscape for HuTry4 activation, which is based on the observation that the more flexible mutant, 193G is 10 times faster than 193A. The factor of 10 between the measured rates can only apply, if the ratio of the theoretical maximum and minimum rates (i.e. the rates for the infinitely flexible and infinitely rigid theoretical trypsin variants, respectively) is at least 10. The theoretical maximum and minimum rates are given as (Eq 34 and Eq 37in Box 4):

$$k_{flex}(T,\eta)=\frac{A}{\eta+\sigma_0\exp\left(\frac{\Delta E_\sigma}{k_B T}\right)}\exp\left(-\frac{\Delta E_a}{k_B T}\right);\ k_{rigid}(T,\eta)=\frac{A}{(\eta+\sigma_0)\exp\frac{\Delta E_\sigma}{k_B T}}\exp\left(-\frac{\Delta E_a}{k_B T}\right) \qquad \text{Eq 43}$$

The ratio of the two rates can be expressed as:

$$\frac{(\eta+\sigma_0)\exp\frac{\Delta E_\sigma}{k_B T}}{\eta+\sigma_0\exp\left(\frac{\Delta E_\sigma}{k_B T}\right)}\geq 10 \qquad \text{Eq 44}$$

After rearrangements we get the following relationship for the height of roughness and solvent viscosity:

$$\exp\frac{\Delta E_\sigma}{k_B T}\geq\frac{10\eta}{\eta-9\sigma_0} \qquad \text{Eq 45}$$

Based on the fitting results in Table 8 we can assume: $\eta >> \sigma_0$ Eq 46

For the resulting barrier height we get: $\frac{\Delta E_\sigma}{k_B T}\geq \ln 10\approx 2.3$ Eq 47

A.7. Expression and purification of HuTry4 enzyme constructs

A.7.1. DNA constructs

The coding sequence for the original wild type HuTry4 was amplified from a commercial human pancreatic cDNA library (Stratagen, no. 937208) with the following oligo- nucleotide primers: HuTry4_upstream: 5'GCT GAA GCT TTC CCC GTT GAC GAT GAT GAC 3', HuTry4_downstream: 5' GAC TGC AGA GCT CCC GGG GGC TTT AGC 3'. The product was subcloned into the Escherichia coli expression vector pTRAP with HindIII (5' end) and SacI (3' end). To increase expression yield the vector was replaced: after digestion with HindIII and SalI the HuTry4 gene was ligated into a modified pET17b vector cut with HindIII and XhoI. The modified pET17b vector contained an adaptor composed of oligonucleotides AGCTTGGGTCGAC and ATATGTCGACCCA between restriction sites NdeI and HindIII instead of the T7 flag to shift the reading frame at the HindIII site.

The 193G and 193A mutations at position 193 were introduced by the megaprimer PCR mutagenesis method using the following primers: HuTry4_R193G: 5' TCC TGC CAG GGT GAC TCC GGT GGC 3' HuTry4_R193A: 5' TCC TGC CAG GCT GAC TCC GGT GGC 3' (Invitrogen, Carlsbad, CA). The PCR products were ligated to pBluescript vector via TA-ligation and were sequenced. Mutant genes were subcloned into the modified pET17b vector as described above for the wild type.

A.7.2. Expression, refolding, purification and activation of the proteins

The proteins were expressed in cultures of BL21(DE3)pLysS E. coli cells transformed with the modified pET17b vectors. Cultures were grown at 37°C in 250 ml Luria-Bertrami medium with 0.4% ampicillin and induced with 0.1 mM isopropyl-1-thio-b-D-galactopyranoside for 4 h after reaching 0.5 absorbance at 600 nm. After centrifugation and lysis with sonication, the inclusion body was washed 3 times with 50ml washing buffer. The pellet was dissolved in 4 ml reducing buffer and was kept for 30 min at 37 °C. The this way denatured and reduced trypsinogen was rapidly diluted into 125 ml of ice-cold, deaerated re-folding buffer and was slowly stirred under N_2 at 4 °C for 16 h.

The trypsinogen solution was exhaustively dialyzed against 2.5 mM HCl, then centrifuged. The clear supernatant was loaded onto a cation-exchange column (SP-Superose FF) and washed. Further purification on an anion-exchange MonoQ column

(5/5), and on a soybean trypsin inhibitor-Sepharose column followed. The latter one served to remove trypsin contamination. The solution was immediately acidified by adding HCl to 30 mM final concentration, and kept in aliquots at -20 °C.

Trypsinogen activation was done in activation buffer with adding porcine enterokinase in a 1:1000 molar ratio. This was followed by affinity purification on benzamidine-Sepharose column with 10mM HCl as elution buffer. The protein containing elution fractions were pooled, concentrated with ultrafiltration using a Centricon filter unit (Amicon) and kept in aliquots at - 20 °C. The theoretical extinction coefficient ε_{280} = 40570 $M^{-1}cm^{-1}$ was used for determining protein concentration. Purity was assessed by 15% SDS-PAGE using the Laemmli buffer system (143). The concentration of the prepared enzymes could also be determined by active site titration with 4-methylumbelliferyl 4-guanidinobenzoate (144).

Luria-Bertrami medium	10.0g Tryptone, 5.0g Yeast extract and 5.0g NaCl in 1000 ml of distilled water, pH 7.0 ± 0.2
inclusion body washing buffer	0.1 M TrisHCl, 2 mM EDTA, pH 8.0
inclusion body reducing buffer	6 M guanidine-HCl, 0.1 M Tris-HCl, pH 8.5, 2 mM EDTA containing 30 mM dithiothreitol, 37°C
re-folding buffer	0.9 M guanidine hydrochloride, 0.1 M Tris-HCl, pH 8.5, 2 mM EDTA, 1 mM L-cysteine, and 1 mM L-cystine, 4°C, deaerated, N^2 saturated
cation-exchange equilibration buffer	25 mM LiOAc, pH 4.0
cation-exchange washing buffer	25 mM LiOAc, pH 4.0, 0–1 M NaCl gradient
anion exchange buffer	20 mM Tris-HCl, pH 8.8, 1 mM EDTA
activation buffer	50 mM Tris-HCl pH 8.0, 100 mM NaCl, 10 mM $CaCl_2$
Laemmli 2x sample buffer	62.5 mM Tris-HCl, pH 6.8, 25% glycerol, 2% SDS, 0.01% Bromophenol Blue, 5% β-mercaptoethanol (710 mM)

Supplementary table 7 Buffers used in the expression and purification of HuTry4 protein

Acknowledgement

This work could not have been done without the work and support of many colleagues.

Most of all I am thankful to my supervisor, András Málnási-Csizmadia, who is a great scientist and an exceptional team leader. I learnt many things from him. To set clear scientific goals and not to investigate phenomena *l'art pour l'art'*, to celebrate and be thankful for every little progress, to focus on important things and not to be deterred by unimportant issues, to trust people and expect responsibility from everyone. He creates the luxury that surrounds us in the lab. I thank him the many opportunities for travel abroad to conferences, courses, consultations, or in the frame of collaboration. I am glad that I could work on several projects and learn a wide range of things. In this project about internal friction he always kept the focus and was aware of the significance of the results, pushed me to go on, which was really encouraging.

Imre Derényi is the person who introduced me to the world of biophysics. It was a challenging world, as the frustrated energy landscapes and their literature can easily become a source of frustration for beginners. Not for him, he did not seem to be frustrated at all. He is really at home in biophysics concepts, and he always seems to find some elegant way that simplifies the message of the published formulae. He is very critical and you can trust the accuracy and consistency of his models. He optimized the fitting of the data and we had long conversations about what our experimental results could mean. He had several enlightening/inspiring ideas and he is the father of the theoretical model, including the details, the numerical simulations and arithmetic calculations.

For decades, Professor László Gráf has been considering the role of flexibility in enzyme mechanism, which thought initiated the examination of the physical background of internal friction. He is an internationally acknowledged expert on serine proteases. He studied HuTry4 and its relatives deeply and he initiated the use of trypsin as a model object for this project. From his research group Julia Toth started the pioneering work on internal friction, she adapted the transient kinetic method, pH jump from chymotrypsin studies. The HuTry4 proteins were expressed and precisely purified by Vilmosné Énekes, I am very grateful for the excellent quality of the enzymes, which made my work much easier. Besides the initiation and the practical help, Professor László Gráf contributed to the theoretical work of the project by very good questions and he was also a prominent teacher during my years at the PhD school.

I joined the project under the leadership of Zoltán Simon, who had conducted the high ionic strength measurements and all the viscosity measurements as well. He was the one who taught me the basics in the lab from the first day on. He has been an invaluable help since then. I admire his precision in handling data files, I learnt a lot

from him, even when he was just listening. He was also very kind to help in proofreading my thesis. Besides Zoli, Máté Gyimesi and Bálint Kintses as senior students also set the example how to work in the lab. Bálint especially helped me a lot as part of a cooperation with Cambridge.

Balázs Jelinek, our scientific manager is a key person in the lab, providing the invisible machine that we all benefit from, which makes the work so smooth. He seems to know everything. I enjoy both working with him and discussing the big issues of life. Besides him, I am thankful to three other people in the lab who provide general support to all of us. We can never value enough the lab order that Ica Ozoróczyné strictly keeps around us. György Hegyi is also someone who has invaluable experience in organic synthesis and fixing things. I enjoy when he talks about the know-hows. Kitti Szamosvölgyi is both a very efficient and a very friendly help in organizing many lab-related issues.

Many of us, students spent years together in 'Malnalab', our research group. I've always enjoyed the different subprojects which we participated in together. I have good memories of the days when Boglárka Várkuti taught me how to work with E.coli. We also "inherited" myosin-projects from each other, Bogi taught me how to measure myosin fluorescence, nucleotide binding, ATPase activity… She is very precise, effective and practical. Miklós Képiró helped me with many software-related issues, which made my life much easier. He also introduced me for a short time to the world of organic synthesis. I like his straightforward manner, perfectionism and honesty about his results. László Végner is one of the most reliable people I know. He helped me in a lot of small things, finding recipes, making a solution. His work proves me that precision creates value. I learnt the basics of molecular dynamics simulations from Zhenhui Yang, Jackie. He changed my attitude towards computer-related problems with setting the example how not to be frustrated when facing a puzzling situation with any kind of software. Probably István Lőrincz is the one I spent the most extreme times together. He is the guy who never runs out of questions, and constantly challenges himself, and pushes his barriers further and further. He doesn't know the word impossible. I'm glad I know him. Ágnes Peragovics is the first from our generation of PhD students, who recently "flew from the nest". She joined one of my favorite ex-projects and she took it to success. We spent a lot of time together, even outside the lab. She witnessed most of my life and encouraged me when I felt low. It was great to have her around as a friend.

Moreover, I am glad that László Nyitray leads the department in a way that there is a very friendly atmosphere, people are very helpful and flexible, which makes the place one of the best departments of the institute. This atmosphere is further supported by the assistants of the department, Kati Kurucz Váradi, Hajnalka Németh, Anna Engel, Éva Magyar. We have a very good cooperative relationship with our neighbors, Stocilab, the common retreats were both relaxing and scientifically inspiring. Mihály Kovács, the PI, has always been open to help in transient kinetics and myosin issues or when I needed a good book. And all of his students, especially Nikolett Nagy, Kata Sarlós, Gábor Harami,

Balázs Takács, Zsuzsa Kocsis helped me in any urgent case when we ran out of gels or plates or antibiotics, restriction enzymes or needed some competitive strain of E.coli. From the rest of the department, I am especially thankful to Bence Kiss, László Radnai, Dániel Süveges, Péter Rapali from the Nyitray Lab, the whole Reményi Lab, especially András Zeke, Ágnes Garai, Gábor Glatz, Anita Alexa, Marianna Rakács, János Varga, and Dávid Héja, Dávid Szakács, József Kardos. Special thanks to Gábor Pál, who carefully read and criticized in detail my master thesis, the first cornerstone of my friction studies.

Besides my colleagues, I am thankful to my family, who have always supported me in my studies and my work. I am very lucky that my parents were interested in the research I was doing, they kept asking questions and sometimes even helped me to prepare for presentations.

The illustrations of the preliminary energy landscapes were done by the graphical artist, Tamás Cserna.

References

1. Henzler-Wildman, K.,Kern, D. (2007) Dynamic personalities of proteins, *Nature 450*, 964-972.
2. Ansari, A., Berendzen, J., Bowne, S. F., Frauenfelder, H., Iben, I. E., et al. (1985) Protein states and proteinquakes, *Proc Natl Acad Sci U S A 82*, 5000-5004.
3. Frauenfelder, H., Chen, G., Berendzen, J., Fenimore, P. W., Jansson, H., et al. (2009) A unified model of protein dynamics, *Proc Natl Acad Sci U S A 106*, 5129-5134.
4. Arrhenius, S. (1889) "About the reaction rate during the inversion of cane sugar through acids". *Z. Phys. Chem. 4*.
5. Kramers, H. A. (1940) Brownian motion in a field of force and the diffusion model of chemical reactions, *Physica 7*, 284-304.
6. Hänggi, P., Talkner, P.,Borkovec, M. (1990) Reaction-rate theory: fifty years after Kramers, *Reviews of Modern Physics 62*, 251-342.
7. Beece, D., Eisenstein, L., Frauenfelder, H., Good, D., Marden, M. C., et al. (1980) Solvent viscosity and protein dynamics, *Biochemistry 19*, 5147-5157.
8. Ansari, A., Jones, C. M., Henry, E. R., Hofrichter, J.,Eaton, W. A. (1992) The role of solvent viscosity in the dynamics of protein conformational changes, *Science 256*, 1796-1798.
9. Frauenfelder, H., Chan, S. S. e., Chan, W. S. e., (Contributor), R. H. A., (Contributor), C. E. S., et al. (2010) *The Physics of Proteins*, Springer, New York Dordrecht Heidelberg London.
10. Ivkovic-Jensen, M. M.,Kostic, N. M. (1997) Effects of viscosity and temperature on the kinetics of the electron-transfer reaction between the triplet state of zinc cytochrome c and cupriplastocyanin, *Biochemistry 36*, 8135-8144.
11. Wensley, B. G., Batey, S., Bone, F. A., Chan, Z. M., Tumelty, N. R., et al. (2010) Experimental evidence for a frustrated energy landscape in a three-helix-bundle protein family, *Nature 463*, 685-688.
12. Wensley, B. G., Kwa, L. G., Shammas, S. L., Rogers, J. M., Browning, S., et al. (2012) Separating the effects of internal friction and transition state energy to explain the slow, frustrated folding of spectrin domains, *Proc Natl Acad Sci U S A 109*, 17795-17799.
13. Borgia, A., Wensley, B. G., Soranno, A., Nettels, D., Borgia, M. B., et al. (2012) Localizing internal friction along the reaction coordinate of protein folding by combining ensemble and single-molecule fluorescence spectroscopy, *Nat Commun 3*, 1195.
14. Soranno, A., Buchli, B., Nettels, D., Cheng, R. R., Muller-Spath, S., et al. (2012) Quantifying internal friction in unfolded and intrinsically disordered proteins with single-molecule spectroscopy, *Proc Natl Acad Sci U S A 109*, 17800-17806.
15. Lavalette, D., Tetreau, C., Tourbez, M.,Blouquit, Y. (1999) Microscopic viscosity and rotational diffusion of proteins in a macromolecular environment, *Biophys. J. 76*, 2744-2751.
16. Yedgar, S., Tetreau, C., Gavish, B.,Lavalette, D. (1995) Viscosity dependence of O2 escape from respiratory proteins as a function of cosolvent molecular weight, *Biophys. J. 68*, 665-670.
17. Hasinoff, B. B. (1981) Diffusion-controlled reaction kinetics of the binding of carbon monoxide to the heme undecapeptide of cytochrome c (microperoxidase 11) in high viscosity solvents, *Arch Biochem Biophys 211*, 396-402.

18. Ansari, A., Jones, C. M., Henry, E. R., Hofrichter, J.,Eaton, W. A. (1994) Conformational relaxation and ligand binding in myoglobin, *Biochemistry 33*, 5128-5145.
19. Goldbeck, R. A., Paquette, S. J.,Kliger, D. S. (2001) The effect of water on the rate of conformational change in protein allostery, *Biophys J 81*, 2919-2934.
20. Hagen, S. J., Hofrichter, J.,Eaton, W. A. (1995) Protein reaction kinetics in a room-temperature glass, *Science 269*, 959-962.
21. Hagen, S. J., Hofrichter, J.,Eaton, W. A. (1996) Geminate Rebinding and Conformational Dynamics of Myoglobin Embedded in a Glass at Room Temperature, *The Journal of Physical Chemistry 100*, 12008-12021.
22. Kleinert, T., Doster, W., Leyser, H., Petry, W., Schwarz, V., et al. (1998) Solvent composition and viscosity effects on the kinetics of CO binding to horse myoglobin, *Biochemistry 37*, 717-733.
23. Steinbach, P. J., Ansari, A., Berendzen, J., Braunstein, D., Chu, K., et al. (1991) Ligand binding to heme proteins: connection between dynamics and function, *Biochemistry 30*, 3988-4001.
24. Tian, W. D., Sage, J. T., Champion, P. M., Chien, E.,Sligar, S. G. (1996) Probing heme protein conformational equilibration rates with kinetic selection, *Biochemistry 35*, 3487-3502.
25. Lavalette, D.,Tetreau, C. (1988) Viscosity-dependent energy barriers and equilibrium conformational fluctuations in oxygen recombination with hemerythrin, *Eur J Biochem 177*, 97-108.
26. Young, R. D., Frauenfelder, H., Johnson, J. B., Lamb, D. C., Nienhaus, G. U., et al. (1991) Time- and temperature dependence of large-scale conformational transitions in myoglobin, *Chemical Physics 158*, 315-327.
27. Steinhoff, H. J. (1990) Residual motion of hemoglobin-bound spin labels and protein dynamics: viscosity dependence of the rotational correlation times, *Eur Biophys J 18*, 57-62.
28. Shibata, Y., Kurita, A.,Kushida, T. (1999) Solvent effects on conformational dynamics of Zn-substituted myoglobin observed by time-resolved hole-burning spectroscopy, *Biochemistry 38*, 1789-1801.
29. Finkelstein, I. J., Massari, A. M.,Fayer, M. D. (2007) Viscosity-dependent protein dynamics, *Biophys J 92*, 3652-3662.
30. Zhou, J. S.,Kostic, N. M. (1993) Gating of photoinduced electron transfer from zinc cytochrome c and tin cytochrome c to plastocyanin. Effects of solution viscosity on rearrangement of the metalloprotein complex, *Journal of the American Chemical Society 115*, 10796-10804.
31. Grove, T. Z., Ullmann, G. M.,Kostic, N. M. (2012) Simultaneous true, gated, and coupled electron-transfer reactions and energetics of protein rearrangement, *J Inorg Biochem 106*, 143-150.
32. Liu, L., Hong, J.,Ogawa, M. Y. (2004) Gated electron transfer as a probe of the configurational dynamics of peptide-protein complexes, *J Am Chem Soc 126*, 50-51.
33. Patel, A. D., Nocek, J. M.,Hoffman, B. M. (2008) Kinetic-dynamic model for conformational control of an electron transfer photocycle: mixed-metal hemoglobin hybrids, *J Phys Chem B 112*, 11827-11837.
34. Danyal, K., Mayweather, D., Dean, D. R., Seefeldt, L. C.,Hoffman, B. M. (2010) Conformational gating of electron transfer from the nitrogenase Fe protein to MoFe protein, *J Am Chem Soc 132*, 6894-6895.

35. Hay, S., Brenner, S., Khara, B., Quinn, A. M., Rigby, S. E., et al. (2010) Nature of the energy landscape for gated electron transfer in a dynamic redox protein, *J Am Chem Soc 132*, 9738-9745.
36. Gutierrez, A., Paine, M., Wolf, C. R., Scrutton, N. S.,Roberts, G. C. (2002) Relaxation kinetics of cytochrome P450 reductase: internal electron transfer is limited by conformational change and regulated by coenzyme binding, *Biochemistry 41*, 4626-4637.
37. Li, W., Fan, W., Elmore, B. O.,Feng, C. (2011) Effect of solution viscosity on intraprotein electron transfer between the FMN and heme domains in inducible nitric oxide synthase, *FEBS Lett 585*, 2622-2626.
38. Feng, C., Kedia, R. V., Hazzard, J. T., Hurley, J. K., Tollin, G., et al. (2002) Effect of solution viscosity on intramolecular electron transfer in sulfite oxidase, *Biochemistry 41*, 5816-5821.
39. Hay, S., Pudney, C. R., Sutcliffe, M. J.,Scrutton, N. S. (2008) Are environmentally coupled enzymatic hydrogen tunneling reactions influenced by changes in solution viscosity?, *Angew Chem Int Ed Engl 47*, 537-540.
40. Heyes, D. J., Sakuma, M.,Scrutton, N. S. (2009) Solvent-slaved protein motions accompany proton but not hydride tunneling in light-activated protochlorophyllide oxidoreductase, *Angew Chem Int Ed Engl 48*, 3850-3853.
41. Allemann, R. K., Evans, R. M.,Loveridge, E. J. (2009) Probing coupled motions in enzymatic hydrogen tunnelling reactions, *Biochem Soc Trans 37*, 349-353.
42. Loveridge, E. J., Evans, R. M.,Allemann, R. K. (2008) Solvent effects on environmentally coupled hydrogen tunnelling during catalysis by dihydrofolate reductase from Thermotoga maritima, *Chemistry 14*, 10782-10788.
43. Loveridge, E. J., Tey, L. H.,Allemann, R. K. (2010) Solvent effects on catalysis by Escherichia coli dihydrofolate reductase, *J Am Chem Soc 132*, 1137-1143.
44. Saxena, A. M., Udgaonkar, J. B.,Krishnamoorthy, G. (2005) Protein dynamics control proton transfer from bulk solvent to protein interior: a case study with a green fluorescent protein, *Protein Sci 14*, 1787-1799.
45. Kao, Y. T., Zhu, X.,Min, W. (2012) Protein-flexibility mediated coupling between photoswitching kinetics and surrounding viscosity of a photochromic fluorescent protein, *Proc Natl Acad Sci U S A 109*, 3220-3225.
46. Jones, A. R., Hardman, S. J., Hay, S.,Scrutton, N. S. (2011) Is there a dynamic protein contribution to the substrate trigger in coenzyme B12-dependent ethanolamine ammonia lyase?, *Angew Chem Int Ed Engl 50*, 10843-10846.
47. Kukita, F. (1997) Solvent-dependent rate-limiting steps in the conformational change of sodium channel gating in squid giant axon, *J Physiol 498 (Pt 1)*, 109-133.
48. Chase, P. B., Denkinger, T. M.,Kushmerick, M. J. (1998) Effect of viscosity on mechanics of single, skinned fibers from rabbit psoas muscle, *Biophys J 74*, 1428-1438.
49. Chase, P. B., Chen, Y., Kulin, K. L.,Daniel, T. L. (2000) Viscosity and solute dependence of F-actin translocation by rabbit skeletal heavy meromyosin, *Am J Physiol Cell Physiol 278*, C1088-1098.
50. Blacklow, S. C., Raines, R. T., Lim, W. A., Zamore, P. D.,Knowles, J. R. (1988) Triosephosphate isomerase catalysis is diffusion controlled. Appendix: Analysis of triose phosphate equilibria in aqueous solution by 31P NMR, *Biochemistry 27*, 1158-1167.

51. Chen, G., Porter, M. D., Bristol, J. R., Fitzgibbon, M. J.,Pazhanisamy, S. (2000) Kinetic mechanism of the p38-alpha MAP kinase: phosphoryl transfer to synthetic peptides, *Biochemistry 39*, 2079-2087.
52. Gavish, B. (1979) Viscosity-dependent structural fluctuations in enzyme catalysis., *Biochemistry 18*, 1269-1275.
53. Goguadze, N. G., Hammerstad-Pedersen, J. M., Khoshtariya, D. E.,Ulstrup, J. (1991) Conformational dynamics and solvent viscosity effects in carboxypeptidase-A-catalyzed benzoylglycylphenyllactate hydrolysis, *Eur J Biochem 200*, 423-429.
54. Kawai, Y., Matsuo, T.,Ohno, A. (2000) Kinetic study on conformational effect in hydrolysis of p-nitroanilides catalyzed by [small alpha]-chymotrypsin, *Journal of the Chemical Society, Perkin Transactions 2*, 887-891.
55. Khoshtariya, D. E., Hammerstad-Pedersen, J. M.,Ulstrup, J. (1991) Substrate specificity of solvent viscosity effects in carboxypeptidase A catalyzed peptide hydrolysis, *Biochim Biophys Acta 1076*, 359-363.
56. Martin, S. F.,Hergenrother, P. J. (1999) Catalytic cycle of the phosphatidylcholine-preferring phospholipase C from Bacillus cereus. Solvent viscosity, deuterium isotope effects, and proton inventory studies, *Biochemistry 38*, 4403-4408.
57. Ng, K.,Rosenberg, A. (1991) Possible coupling of chemical to structural dynamics in subtilisin BPN' catalyzed hydrolysis, *Biophys Chem 39*, 57-68.
58. Skamnaki, V. T., Owen, D. J., Noble, M. E., Lowe, E. D., Lowe, G., et al. (1999) Catalytic mechanism of phosphorylase kinase probed by mutational studies, *Biochemistry 38*, 14718-14730.
59. Tlapak-Simmons, V. L., Baron, C. A.,Weigel, P. H. (2004) Characterization of the purified hyaluronan synthase from Streptococcus equisimilis, *Biochemistry 43*, 9234-9242.
60. Uribe, S.,Sampedro, J. G. (2003) Measuring Solution Viscosity and its Effect on Enzyme Activity, *Biol Proced Online 5*, 108-115.
61. Eftink, M. R.,Hagaman, K. A. (1986) Viscosity dependence of the solute quenching of the tryptophanyl fluorescence of proteins, *Biophys Chem 25*, 277-282.
62. Somogyi, B., Punyiczki, M., Hedstrom, J., Norman, J. A., Prendergast, F. G., et al. (1994) Coupling between external viscosity and the intramolecular dynamics of ribonuclease T1: a two-phase model for the quenching of protein fluorescence, *Biochim Biophys Acta 1209*, 61-68.
63. Khajehpour, M., Troxler, T.,Vanderkooi, J. M. (2003) Effect of protein dynamics upon reactions that occur in the heme pocket of horseradish peroxidase, *Biochemistry 42*, 2672-2679.
64. Suhling, K., Davis, D. M.,Phillips, D. (2002) The Influence of Solvent Viscosity on the Fluorescence Decay and Time-Resolved Anisotropy of Green Fluorescent Protein, 91-95.
65. Gonnelli, M.,Strambini, G. B. (1993) Glycerol effects on protein flexibility: a tryptophan phosphorescence study, *Biophys J 65*, 131-137.
66. Almagor, A., Yedgar, S.,Gavish, B. (1992) Viscous cosolvent effect on the ultrasonic absorption of bovine serum albumin, *Biophys J 61*, 480-486.
67. Somogyi, B., Norman, J. A., Zempel, L.,Rosenberg, A. (1988) Viscosity and transient solvent accessibility of Trp-63 in the native conformation of lysozyme, *Biophys Chem 32*, 1-13.
68. Pabit, S. A., Roder, H.,Hagen, S. J. (2004) Internal friction controls the speed of protein folding from a compact configuration, *Biochemistry 43*, 12532-12538.

69. Hagen, S. J. (2010) Solvent viscosity and friction in protein folding dynamics, *Curr Protein Pept Sci 11*, 385-395.
70. Plaxco, K. W.,Baker, D. (1998) Limited internal friction in the rate-limiting step of a two-state protein folding reaction, *Proc Natl Acad Sci U S A 95*, 13591-13596.
71. Jacob, M., Geeves, M., Holtermann, G.,Schmid, F. X. (1999) Diffusional barrier crossing in a two-state protein folding reaction, *Nat Struct Biol 6*, 923-926.
72. Qiu, L.,Hagen, S. J. (2004) A limiting speed for protein folding at low solvent viscosity, *J Am Chem Soc 126*, 3398-3399.
73. Bieri, O., Wirz, J., Hellrung, B., Schutkowski, M., Drewello, M., et al. (1999) The speed limit for protein folding measured by triplet-triplet energy transfer, *Proc Natl Acad Sci U S A 96*, 9597-9601.
74. Jas, G. S., Eaton, W. A.,Hofrichter, J. (2000) Effect of Viscosity on the Kinetics of α-Helix and β-Hairpin Formation, *The Journal of Physical Chemistry B 105*, 261-272.
75. Cellmer, T., Henry, E. R., Hofrichter, J.,Eaton, W. A. (2008) Measuring internal friction of an ultrafast-folding protein, *Proc Natl Acad Sci U S A 105*, 18320-18325.
76. Narayanan, R., Pelakh, L.,Hagen, S. J. (2009) Solvent friction changes the folding pathway of the tryptophan zipper TZ2, *J Mol Biol 390*, 538-546.
77. Banachewicz, W., Johnson, C. M.,Fersht, A. R. (2011) Folding of the Pit1 homeodomain near the speed limit, *Proc Natl Acad Sci U S A 108*, 569-573.
78. Neuweiler, H., Johnson, C. M.,Fersht, A. R. (2009) Direct observation of ultrafast folding and denatured state dynamics in single protein molecules, *Proc Natl Acad Sci U S A 106*, 18569-18574.
79. Toth, J., Simon, Z., Medveczky, P., Gombos, L., Jelinek, B., et al. (2007) Site directed mutagenesis at position 193 of human trypsin 4 alters the rate of conformational change during activation: role of local internal viscosity in protein dynamics, *Proteins 67*, 1119-1127.
80. Qin, L.,Kostic, N. M. (1994) Photoinduced electron transfer from the triplet state of zinc cytochrome c to ferricytochrome b5 is gated by configurational fluctuations of the diprotein complex, *Biochemistry 33*, 12592-12599.
81. Scott, K. A., Batey, S., Hooton, K. A.,Clarke, J. (2004) The folding of spectrin domains I: wild-type domains have the same stability but very different kinetic properties, *J Mol Biol 344*, 195-205.
82. Wensley, B. G., Gartner, M., Choo, W. X., Batey, S.,Clarke, J. (2009) Different members of a simple three-helix bundle protein family have very different folding rate constants and fold by different mechanisms, *J Mol Biol 390*, 1074-1085.
83. Ivkovic-Jensen, M. M.,Kostic, N. M. (1996) Effects of temperature on the kinetics of the gated electron-transfer reaction between zinc cytochrome c and plastocyanin. Analysis of configurational fluctuation of the diprotein complex, *Biochemistry 35*, 15095-15106.
84. Pletneva, E. V., Fulton, D. B., Kohzuma, T.,Kostic, N. M. (2000) Protein Docking and Gated Electron-Transfer Reactions between Zinc Cytochrome c and the New Plastocyanin from the Fern Dryopteris crassirhizoma. Direct Kinetic Evidence for Multiple Binary Complexes, *Journal of the American Chemical Society 122*, 1034.
85. Rauscher, A., Derenyi, I., Graf, L.,Malnasi-Csizmadia, A. (2013) Internal friction in enzyme reactions, *IUBMB Life 65*, 35-42.
86. Ohta, Y., Mukouyama, E. B.,Suzuki, H. (2006) Kinetic isotope effect of the L-phenylalanine oxidase from Pseudomonas sp. P-501, *J Biochem 139*, 551-555.

87. Gottfried, D. S., Peterson, E. S., Sheikh, A. G., Wang, J., Yang, M., et al. (1996) Evidence for Damped Hemoglobin Dynamics in a Room Temperature Trehalose Glass, *The Journal of Physical Chemistry 100*, 12034-12042.
88. Brunger, A. T., Huber, R.,Karplus, M. (1987) Trypsinogen-trypsin transition: a molecular dynamics study of induced conformational change in the activation domain, *Biochemistry 26*, 5153-5162.
89. Matrai, J., Verheyden, G., Kruger, P.,Engelborghs, Y. (2004) Simulation of the activation of alpha-chymotrypsin: analysis of the pathway and role of the propeptide, *Protein Sci 13*, 3139-3150.
90. Wroblowski, B., Diaz, J. F., Schlitter, J.,Engelborghs, Y. (1997) Modelling pathways of alpha-chymotrypsin activation and deactivation, *Protein Eng 10*, 1163-1174.
91. Vitkup, D., Ringe, D., Petsko, G. A.,Karplus, M. (2000) Solvent mobility and the protein 'glass' transition, *Nat. Struct. Biol. 7*, 34-38.
92. Walser, R.,van Gunsteren, W. F. (2001) Viscosity dependence of protein dynamics, *Proteins 42*, 414-421.
93. Zagrovic, B.,Pande, V. (2003) Solvent viscosity dependence of the folding rate of a small protein: distributed computing study, *J Comput Chem 24*, 1432-1436.
94. Feig, M. (2007) Kinetics from Implicit Solvent Simulations of Biomolecules as a Function of Viscosity, *J. Chem. Theory Comput. 3*, 1734-1748.
95. Kossiakoff, A. A., Chambers, J. L., Kay, L. M.,Stroud, R. M. (1977) Structure of bovine trypsinogen at 1.9 A resolution, *Biochemistry 16*, 654-664.
96. Walter, J., Steigemann, W., Singh, T. P., Bartunik, H., Bode, W., et al. (1982) On the Disordered Activation Domain in Trypsinogen. Chemical Labelling and Low-Temperature Crystallography, *Acta Crystallogr. Sect.B 38*, 1462-1472.
97. Verheyden, G., Matrai, J., Volckaert, G.,Engelborghs, Y. (2004) A fluorescence stopped-flow kinetic study of the conformational activation of alpha-chymotrypsin and several mutants, *Protein Sci. 13*, 2533-2540.
98. Fersht, A. R.,Renard, M. (1974) pH dependence of chymotrypsin catalysis. Appendix: substrate binding to dimeric alpha-chymotrypsin studied by x-ray diffraction and the equilibrium method, *Biochemistry 13*, 1416-1426.
99. Heremans, L.,Heremans, K. (1989) Raman spectroscopic study of the changes in secondary structure of chymotrypsin: effect of pH and pressure on the salt bridge, *Biochim. Biophys. Acta 999*, 192-197.
100. Stoesz, J. D.,Lumry, R. W. (1978) Refolding transition of alpha-chymotrypsin: pH and salt dependence, *Biochemistry 17*, 3693-3699.
101. DeLano, W. L. (2006) PyMOL, DeLano Scientific LLC.
102. Gombos, L., Kardos, J., Patthy, A., Medveczky, P., Szilagyi, L., et al. (2008) Probing conformational plasticity of the activation domain of trypsin: the role of glycine hinges, *Biochemistry 47*, 1675-1684.
103. Bobofchak, K. M., Pineda, A. O., Mathews, F. S.,Di Cera, E. (2005) Energetic and structural consequences of perturbing Gly-193 in the oxyanion hole of serine proteases, *J Biol Chem 280*, 25644-25650.
104. KinTek Corporation Products website, http://www.kintek-corp.com/products/sf2004.php, July 10, 2013
105. BIO-LOGIC homepage, http://www.bio-logic.info/instruments/sfm-200030004000/ and http://www.bio-logic.info/rapid-kinetics-spectroscopy-bio-lab/instruments/rapid-mixing-temperature-jump-system-mt-jump/, May 5, 2013

106. Katona, G., Berglund, G. I., Hajdu, J., Graf, L.,Szilagyi, L. (2002) Crystal structure reveals basis for the inhibitor resistance of human brain trypsin, *J. Mol. Biol. 315*, 1209-1218.
107. Chi, Z., Liu, R., Yang, H., Shen, H.,Wang, J. (2011) Binding of tetracycline and chlortetracycline to the enzyme trypsin: spectroscopic and molecular modeling investigations, *PLoS One 6*, e28361.
108. UV absorption of aromatic residues, http://www.huichun.tcu.edu.tw/MMP/Amino%20Acids/doc/Amino%20Acids-64.htm, May 7, 2013
109. Hu, X., Yu, Z.,Liu, R. (2013) Spectroscopic investigations on the interactions between isopropanol and trypsin at molecular level, Spectrochim Acta A Mol Biomol Spectrosc 108, 50-54.
110. Hamamatsu Online Catalogue, http://www.hamamatsu.com/resources/pdf/etd/Xe-HgXe_TLSX1044E05.pdf, May 7, 2013
111. COMAR interference filter catalogue, http://www.comaroptics.com/components/filters/interference-filters, May 7, 2013
112. Baucke, E., Behrends, R., Fuchs, K., Hagen, R.,Kaatze, U. (2004) Kinetics of Ca2+ complexation with some carbohydrates in aqueous solutions, *J Chem Phys 120*, 8118-8124.
113. Wang, Q., Liang, K. C., Czader, A., Waxham, M. N.,Cheung, M. S. (2011) The effect of macromolecular crowding, ionic strength and calcium binding on calmodulin dynamics, *PLoS Comput Biol 7*, e1002114.
114. Vaidya, A. P., Wigent, R. J., Moore, J. C.,Schwartz, J. B. (2007) Protective effect of Carbopol on enzymatic degradation of a peptide-like substrate. I: Effect of various concentrations and grades of Carbopol and other reaction variables on trypsin activity, *Pharm Dev Technol 12*, 89-96.
115. A recipe calculator for thermodynamically correct buffers for pH control, http://www.liv.ac.uk/buffers/buffercalc.html, August 1 2008
116. Barshtein, G., Almagor, A., Yedgar, S.,Gavish, B. (1995) Inhomogeneity of viscous aqueous solutions, Phys. Rev. E. Stat. Phys. Plasm*as Fluids Relat. Interdiscip. Topics 52*, 555-557.
117. Albright, P. S. (1937) Experimental Tests of Recent Theories Descriptive of the Salting-out Effect1, *Journal of the American Chemical Society 59*, 2098-2104.
118. Weast, R. C., Astle, M. J.,Beyer, W. H., (Eds.) (1988-1989) *CRC Handbook of Chemistry and Physics*, 69th ed., CRC Press, Boca Raton, Florida.
119. Fuchs, K.,Kaatze, U. (2002) Dielectric spectra of mono- and disaccharide aqueous solutions, *The Journal of Chemical Physics 116*, 7137-7144.
120. Rampp, M., Buttersack, C.,Lüdemann, H.-D. (2000) c,T-Dependence of the viscosity and the self-diffusion coefficients in some aqueous carbohydrate solutions, *Carbohydrate Research 328*, 561.
121. Williams, T., Kelley, C.,al., E. gnuplot.
122. Szilagyi, L., Kenesi, E., Katona, G., Kaslik, G., Juhasz, G., et al. (2001) Comparative in vitro studies on native and recombinant human cationic trypsins. Cathepsin B is a possible pathological activator of trypsinogen in pancreatitis, *J. Biol. Chem. 276*, 24574-24580.
123. Toth, J., Gombos, L., Simon, Z., Medveczky, P., Szilagyi, L., et al. (2006) Thermodynamic analysis reveals structural rearrangement during the acylation

step in human trypsin 4 on 4-methylumbelliferyl 4-guanidinobenzoate substrate analogue, *J. Biol. Chem. 281*, 12596-12602.
124. Kintses, B., Simon, Z., Gyimesi, M., Toth, J., Jelinek, B., et al. (2006) Enzyme kinetics above denaturation temperature: a temperature-jump/stopped-flow apparatus, *Biophys. J. 91*, 4605-4610.
125. Jahn, W. (2007) The association of actin and myosin in the presence of gamma-amido-ATP proceeds mainly via a complex with myosin in the closed conformation, *Biochemistry 46*, 9654-9664.
126. Wray, J.,Jahn, W. (2002) Gamma-amido-ATP stabilizes a high-fluorescence state of myosin subfragment 1, *FEBS Lett 518*, 97-100.
127. Malnasi-Csizmadia, A., Pearson, D. S., Kovacs, M., Woolley, R. J., Geeves, M. A., et al. (2001) Kinetic resolution of a conformational transition and the ATP hydrolysis step using relaxation methods with a Dictyostelium myosin II mutant containing a single tryptophan residue, *Biochemistry 40*, 12727-12737.
128. Malnasi-Csizmadia, A., Woolley, R. J.,Bagshaw, C. R. (2000) Resolution of conformational states of Dictyostelium myosin II motor domain using tryptophan (W501) mutants: implications for the open-closed transition identified by crystallography, *Biochemistry 39*, 16135-16146.
129. Schlarb-Ridley, B. G., Mi, H., Teale, W. D., Meyer, V. S., Howe, C. J., et al. (2005) Implications of the effects of viscosity, macromolecular crowding, and temperature for the transient interaction between cytochrome f and plastocyanin from the cyanobacterium Phormidium laminosum, *Biochemistry 44*, 6232-6238.
130. Viswanath, D. S., Ghosh, T. K., Prasad, D. H. L., Dutt, N. V. K.,Rani, K. Y. (2007) *Viscosity of liquids*, Springer, Dordrecht.
131. de Gennes, P. G. (1979) *Scaling Concepts in Polymer Physics*, Cornell University Press, Ithaca, NY.
132. Zwanzig, R. (1992) Dynamical disorder: Passage through a fluctuating bottleneck, *J. Chem. Phys. 97*, 3587-3589.
133. Agmon, N.,Hopfield, J. J. (1982) Transient kinetics of chemical reactions with bounded diffusion perpendicular to the reaction coordinate: Intramolecular processes with slow conformational changes, *J. Chem. Phys. 78*, 6947-6959.
134. Frauenfelder, H., Fenimore, P. W., Chen, G.,McMahon, B. H. (2006) Protein folding is slaved to solvent motions, *Proc Natl Acad Sci U S A 103*, 15469-15472.
135. Grote, R. F.,Hynes, J. T. (1980) The stable state picture of chemical reactions. II., *J. Chem. Phys. 73*, 2715-2732.
136. Zwanzig, R. (1988) Diffusion in a rough potential, *Proc Natl Acad Sci U S A 85*, 2029-2030.
137. Festa, R.,d'Agliano, E. G. (1978) Diffusion coefficient for a Brownian particle in a periodic field of force : I. Large friction limit, *Physica A: Statistical and Theoretical Physics 90*, 229.
138. Rauscher, A. A., Simon, Z., Szollosi, G. J., Graf, L., Derenyi, I., et al. (2011) Temperature dependence of internal friction in enzyme reactions, *Faseb J 25*, 2804-2813.
139. Ivanovska, I. L., de Pablo, P. J., Ibarra, B., Sgalari, G., MacKintosh, F. C., et al. (2004) Bacteriophage capsids: tough nanoshells with complex elastic properties, *Proc Natl Acad Sci U S A 101*, 7600-7605.
140. Davis, J. S.,Epstein, N. D. (2007) Mechanism of tension generation in muscle: an analysis of the forward and reverse rate constants, *Biophys J 92*, 2865-2874.

141. Davis, J. S.,Epstein, N. D. (2009) Mechanistic role of movement and strain sensitivity in muscle contraction, *Proc Natl Acad Sci U S A 106*, 6140-6145.
142. Ramachandran, G. N., Ramakrishnan, C.,Sasisekharan, V. (1963) Stereochemistry of polypeptide chain configurations, *J Mol Biol 7*, 95-99.
143. Laemmli, U. K. (1970) Cleavage of structural proteins during the assembly of the head of bacteriophage T4, *Nature 227*, 680-685.
144. Jameson, G. W., Roberts, D. V., Adams, R. W., Kyle, W. S.,Elmore, D. T. (1973) Determination of the operational molarity of solutions of bovine alpha-chymotrypsin, trypsin, thrombin and factor Xa by spectrofluorimetric titration, *Biochem J 131*, 107-117.